EXPERIMENTAL STUDY OF

REVERSE CREVICE CORROSION

OF COPPER

A Thesis

Submitted to the College of Graduate Studies and Research

In Partial Fulfillment of the Requirement for the Degree of

Master of Science

In the Department of Chemical Engineering

University of Saskatchewan

Saskatoon, Saskatchewan

Canada

By

Lin Lu

PERMISSION TO USE

The author grants permission to the University of Saskatchewan Libraries to make this thesis available for inspection. Copying of this thesis, in whole or in part, for scholarly purpose may be granted by my supervisor (Dr. Richard W. Evitts), the head of the department of Chemical Engineering, or the Dean of the college of Engineering. It is understood that any copying or publication or use of this thesis or parts thereof for financial gain shall not be allowed without my written permission. It is also understood that due recognition to me and the University of Saskatchewan must be granted in any scholarly use which maybe made of any material in this thesis.

Requests for permission to copy or to make other use of the material in this thesis in whole or in part should be addressed to:

Head, Department of Chemical Engineering
57 Campus Drive
University of Saskatchewan
Saskatoon, SK
Canada
S7N 5A9

ACKNOWLEDGEMENT

First of all, I would like to express my sincere and deepest appreciation to my supervisor, Dr. Evitts for his guidance, support, encouragement, kindness and help during the course of my graduate study. His in-depth knowledge, expertise and vision have guided me through the past three years of study and research. I am lucky enough to have Professor, Dr. Evitts as my supervisor. The research experience and knowledge gained here will benefit greatly my professional career.

I would like to thank my thesis committee members, Dr. Postlethwaite, Dr. Phoenix, and Dr. Nemati for their valuable advice, help and support. I have learned a lot from all of the committee members in many different aspects. Without their help, I would not achieve what I have achieved today. Thanks to Mr. D. Cekic and Mr. T. Wallentiny for providing technological assistance for the experiment studies.

Many thanks also go to many of my lab mates and friends. We have shared many happiness and some times, sadness during the past three years of study. At difficult times, they offered great help and encouragement. At good times, they shared the happiness with me.

Lastly, and also most importantly, I would like to thank my Mom, Zuyu Qu, Dad, Yanping Lu, and my Brother, Ying Lu for their love, support, encouragement, and understanding. I know I can always count on them for whatever I need. I would like to dedicate this thesis to them.

This research was funded by NSERC (Natural Sciences and Engineering Research Council of Canada)

DEDICATION

This thesis is dedicated to My Parents

ABSTRACT

Crevice corrosion generally occurs on the crevice surface while the exterior or bold surfaces are not damaged. However, for copper and its alloys, the opposite is true; the bold surface is corroded while the crevice remains relatively corrosion-free. This unique type of corrosion is referred to as reverse crevice corrosion (RCC). In this research, commercially pure copper was chosen as the target metal to investigate RCC. Based on electrochemical measurements and surface analysis, reverse crevice corrosion was found to occur at room temperature. At elevated temperature only uniform corrosion was observed while under a deoxygenated environment, as expected, no corrosion was observed.

A multiple crevice assembly and a working electrode were designed especially for this research. Exposure test experiments were first performed at room temperature and 50 ºC. Several types of electrochemical tests were conducted including open circuit potential measurement, potentiodynamic measurement and electrochemical impendence spectroscopy (EIS). Atomic Force Microscopy (AFM) and Raman Spectroscopy were used to analyze the surfaces of the copper coupon.

The results of the exposure tests showed that RCC occurred at room temperature, but not at elevated temperature. Only uniform corrosion was observed at elevated temperature and no corrosion was occurred under a deoxygenated environment. It was found, based on the open circuit potential measurement, that the RCC process can be divided into three steps, a uniform corrosion phase, a corrosion slow-down step and a reverse crevice corrosion step. The first two steps can be combined into one phase, incubation phase. This hypothesis is supported with the results from Raman spectra and AFM. The EIS measurements revealed that the diffusion process from bulk solution to copper coupon surface is the rate controlling step for incubation phase and this diffusion process combined with the reduction of Cu (I) oxide in the crevice are the rate-controlling step corresponding to the last step.

TABLE OF CONTENTS

LIST OF TABLES

LIST OF FIGURES

NOMENCLATURE

a	a constant in Tafel equation (V)
b_a	Tafel slope of anodic polarization curve (V/decade)
b_c	Tafel slope of cathodic polarization curve (V/decade)
C_{dl}	Double layer capacitance (F/cm^2)
E	Electrode potential (V)
E^0	Standard potential of the electrode (V)
E*	the amplitude of signal
E_i	Polarization potential (V)
E_t	Potential at time t (V)
f	Frequency (Hz)
F	Faraday's constant (Coulombs)
ΔG	Gibbs free energy (kJ/mol)
I	current (A)
I_{corr}	corrosion current (A)
I_0	the amplitude of response signal (A)
I_t	the response signal (A)
i_0	exchange current density (A/cm^2)
i_{corr}	corrosion current density (A/cm^2)
K	substitution for $b_a \cdot b_c/(2.3\ (b_a+b_c))$
n	the number of electrons in the reaction
P_{eq}	the number of equivalent weights
r	penetration rate (μm/year)
R	Universal gas constant (8.314 J/mol·K)
R_p	polarization resistance (Ω·cm^2)
R_{ct}	resistance resulting from charge transfer reactions (Ω·cm^2)
R_Ω	Ohmic resistances resulting from the electrolyte, surface film, circuit leads (Ω·cm^2)
t	time (h)
T	absolute temperature (K)
W	weight loss (g)

Z impedance ($\Omega \cdot cm^2$)

$|Z|$ the module of Z

Z_0 the magnitude of impedance Z ($\Omega \cdot cm^2$)

$\overline{Z}$ complex impedance

Z' real component of impedance ($\Omega \cdot cm^2$)

Z'' imaginary component of impedance ($\Omega \cdot cm^2$)

Greek Symbols

γ activities of species

η overpotential (V)

η_a activation overpotential (V)

η_c concentration overpotential (V)

η_T total overpotential (V)

ω frequency (radians/s)

ω_{max} the maximum frequency (radians/s)

φ Phase shift

Φ Potential (V)

Φ_{corr} Corrosion potential (V)

CHAPTER 1

INTRODUCTION

1.1 Overview

Corrosion of metal is the degradation of materials by electrochemical reactions. It is most commonly seen on metals in the form of oxide films. However, similar processes also occur in non-metals, such as plastic, concrete and ceramics but the corrosion process is not electrochemical. A recent survey on the costs of corrosion showed that the direct cost of corrosion was $276 billion in the United States for 2002, which is approximately 4% of their Gross National Product (NACE International, 2005).

From an economical viewpoint, some of the corrosion damage cannot be completely avoided. However, many losses can be reduced. This can be accomplished through programs that promote public awareness and further development in mitigation technologies. Corrosion takes on two basic forms: uniform corrosion and localized corrosion. Uniform corrosion is characterized by corrosive attack that takes place evenly over the entire surface area or a large fraction of the total area of a metal surface. In contrast, localized corrosion has some selectivity, which often occurs in small areas or zones on a metal surface in contact with corrosive media. Some of the more common forms of localized corrosion are pitting corrosion, crevice corrosion, galvanic corrosion and erosion-corrosion.

Compared to uniform corrosion, localized corrosion is more problematic since it is very difficult to detect, predict and design against. This is because localized corrosion morphologies are typically small in size and the locations of corrosion (e.g., pit or crevice) are often covered with corrosion products. In addition, localized corrosion is difficult to measure quantitatively on any instrument due to the small size of the corroding areas (Fontana, 1967).

Copper alloys are widely used in many fields, especially for marine applications, such as seawater valves. As a comparatively noble metal, copper has good resistance to corrosion in most cases. However, it still will undergo corrosion in such forms as pitting, crevice and stress corrosion cracking, and its alloys are subject to selective leaching (Polan, 1987). Among these types of corrosion, crevice corrosion is of particular interest to copper since valves are connected to piping systems with flanges and they contain numerous internal crevices.

Usually, the appearance of crevice corrosion on all metals except copper is manifested as a corroded crevice with a somewhat cathodically-protected bold metal surface around the crevice mouth. Figure1-1(a) shows a type 904L stainless steel coupon (20Cr-25Ni-4.5Mo-l.5Cu) that underwent crevice corrosion after only 30 days of exposure in ambient-temperature seawater (ASM International, 2001). In contrast, copper and its alloys undergo a different process that is referred to as reverse crevice corrosion (RCC). In the RCC phenomenon, the external or bold surfaces are attacked instead of the interior walls of the crevice. Figure 1-1(b) shows a 70Cu-30Ni coupon after 2 months exposure in ambient-temperature seawaters. In this figure, it is seen that corrosion has occurred nearby the crevice mouth on the bold surface. However, it looks not severe even after 2 months of immersion (ASM International, 2001). In comparison, crevice-related corrosion of Alloy 400 (70Ni-30Cu) is more severe after only 45 days (Figure 1-1(c)) where corrosion occurred within as well as outside the crevice (ASM International, 2001).

The reverse crevice corrosion phenomenon has been known about for many years. There is, however, little research on it and, as a result, very little is known about it or why it occurs. Copper has extensive applications in modern industries due to its excellent thermal and electrical properties. Thus, it is essential to carry out further research on the RCC phenomenon. This study focuses on furthering this research. A knowledge of the mechanism of this type of attack will help in the design of mitigation technology. Moreover, from an economic perspective, it is also important to reduce natural resource wastage and cut down on the expenses caused by parts replacement resulting from RCC.

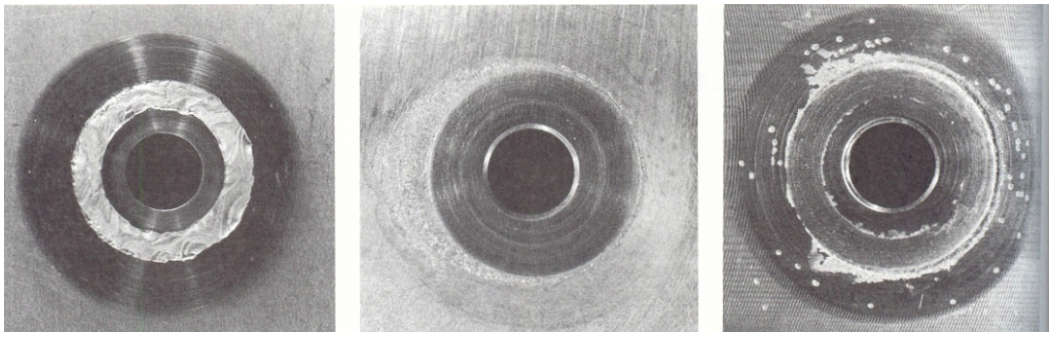

(a) (b) (c)

Figure 1- 1: Crevice-related corrosion for different alloys in natural seawater. (a) Alloy 904L (20Cr-25Ni-4.5Mo-1.5Cu) after 30 days. (b) 70Cu-30Ni after 2 months (c) Alloy 400 (70Ni-30Cu) after 45 days (ASM International, 2001).

1.2 Objectives

The general objective of this study was to examine the RCC process and to postulate a theory to explain the phenomenon. Specifically, this study aimed to fulfill the following three objectives:

1. To reaffirm the existence of reverse crevice corrosion in copper.
2. To conduct experimental investigations on how temperature and the presence of oxygen affect reverse crevice corrosive behavior.
3. To determine the chemistry composition and morphology of corrosion products generated on the bold surface (outside of crevice) and in the crevice, and to relate these to a mechanism.

To fulfill these objectives, three research phases were undertaken.

Phase I: This phase was intended to:

1. Design a crevice assembly to be used in this study and a set of working electrode parts suitable for the crevice assembly based on past literature. According to the design, proper materials are selected and used for manufacturing these parts.
2. Determine the applicable electrochemical measurement techniques to generate valid data.
3. Design and set up an experimental apparatus to meet the different demands of the electrochemical techniques used in this study.

Phase II was intended to apply the different electrochemical methods to study RCC. The phase II goals were:

1. To observe corrosion behavior of creviced copper coupons in the laboratory by means of exposure tests and examine the reproducibility of RCC phenomenon under the following conditions: room temperature (22 ~ 24 ºC) with O_2, temperature of 50 ºC with O_2 and room temperature without O_2.
2. To monitor the open circuit potential to see if it changes during the onset of reverse crevice corrosion under different temperatures for samples immersed in solutions exposed to air and deaerated.
3. To perform potentiodynamic and potentiostatic studies to examine the kinetics of the phenomenon at room temperature.
4. To use electrochemical impedance spectroscopy (EIS) to provide information on the mechanism of the RCC process at room temperature.

In Phase III of this research, surface analysis experiments were conducted to examine the surface structure and the composition of corrosion products. This phase involved 2 steps:

1. Use atomic force microscopy (AFM) to detect the surface morphology of a copper coupon after it undergoes corrosion at room temperature with O_2, temperature of 50 ºC with O_2 and room temperature without O_2.
2. Apply Raman spectroscopy to analyze the chemistry composition of corrosion products produced in the crevice and on the bold surface.

1.3 Experimental Methods Used in This Study

In this research, the experimental methods for corrosion studies are classified into two categories: electrochemical and surface analysis. These two methods were applied to examine the nature of reverse crevice corrosion phenomenon in copper.

For electrochemical measurements, there are several methods available that measure different aspects of corrosion behavior. For example, the measurement of corrosion potential can be used to provide a general description of corrosion tendency over a long period of time. In comparison, potentiodynamic or

potentiostatic measurement provides a rapid measurement of the corrosion process under specific environmental conditions by applying an external voltage. Potentiodynamic and potentiostatic methods are often used to determine the kinetic properties associated with corrosion processes. The difference between these two types of tests is as follows. Potentiodynamic measurement is based on a transient state while potentiostatic is conducted under steady state. However, both measurements are based on direct current and involve Tafel theory. In contrast, electrochemical impedance spectroscopy uses an alternating current excitation signal to deduce measurement errors (Mansfeld, 1981). In addition, it is a non-destructive measurement as long as the amplitude of the excitation signal is less than 50 mV (Global Spec, Inc., 2005).

As the approaches of surface analysis, Atomic Force Microscopy (AFM) and Raman spectroscopy were used to measure the surface morphology and the chemical composition of corrosion products in the crevice and bold surface of the copper coupon.

1.4 Thesis Outline

This thesis is arranged into five chapters. Following this introductory chapter, a literature review is presented in Chapter 2. The review is divided into three basic compartments: the corrosion resistance of copper alloys; the mechanism of crevice corrosion; and the pertinent experimental approaches for corrosion studies. The experimental work conducted in this research and the results are covered in Chapters 3 and 4, respectively. Finally, Chapter 5 contains the conclusions from this research and some recommendations for future studies in this area.

CHAPTER 2

LITERATURE REVIEW

Reverse crevice corrosion (RCC) of copper and its alloys has been known about for many years, although the information in the literature is somewhat sparse. There are few references on experimental studies of RCC in copper. In light of this, the literature review presented here covers a large number of topics that are concerned with the corrosion behavior of copper and crevice corrosion in general. In addition, some fundamental electrochemistry concepts are briefly introduced because they are the basis of corrosion measurement techniques. The experimental techniques used in this study are also summarized.

2.1 Copper and Its Alloys

In nature, copper exists is its metallic state in certain geological formations. Copper metal has been used for more than 10,000 years. Copper and its alloys have many industrial applications because of their excellent corrosion resistance properties as well as superior electrical and thermal performance (Leidheiser, 1979). Although copper is malleable and machinable, it is not very durable. If a high strength material is desired, copper has to be alloyed with other metals, such as zinc, tin, aluminum and nickel (Leidheiser, 1979). The application of copper and its alloys is generally classified into five sections shown as in Table 2-1:

Table 2 - 1: Applications of copper and its alloys under different environments (Cieslewicz and Schweitzer, 1989)

Applications	Examples	Approximate corrosion rate*
Construction	Roofing, building fronts, hand rails and door knobs.	Atmosphere: 0.5~2.5μm/year
Fresh water	Fresh water supply line and plumbing fittings.	Fresh water: about 10μm/year Soil: 1~50μm/year
Marine	Seawater supply line, shafting, valve stems and marine hardware.	Sea water: about 50μm/year
Industrial	Heat exchanger, condenser and chemical plant process equipments.	Variable (depends upon environment)
Electrical	Electrical wiring, connectors, printed circuit boards and semiconductor packages.	Variable

2.2 Corrosion Resistance of Copper and Its Alloys

2.2.1 Pourbaix diagram

Copper is a comparatively noble metal. Compared with other corrosion-resistant alloys, copper and its alloys exhibit a unique performance. This can be explained partly by the Pourbaix diagram for the Cu-H_2O system at 25 ^oC. In Figure 2-1, between two dashed lines a and b, there is a stable domain for water. It can be seen that the immunity domain of copper partly overlaps with the stability domain of water. That is to say, copper will not corrode in water without oxygen being present. For most metals in a deaerated environment, corrosion takes place and the anodic reaction is the dissolution of the metal while the cathodic reaction is the evolution of hydrogen gas from the electrolyte. However, if oxygen is present, copper is susceptible to corrosion as indicated by the corrosion domains in Figure 2-

1. In other words, the primary cathodic reaction for copper corrosion in aqueous systems is the reduction of oxygen to form hydroxide ions.

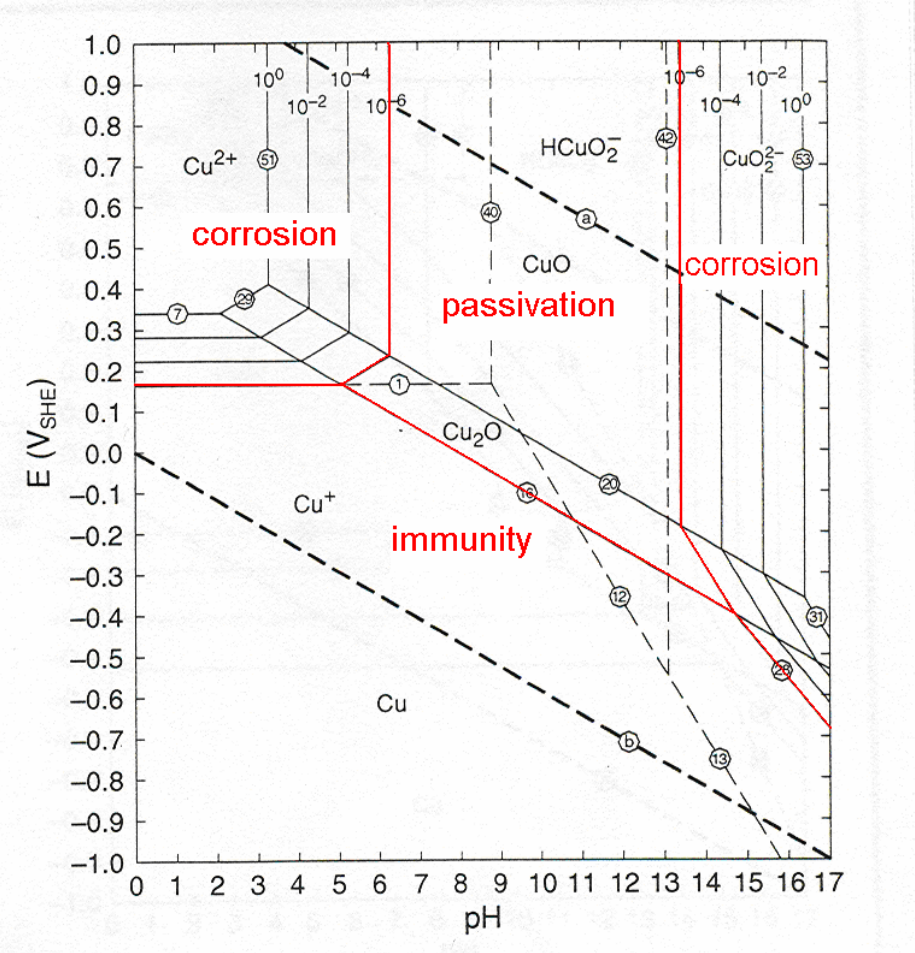

Figure 2 - 1: Pourbaix diagram for the Cu – H_2O system at 25 °C (Pourbaix, 1974).

The circled numbers on the diagram indicate the presence of a chemical reaction and the activity of dissolved species at which the lines were calculated is indicated by the other numbers.

Bianchi and Longhi (1973) determined the Pourbaix diagrams for copper in seawater at 25 °C. Figure 2-2 is an example of one of these diagrams. Compared with Figure 2-1, Figure 2-2 considers the reactions between a chloride ion and copper as well as copper and water. As a result, it can be seen that there are two new chemical species in the figure, $Cu_2(OH)_3Cl$ and CuCl. In addition, the range each species occupies is different due to the existence of these new compositions.

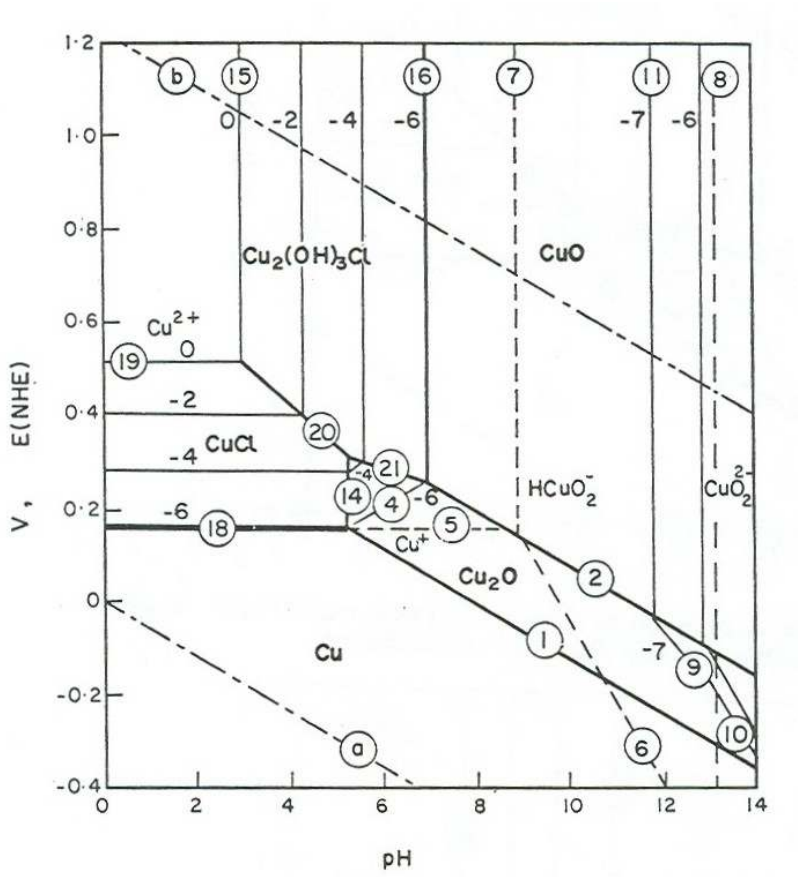

Figure 2 - 2: Pourbaix diagram for copper in sea water at 25 ^{o}C (Bianchi and Longhi, 1973).

2.2.2 Anodic behavior of copper

Unlike a passive metal, copper can not produce a passive film. But the corrosion product formed on copper and its alloys do provide a protection from corrosion to some extent. In most cases, the protective oxide film on copper is Cu (I) oxide in aqueous environments at room temperature. This film is adherent and relatively impervious and acts as a diffusion barrier, but easily affected by change in hydrodynamic intensity. In addition, basic copper salts may also provide a certain degree of protection (ASM International, 2001).

To explore the key factors affecting the anodic behavior in copper, many researchers have investigated the influence of pH, flow rate, temperature, the presence of chloride ion and crystallography on the corrosion rate of copper under

various environments. These factors will be further detailed in the following sections:

2.2.2.1 Influence of pH

Depending on pH, the anodic polarization of copper may result in anodic dissolution or film formation. Generally speaking, the propensity for film formation increases with increasing acidity especially at low temperatures. In acidic aqueous solutions, such as HCl and H_2SO_4, Cu (I) complexes are formed by bonding with Cl^- or SO_4^{2-}. These porous corrosion products do not prevent the copper from the further dissolution. However, a more protective Cu_2O film is formed in 10 M concentrated sulfuric acid solution. The film formation phenomenon has also been found to occur in alkaline solutions (Leckie, 1970). Leckie (1970) proposed a variety of corrosion products for copper in alkaline solutions as shown in equation 2.1 to 2.7. The exact corrosion products depend on the applied current in the galvanostatic measurements that were used in the study.

$$2Cu + 2OH^- \rightarrow Cu_2O + H_2O + 2e^- \qquad \Delta G = \text{-52.342 kJ/mol} \qquad (2.1)$$

$$Cu_2O + 2OH^- + H_2O \rightarrow Cu(OH)_2 + 2e^- \qquad \Delta G = 645.628 \text{ kJ/mol} \qquad (2.2)$$

$$Cu(OH)_2 + OH^- \rightarrow HCuO_2^- + H_2O \qquad \Delta G = \text{-301.177 kJ/mol} \qquad (2.3)$$

$$HCuO_2^- + OH^- \rightarrow Cu_2O^{2-} + H_2O \qquad \Delta G = \text{-4.905 kJ/mol} \qquad (2.4)$$

$$Cu + 3OH^- \rightarrow HCuO_2^- + H_2O + 2e^- \qquad \Delta G = \text{-22.379 kJ/mol} \qquad (2.5)$$

Earlier studies on the corrosion mechanisms and products of copper corrosion were limited to either acidic or alkaline environments, but recently, Feng et al. (1997) systematically investigated copper corrosion in simulated tap water over a wide pH range. The results of this study are summarized in Table 2-2. The thickness of the oxide films and the dependence of corrosion rate on pH were measured as shown in Figure 2-3 and 2-4. In Figure 2-3, dissolution of oxide films takes place when the pH is less than 4; between a pH of 4 and 10, cubic Cu_2O crystals grow while the crystal size becomes smaller and the thickness of the film becomes thinner; when pH is greater than 10, monoclinic CuO films start to form.

Table 2 - 2: Corrosion products and controlling mechanism of copper in aqueous solutions at various pH values (Feng et al., 1997).

pH value	Oxide films	Morphology of corrosion products	Controlling mechanism	Corrosion rate	
				Tendency	Explanation
3	Cu_2O	Porous corrosion products	Diffusion in solution	↑	The corrosiveness of solutions increases
4-5	Cu_2O	Cubic Cu_2O provides a barrier to copper dissolution	Mixed diffusion of copper ions in oxide films and in solution	increase	From pH 4 to 5, the film becomes more protective
6-9	Cu_2O	Cubic Cu_2O is more protective	Diffusion in oxide film		Keep constant
10	Cu_2O	A thick , compact cubic Cu_2O film	Passivation	minimum	passivity
12-13	CuO	A protective monoclinic layer	Diffusion in the oxide films	increase ↓	Increased solubility of CuO film

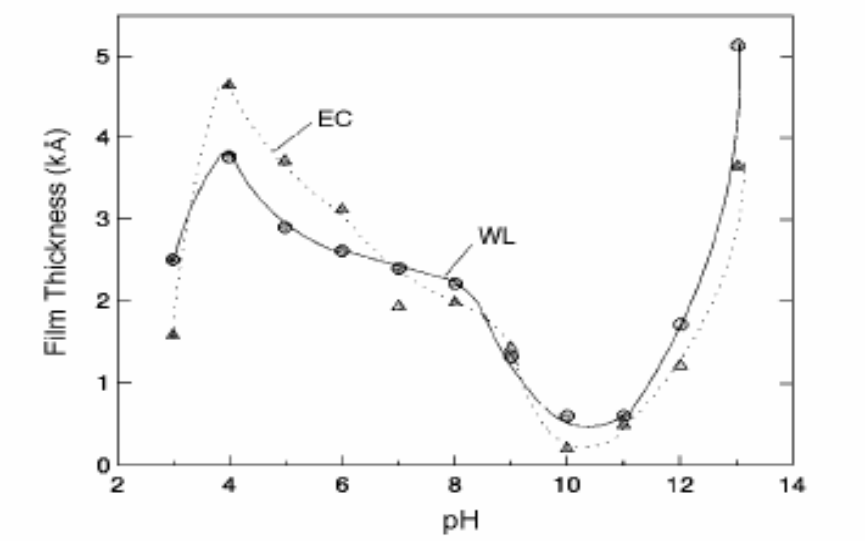

Figure 2 - 3: Variation of oxide film thickness with pH (EC, electrochemical method; and WL: weight-loss method; T = 30 °C; and immersion time 24 h) (Feng et al., 1997).

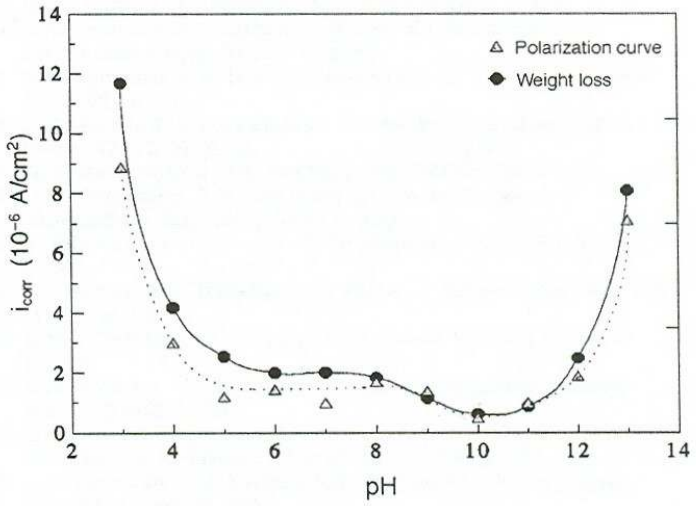

Figure 2 - 4: Current density of copper in the solutions of various pH values (T = 30 ^{o}C, immersion time 24 h) (Feng et al., 1997).

2.2.2.2 Influence of flow rate

Fluid velocity factor is one of the key parameters that affect on the corrosion rate of copper. According to Braun and Nobe (1973), who used a rotating disk electrode in acidic chloride media, the current plateau/limiting current was always proportional to the square root of the rate of rotation which directly affected the formation or dissolution of a multilayer film CuCl. Turner and Brook (1973) found that current densities increased with increasing flow rate as did the potential and the corrosion current before the limiting current was achieved. Moreover, the flow rate had some effect on thinning the critical thickness (the minimum thickness to form a stable film) of the CuCl film. Giuliani et al. (1971) found that the sensitivity of Cu-Ni alloy corrosion rates to the flow rate was relatively low in Cl^- solution.

2.2.2.3 Influence of temperature

The literature is unclear when it comes to the effect of temperature on the corrosion rate of copper. Melchers (2001) examined the literature to investigate if any relationship would be formed between corrosion rate and temperature of 90:10 Cu-Ni alloys immersed in sea-water. It was revealed that there was no obvious difference in corrosion rate for short-term exposure tests at temperature of 10, 20 and 30 ^{o}C. However, the corrosion rate was found to be lower at 40 and 50 ^{o}C than

at 30 ^{o}C. In long-term exposure tests, the highest corrosion rate was found to occur in the18 ^{o}C – 28 ^{o}C temperature ranges.

2.2.2.4 Chloride ion effects

Due to the aggressive nature of halide ions, many researchers have studied the anodic behavior of copper in solutions containing various concentrations of halide ions. Among the halide ions, chloride is the most aggressive one (Turner and Brook, 1973).

In solutions containing Cl^-, the corrosion products of copper are mainly the chloro-complexes, which form a non-adherent layer on the surface of the metal. Moreover, the concentration of chloride produces an effect on the composition of corrosion products. For example, Braun and Nobe (1973) found that $CuCl_3^{2-}$ was the primary product in concentrated chloride solutions, while $CuCl_2^-$ was predominant in solutions with a chloride ion concentration less than 0.7 M. In more dilute solutions, Cu^{2+} appeared as the corrosion product (Leckie, 1970). According to Beccaria et al. (1987), the influence of chloride is weak on the corrosion behavior of aluminum brass in sulfate solutions. In most acidic solutions, the presence of chloride ions promoted the occurrence of dezincification or localized corrosion. In chlorinated seawater, Klein et al. (1991) found that 70:30 copper-nickel alloy exhibited a better corrosion resistance in the seawater with 1 ppm addition of chlorine. In addition, in a high chlorine-containing environment (the concentration of chlorine = 90 ppm), the corrosion rate was found to increase significantly.

2.2.2.5 Crystallographic factors

Anodic dissolution is often employed in the process of electrochemical machining or polishing. Crystallographic factors were considered to have some influence on this process (Landolt et al., 1971). It was shown that if copper surface was treated with active dissolution, the anodic attack depends on the crystallographic orientations that result in differentiation between grains in polycrystalline materials. However, after transpassive dissolution, the attack is not sensitive to the orientation of the crystals. The difference between active dissolution and transpassive dissolution lies on the various flow velocity of the solution used for anodic dissolution.

2.2.2.6 Alloying elements

Doping with divalent or trivalent cations is an effective way of improving the corrosion resistance of copper. The ionic or electronic conductivity of films formed due to alloying elements is reduced and thus the migration velocity essential for the corrosion reaction is slowed down. In practice, aluminum, zinc, tin, iron, and nickel often serve as the alloying additions and reduce the corrosion rate noticeably on copper alloys. The following table summarizes the effects of alloy compositions (Polan, 1987).

Table 2 - 3: The corrosion performance of copper and its alloys (Polan, 1987)

<table>
<tr><th colspan="2" rowspan="2">Classifications</th><th rowspan="2">Composition</th><th colspan="2">Corrosion performance</th></tr>
<tr><th>Corrosion resistance</th><th>Corrosion susceptibility</th></tr>
<tr><td colspan="2">Coppers</td><td>>99.3% copper</td><td rowspan="3">• Seawater corrosion
• Biofouling</td><td rowspan="3">• Erosion corrosion</td></tr>
<tr><td rowspan="2">High – Copper Alloys</td><td>wrought</td><td>>96% copper</td></tr>
<tr><td>cast</td><td>>94% copper</td></tr>
<tr><td colspan="2">Brasses</td><td>Cu-Zn</td><td>• Alloys containing 15% zinc or less have good corrosion resistance in aqueous solution.
• High zinc brasses resist sulfides well.
• Tin brasses have good resistances to dezincification.
• Aluminum brasses increase resistance to impingement attack in turbulent high-velocity saline water.</td><td>• Above 15% Zn, dezincification may occur.
• Susceptibility to stress-corrosion cracking increases as zinc content decreases from 15% to 0%.</td></tr>
</table>

Table 2-3 cont.

Classifications	Composition	Corrosion performance	
		Corrosion resistance	Corrosion susceptibility
Phosphor bronzes	Cu-Tin	• Good resistance to flowing seawater and to most nonoxidizing acids except hydrochloric.	
Aluminum bronzes	Cu-Al	• Excellent resistance to impingement corrosion and high temperature oxidation. • Resistance to potash solution, nonoxidizing mineral acids, many organic acids and alkalis.	
Copper – Nickel Alloys	Cu-Ni	• The best general resistance to aqueous corrosion of all the copper alloys. • Great superiority to copper and other copper alloys in resisting acid solution, SCC and impingement corrosion.	

2.3 Corrosion Forms Found in Copper and Its Alloys

Copper and its alloys are subject to almost all kinds of corrosion attacks depending upon the environment. The following section is a summary of the relevant information from ASM hand book (ASM International, 2001) on the types occurring on copper and its alloys.

2.3.1 Uniform corrosion

Uniform corrosion is characterized by corrosive attack proceeding evenly over the entire surface area. Since uniform corrosion is relatively easy to measure and predict, it seldom causes disastrous failures. In environments like fresh or salt water, soils, and alkaline or acid salt solutions, the rate of uniform thinning is very low. However, as far as copper and its alloys being concerned, the corrosion rate of copper is a little faster in oxidizing acid, sulfur-bearing compounds, NH_3 and cyanides (ASM International, 2001).

2.3.2 Pitting

Pitting of copper and its alloys always occurs under relatively low flow velocity. Long-term exposure tests (ASM International, 2001) have shown that there is a certain limit in pitting depth, beyond which an increase in pit depth is not obvious.

To prevent a copper alloy from pitting, the correct choice of copper alloy for the environment is necessary. For example, aluminum brass is the best choice for protection against pitting attack, while the high-copper alloys are somewhat more inclined to pitting (ASM International, 2001).

2.3.3 Erosion corrosion

Copper alloys are relatively sensitive to erosion corrosion when they are exposed to water with high flowing velocity, and especially when turbulence occurs. Because rapidly flowing water can locally strip away any protective film, copper corrosion rates will be high. A steady state is achieved when the film growth rate due to corrosion matches the rate at which the protective film is stripped. Sometimes, horseshoe-shaped and accompanied by pitting, this kind of attack is characterized by broad pits which are free from corrosion products and by undercuts in the direction of flow.

2.3.4 Selective corrosion

The dezincification of brass is the selective dissolution of the zinc from the alloy leaving a porous mass of copper with poor strength. Brass can be dezincified

by contact with water and by exposure to an outdoor-atmosphere. The attack is accelerated by the presence of chloride and elevated temperatures. Aluminum bronze with more than 8 wt % Al has very good strength characteristics and good corrosion resistance, but it is very sensitive to selective corrosion, i.e. dealuminization.

2.3.5 Stress corrosion cracking

Stress corrosion cracking in copper materials is caused by tensile stresses, usually residual stresses from cold working, in combination with a corrosive environment which contains ammonia, moisture or mercury. In general, zinc-rich brass is most susceptible to stress corrosion cracking. However, under some conditions, other copper materials, even pure copper, can also be damaged by this type of corrosion.

2.3.6 Galvanic corrosion

Galvanic corrosion refers to the corrosion damage induced when two dissimilar materials are coupled in a corrosive electrolyte. According to galvanic series, when two metals are coupled together, the electronegative member of the couple is corroded (anode) while the electropositive member is protected (cathode). Copper and its alloys almost always serve as cathode due to their positions in galvanic series.

The severity of galvanic corrosion is mainly dependent on two factors: galvanic potential difference between the couple and the area ratio. The greater the galvanic potential difference is between the couple, the more severe in the corrosion. In addition, it is not desirable to have a situation where a large cathodic area is combined with a small anodic area.

2.3.7 Crevice corrosion

Crevice corrosion is a localized form of corrosion usually associated with a stagnant solution on the micro-environmental level. Such stagnant microenvironments tend to occur in crevices (shielded areas) such as those formed

under gaskets, washers, insulation material, fastener heads, surface deposits, disbonded coatings, threads, lap joints and clamps.

Classic crevice corrosion results from oxygen depletion and it attacks the inside crevice. For copper and its alloys, the reverse is true; the attack occurs on the surface outside the crevice while the crevice remains relatively corrosion-free.

2.4 Case Studies of Copper Corrosion

In spite of being a relatively noble metal, copper sometimes suffers corrosive attack, especially localized corrosion. Most studies have focused on the general anodic behavior of copper under specific conditions produced in the laboratory, but these conditions are often dissimilar to those found in practical settings. The following two cases are good examples which illustrate most of the important factors involved in the copper corrosion processes, and the commonly seen corrosion forms.

2.4.1 Pipe corrosion in drinking water (Royuela and Otero, 1993)

Generally, uniform corrosion of copper happens in acidic and soft waters, or when the water contains sulphides or ammonia. However, in most conditions, pitting is observed as a result of the formation of differential aeration cells. Several factors, such as suspended solid particles, the hydrolysis of manganese salts and so on, were found to promote susceptibility to pitting. In their study, parameters such as copper chemistry, water, oxygen, pH, temperature, rate of flow and deposited films were taken into account to evaluate the resulting corrosion risks to copper. Polarization resistance measurement, potentiostatic measurements and cyclic polarization measurements were used to determine the rate of corrosion, to analyze the relationship between current and time and to obtain the pitting potentials respectively.

2.4.2 Cavitation erosion and corrosion in seawater (Wood and Fry, 1989)

Copper-nickel alloys are widely used in many marine applications, such as propeller blades, pump impellers and valves of board ships. The corrosion behavior

of copper alloys under such situations has always been of great interests to many researchers.

In seawater, copper components are often subjected to both cavitation erosion and corrosion simultaneously (Wood and Fry, 1989). Pure erosion and pure corrosion were investigated separately as well as in combination for copper and 70:30 copper-nickel alloys in a flowing seawater system. Potentiostatic measurements were used to provide different overpotentials resulting in various corrosion rates. Additionally, the depth of penetration was determined. It was found that the synergistic effects of cavitation erosion and corrosion must be kept in mind when designing a structure under a mildly corrosive environment for erosion-corrosion.

2.5 Mechanism of Crevice Corrosion

2.5.1 The history of crevice corrosion mechanism development

In 1922, R. J. McKay (1922) was the first research to demonstrate that crevice corrosion is a serious corrosion hazard. In the following years, an increasing number of researchers studied the mechanism of crevice corrosion due to its potential serious influence on people's life. When crevice corrosion occurs, the crevice becomes anodic while the cathodic reactions that power the corrosion cell proceed on the external surface. McKay (1925) in a later paper defined electrolytic concentration cells, in which the cell was powered by potential difference, a result of two electrodes of the same material in different electrolytes.

According to Wyche et al. (1959), crevice corrosion is caused by the formation of oxygen concentration cells and maintained by galvanic effects between the "active" crevice and the "passive" bulk metal. Schafer and Foster (1959) reaffirmed that all types of crevice corrosion can be attributed to oxygen concentration cells and the only differences between them are crevice geometry and the composition of the solution. In addition, they stated that the formation of a differential aeration cell was the key point in crevice initiation stage and the consequent propagation of attack was sustained by the acidification of the crevice resulting from the hydrolysis of metal ions.

Based on the work of Schafer and Foster (1959), Fontana and Greene (1967) postulated a unified crevice corrosion mechanism. Figure 2-5 shows the processes involved in this mechanism. In the beginning (see Figure 2-5 (a)), the overall reactions, inside and outside the crevice, were the dissolution of metal (*M*) and the reduction of oxygen to hydroxide ions, as shown in equation (2.6) and (2.7).

$$\mathrm{M} \leftrightarrow \mathrm{M}^{n+} + ne^{-} \tag{2.6}$$

$$\mathrm{O_2} + 2\mathrm{H_2O} + 4e^{-} \leftrightarrow 4\mathrm{OH}^{-} \tag{2.7}$$

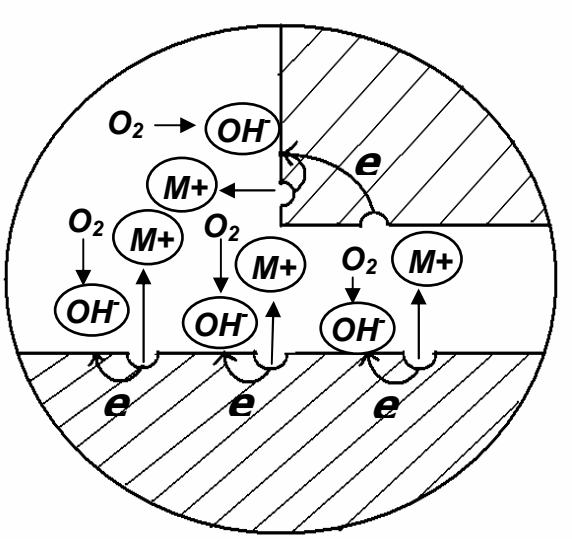

(a): Crevice corrosion-initial stage

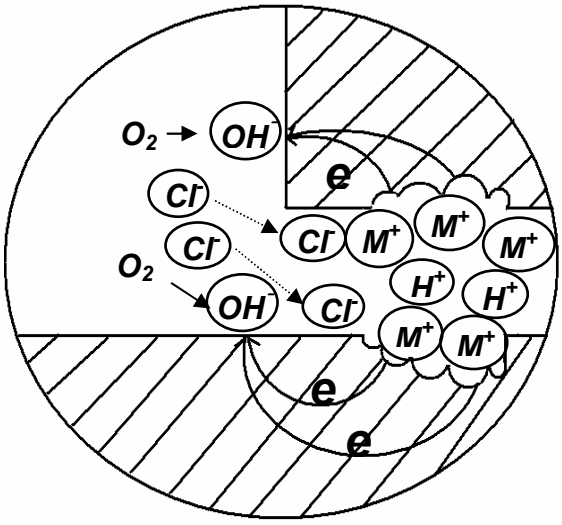

(b): Crevice corrosion-later stage

Figure 2 - 5: Crevice corrosion mechanism (Fontana, 1978).

Later, due to flow restrictions, the crevice is depleted of oxygen. The reduction of oxygen in the crevice cannot proceed while metal dissolution continues in the crevice. To maintain the electroneutrality of the crevice solution, negative ions, such as chloride ions, migrate into the crevice. The hydrolysis of metal ions, as shown in equation 2.8, leads to a decrease in pH as there is no generation of hydroxide ions in the crevice.

$$M^{n+} + nH_2O \leftrightarrow M(OH)_n + nH^+ \tag{2.8}$$

Due to the combination effect of low pH and chloride ion, the passive film on the metal in the crevice is broken down. In the meantime, the oxygen reduction reaction occurring outside the crevice cathodically protects the adjacent surfaces. Figure 2-5 (b) shows the main processes related to the later stage in which chloride ions migrates into the crevice and the hydrogen ions, produced by the hydrolysis reaction, accumulate in the crevice while the reduction of oxygen proceeds on the exterior surface of metal.

Many numerical models have been developed by many researchers to simulate the crevice corrosion processes. These models have described the chemical and electrochemical nature of crevice corrosion to various extents. Oldfield and Sutton (1978) predicted the incubation period of crevice corrosion of stainless steels. In this model, it was assumed that no concentration gradients existed in the crevice, and mass transport occurred only between bulk solution and crevice. The numerical predictions were verified by experimental data. In Bernhardsson et al.'s (1983) work, chemical and electrochemical reactions were integrated by taking into account the effect of cation production, chemical reaction, electromigration, diffusion, and electroneutrality. The initiation period of crevice corrosion of aluminum was modeled by Alkire and Siitari (1982), in which mononuclear hydrolysis of cations was assumed as the chemical reaction mechanism. Later, Hebert and Alkire (1983) further improved this model and a better agreement between the simulation and experiment data was achieved.

Fu and Chan (1984) developed a mass transport model of localized corrosion. Many factors, including electrostatic potential, diffusion potential, and chemical potential gradients were considered in this model. This model was validated by

experimental results obtained from an artificial crevice cell. Elevated temperature effects were incorporated in Sharland's model for stainless steel (1988). The comparison with experimental data showed reasonable agreement. Later on, Evitts et al. (1993, 1995), Evitts and Postlethwaite (2000) and Postlethwaite et al. (1994) et al. numerically simulated the initial stage of the crevice corrosion behavior of passive metals, such as stainless steel, nickel and titanium, in its initial stage at elevated temperatures. All of their models were based on dilute solution theory and some took into account the effects of temperature on the transport properties, chemical equilibrium, and the passive current. Evitts et al. (1996) proposed a unique algorithm to study the effect of the bold surface on the crevice corrosion process. Distinct from other models, this work coupled a 1-D model with a 2-D model and applied a mixed potential theory to the simulation.

Oldfield et al. (1996) produced a model that generated kinetic corrosion diagrams at each time step. A numerical crevice corrosion model based on a moderately concentrated solution was developed by Walton et al. (1996), in which the transport of ions was described by diffusion and electromigration. Their results were largely in agreement with their experimental data. The latest study of numerical simulations of crevice corrosion was accomplished by Heppner et al. (2002a, 2002b, 2004 and 2005) and Heppner and Evitts (2004) in which a computational model for initiation of crevice corrosion was developed. This model could be applied to more situations and is suitable for several passive metals, the applicability of which was verified by the experimental data of type 304 stainless steel from others' work.

There are some specific mechanisms that have been used to describe copper crevice corrosion. Wyche et al. (1959) found that two types of crevice corrosion of copper alloys could be ascribed to different kinds of concentration cells. When an oxygen concentration cell was present in the crevice, attack occurred within the crevice as it did in other alloys. However, when sufficient metal ions are accumulated in the crevice, due to the restriction of crevice geometry, a metal ion concentration cell is established. In this cell, the concentration of metal ion in the crevice is high while that on the bold surface is low. This theory has not been

validated. Schafer and Foster (1959) also suspected it to be the correct mechanism for RCC.

2.5.2 Factors affecting crevice corrosion

To determine a material's susceptibility to crevice corrosion, many factors should be considered. It was demonstrated that temperature was an important parameter in crevice corrosion (Postlethwaite, 1983). Generally, as temperature increases, the rate of corrosion and severity of attack increases.

Abdulsalam (2002) discussed the relationships between temperature and other corrosion variables for a commercially pure nickel (99.53 wt %) in 1 N H_2SO_4. Figure 2-6 shows the effect of temperature effect on the anodic polarization behavior of nickel. In this figure, the active peak, i_{pass}, and the passivation potential, E_{pass}, increase to a more noble value as temperature increases. That is, pure nickel is more difficult to passivate as the temperature increases. Figure 2-7 illustrates the potential distribution as a function of crevice depth and temperature. It is clear that the potential drop becomes larger as temperature increases. It is evident then that there will be a critical temperature below which crevice corrosion will not occur.

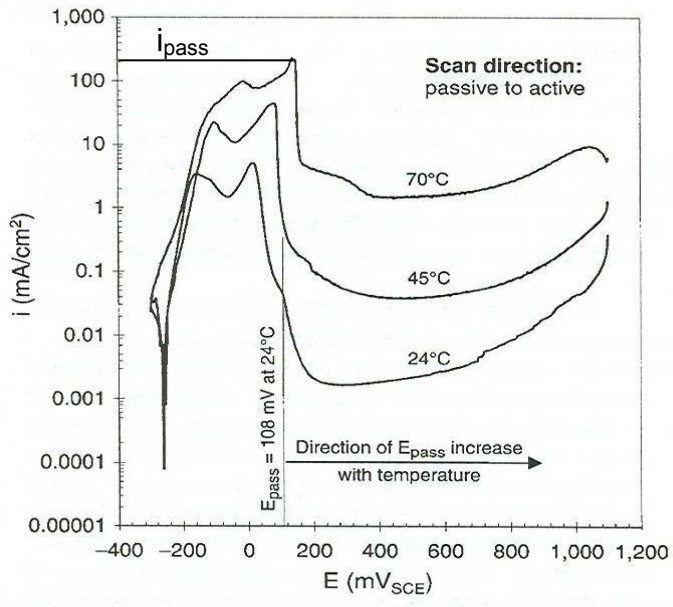

Figure 2 - 6: Anodic polarization curves for the commercially pure nickel (99.53 wt%) in deaerated 1 N H_2SO_4 at 24, 45, and 70 ^oC. Scan direction is from passive to active potentials (Abdulsalam, 2002).

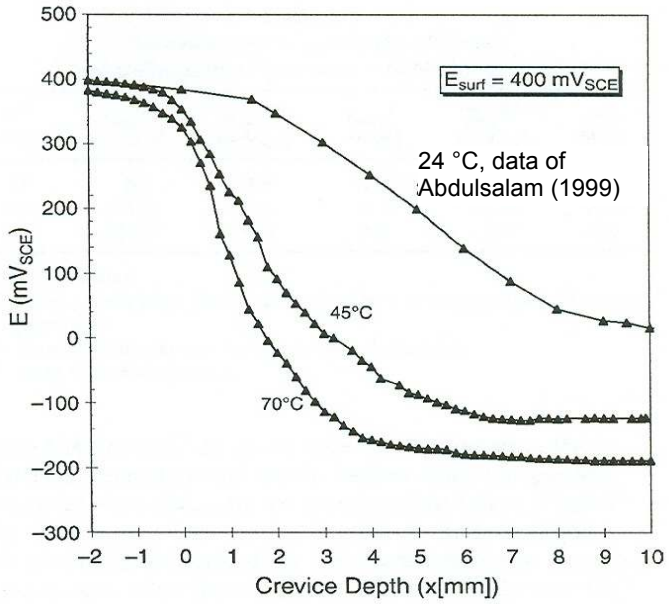

Figure 2 - 7: Initial variation of potential with depth inside the crevice for the commercially pure nickel (99.53 wt%) nickel in 1 N H_2SO_4 at 24, 45, and 70 ^oC (Abdulsalam, 2002).

The critical crevice temperature (CCT) is the temperature above which an alloy is susceptible to crevice corrosion. Steinsmo et al. (1997) defined CCT as the temperature at which an anodic current density of more than 10 $\mu A/cm^2$ persists for at least 4 hours. Initiation was marked as a sudden increase in corrosion current density as shown in Figure 2-8. In this case, the CCT was 80 ^oC. In addition, it was found that after the initiation of crevice corrosion, the corrosion current decreased little with the drop-off of temperature until the repassivation temperature was achieved. In Figure 2-8, the repassivation temperature is approximately 30 ^oC.

Pardo et al. (2000) studied the effect of temperature, pH and the concentration of chloride ions on the crevice corrosion of superduplex (SD) and superaustenitic (SA) stainless steels. Critical potentials and critical temperatures were measured in this study by cyclic polarization. As shown in Figure2-9, the repassivation potential (E_r) decreased as the temperature, pH and concentration of chloride ions increased.

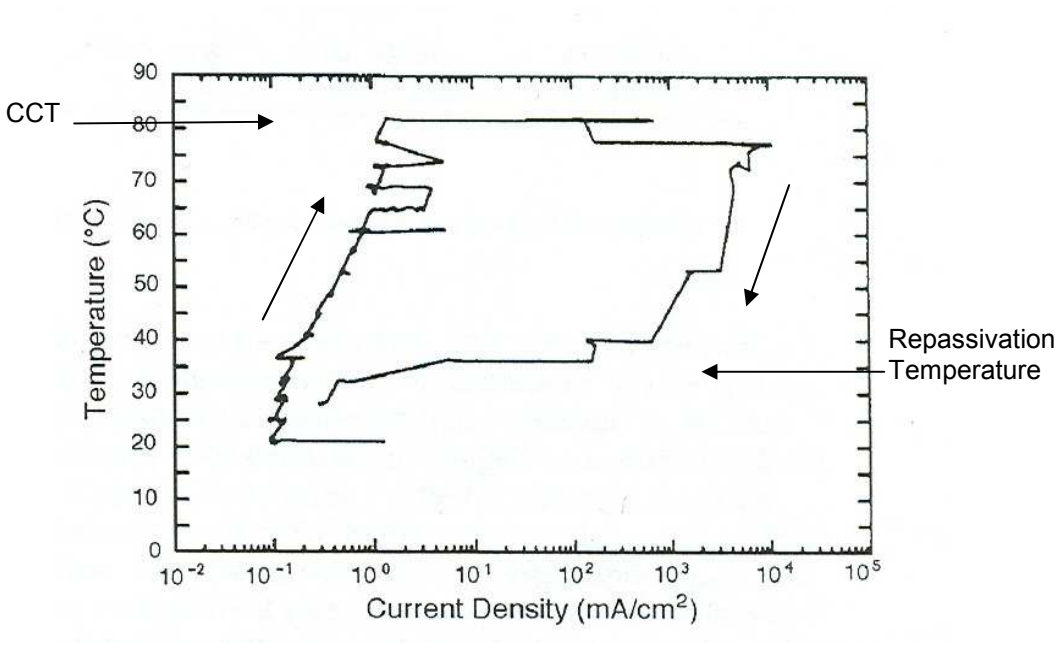

Figure 2 - 8: Anodic current density at 600 mV_{SCE} vs. temperature for high alloyed stainless steel (N08367) in air-saturated 3 wt% NaCl (Steinsmo et al., 1997).

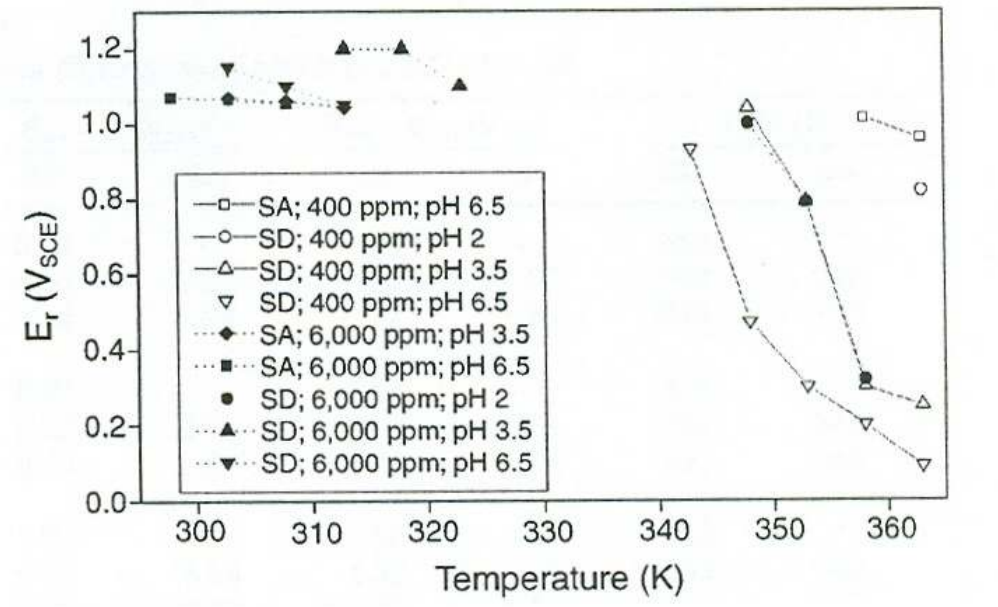

Figure 2 - 9: E_r vs temperature and pH for SD and SA stainless steels in solutions with 400 ppm and 6000 ppm Cl^- (Pardo et al., 2000).

Crevice geometry is another important factor in crevice corrosion susceptibility. It is believed that a critical characteristic dimension is the criterion to

determine the onset of crevice corrosion, which can be converted from a critical species concentration by numerical method (Vankeerberghen, 2004). In Vankeerberghen's work, a criterion was developed for aluminum to determine its susceptibility to crevice corrosion in aqueous NaCl solution. The crevice used in this study was constructed by two disks with a radius of R_0 and the gap between them is H. R_0^2/H was defined as the characteristic dimension. Figure 2-10 shows the result of this study, in which the concentration and pH in the center of the disk-like crevice and the potential drop over the disk-like crevice are correlated to the crevice characteristic dimension.

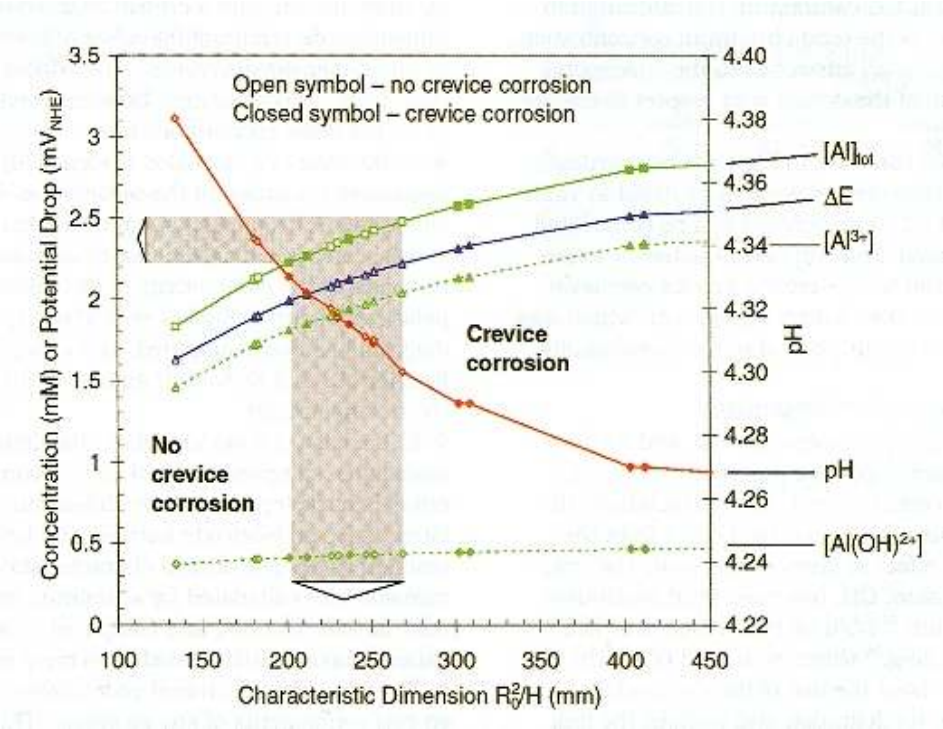

Figure 2 - 10: Influence of the characteristic dimension on the concentration and pH in the center of the disk-like crevice and on the potential drop over the disk-like crevice for aluminum in an aqueous 0.05 M NaCl solution (Vankeerberghen, 2004).

2.6 Design of an Artificial Single Crevice

There are several difficulties encountered when constructing a single crevice including maintaining a uniform geometry. Recently, Alavi and Cottis (1987), Chin and Sabde(1999), DeJong (1999) and Klassen et al. (2001) have fabricated artificial single crevices. Among their methods, the single crevice constructed by DeJong's

(1999) semiconductor microfabrication technique is more impressive than other methods by its uniform size and a regular surface. However, compared with other techniques, it is more expensive and quite complicated.

2.6.1 Semiconductor microfabrication technique (DeJong, 1999)

DeJong (1999) manufactured a crevice by using the following procedure: wafer Cleaning; film growth or deposition; lithography; Etching; metal lift off; surface Characterization. After fabrication, dicing, and cleaning, the crevice substrates and formers were assembled, as shown Figure 2-11.

The crevice produced in this way is of good quality and has uniform size and regular surfaces. The apparatus can be used to make several single-crevices at the same time, which makes the experiment more reproducible. It was used to verify the simulation results in DeJong's work and a good agreement between experiments and simulations was achieved.

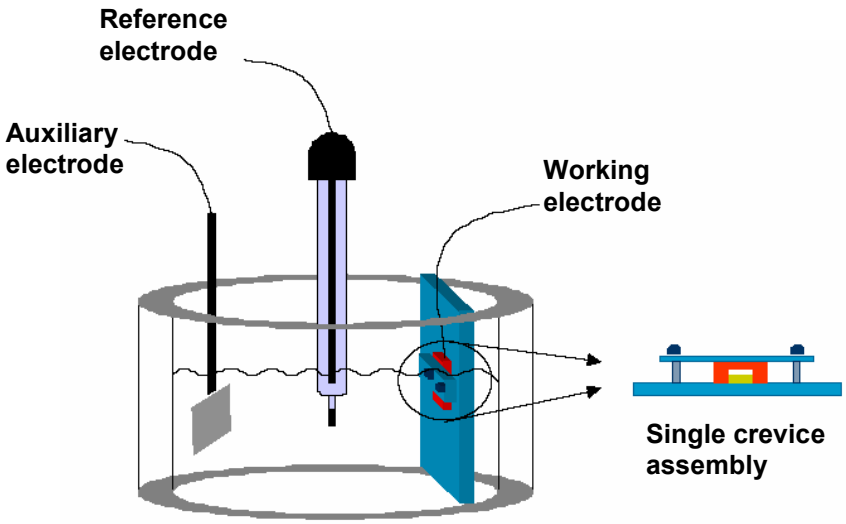

Figure 2 - 11: Schematic of artificial crevice by microfabrication (DeJong, 1999).

2.6.2 Artificial crevice of Klassen et al. (2001)

The Klassen et al.'s (2001) crevice assembly shown in Figure 2-12 consists of two parts: a metal embedded in a cylindrical epoxy mount and a crevice plate made from Perspex® (polymethylmethacrylate). A conducting wire connects the

measurement instruments to the metal sample. After the epoxy is cured, the sample was polished to 600 grit. Three thicknesses (2.0, 4.0 and 6.0 mm) of the crevice plate were used. A crevice hole was drilled into the plates with a diameter of 0.18 mm, which was rinsed by the experimental solution to reduce air bubble before it was immersed in the bulk solution. The edges of the crevice plate were sealed with silicone.

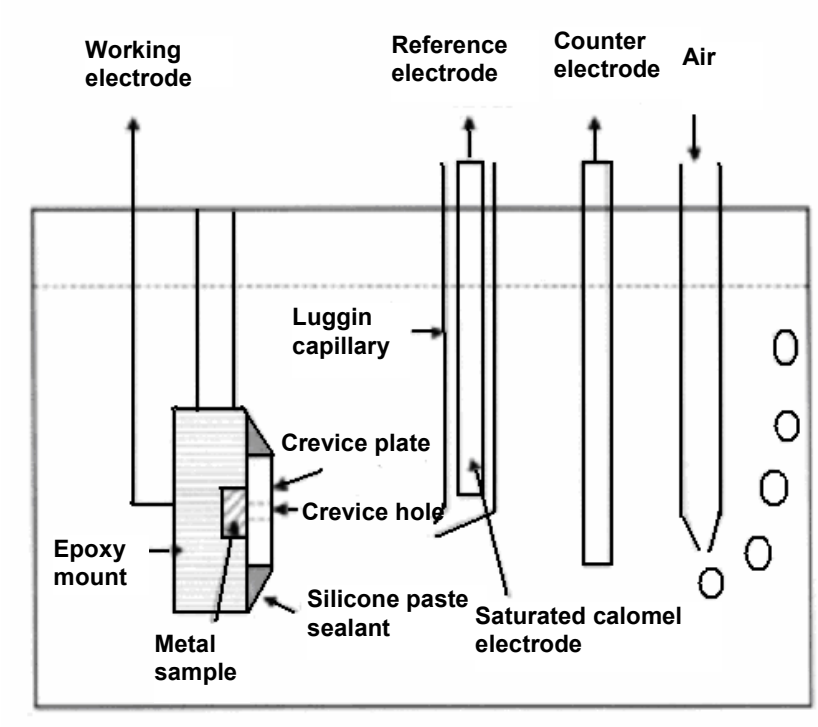

Figure 2 - 12: Schematic of the experimental crevice apparatus by Klassen et al. (2001).

Klassen et al.'s apparatus is relatively simple and easy to produce, and it is convenient to observe the solution in the crevice due to the transparency of Perspex®. However, it is doubtful that using a hole to simulate a crevice could really mimic the real crevice corrosion processes.

2.6.3 Two-Plate crevice of Alavi and Cottis (1987)

The artificial crevice used in Alavi and Cottis's experiments (1987), was formed by two parts, a metal plate, encased in epoxy resin, and a Perspex electrode

holder, as shown in Figure 2-13. The surface of epoxy-embedded specimen was polished flat enough to guarantee a uniform crevice gap in this experiment.

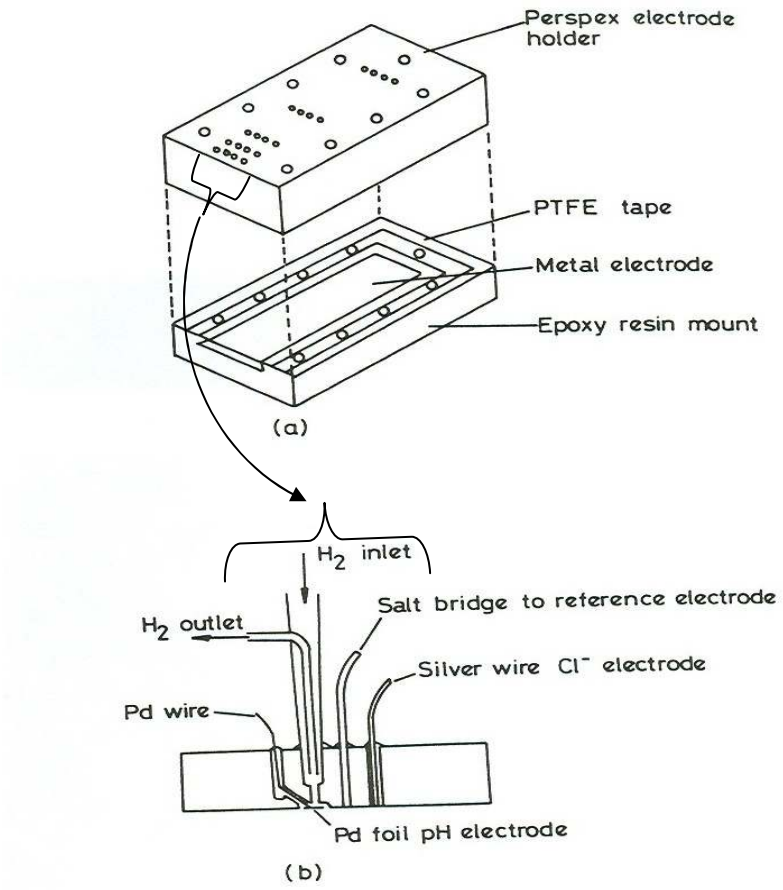

Figure 2 - 13: Schematic of artificial crevice in Alavi and Cottis's experiment (1988).

This method is better than other ones because it can measure current density or potential in different places with multiple electrode holders. As a result, the distribution of current and potential in the crevice can be acquired.

2.6.4 Chin and Sabde's crevice cell (1999)

A crevice cell with a crevice depth-to-thickness (length to gap) ratio of 110 was constructed, the schematic of which is shown in Figure 2-14 (Chin and Sabde, 1999). The crevice was produced by bolting a circular polymethyl methacrylate (PMMA) plate to a carbon steel plate. The dimensions of PMMA plate were 254 mm (diameter) and 19 mm (thickness) and the steel plate had the same diameter as PMMA plate and a thickness of 13 mm. A 10 mm-diameter hole was drilled at the

center of the PMMA plate to serve as a route to connect the crevice to the bulk solution. The crevice gap was set at 0.8mm by inserting a polytetrafluoroethylene (PTFE) gasket with a 190 mm inner diameter and a 254 mm outer diameter between the steel and PMMA plates. A PMMA cylinder was glued to the top side of the PMMA plate to serve as the bulk solution compartment.

With this apparatus, the local current density at various locations in the crevice can be measured by installing a number of microelectrodes on the working electrode surface.

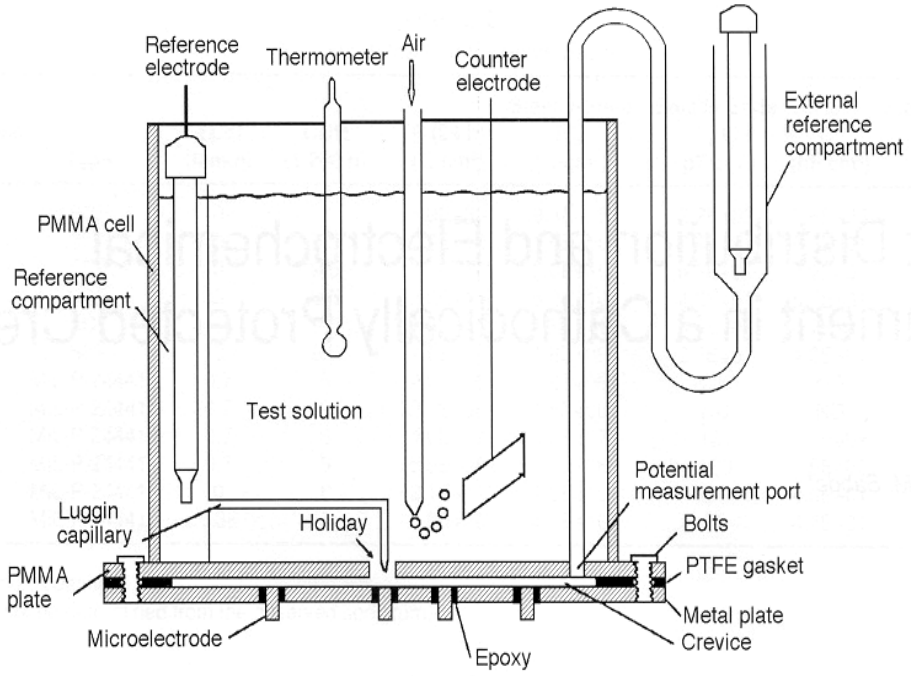

Figure 2 - 14: Schematic of a crevice cell made by Chin and Sabde (1999).

2.7 Electrochemical Measurement of Corrosion Rate

Thermodynamics predicts whether it is possible for corrosion of an alloy or metal to occur. However, it does not determine the rate of corrosion. If the corrosion rate is very small, then the damage caused is of little practical importance.

The corrosive extent can be measured by many techniques, such as weight loss of material, depth of penetration, and number of pits per unit area. Although these methods are widely used by researchers, they provide time-average values

over a very long period. However, electrochemical techniques can be used to rapidly determine corrosion rates.

2.7.1 Faraday's law

When faraday's 1st and 2nd laws apply to corrosion field, the law can be expressed as the quantity of material (W) converted during electrode reactions that is proportional to the amount of current ($I \times t$) which passes through the electrode surface. In other words, when 96,487 coulombs of electrical charge is placed through an electrolytic solution, one equivalent of substance is plated out onto an electrode (Piron, 1991).

$$W = \frac{P_{eq} \times I \times t}{F} \tag{2.9}$$

$$P_{eq} = \frac{atomic\ weight}{n} \tag{2.10}$$

where I is the electrical current involved in electrochemical process; F is Faraday's constant; P_{eq} is the number of equivalent weights reacted per second and n is the number of electrons in the reaction.

The penetration rate, r, can be calculated from the weight loss of one year, W, by equation (2.9). Therefore, the penetration rate, r, can be calculated by equation 2.11.

$$r = \frac{W}{t \times A \times D} \tag{2.11a}$$

For penetration rate in micro-meter per year (μm/year), equation 2.11a can be simplified to

$$r = 3.27 \frac{P_{eq} \times I}{A \times D} \tag{2.12b}$$

where I is the current (μA), A is the surface area (cm^2), D is the material density (g/cm^3).

2.7.2 Linear polarization/polarization resistance

2.7.2.1 Polarization and overpotential

When a metal is exposed to an aqueous solution that contains the ions of that metal, oxidation of the metal and reduction of the metal ions will occur at the same time, as expressed by Equation 2.8. It has to be mentioned here that all potentials used in this section is half-cell potential.

Because the reactions take place in two directions, the rate of these two reactions can be given by the partial anodic current density, $\vec{i}$, and the partial cathodic current density, $\overleftarrow{i}$. Assuming there are no other electrode reactions occurring at the electrode surface, the two current densities will be equal and opposite at equilibrium, which is called exchange current density, i_0. The equilibrium potential E can be calculated according to the Nernst equation.

$$E = E^0 + \frac{RT}{nF}\ln(\frac{\gamma_{ox}}{\gamma_{red}}) \tag{2.12}$$

Here R is the gas constant; T is the temperature in K; n is the number of electron involved in the electrochemical reaction; γ_{ox}/γ_{red} is the activity of oxidized/reduced species (often approximated by using the concentration of the oxidized/reduced species); E^0 is the standard electrode potential.

After applying an external current density, i, to the electrode surface, $\vec{i}$ will not be equal to $\overleftarrow{i}$ in quantity, which also causes the change of electrode potential. The electrode is said to be polarized. The change of electrode potential is referred to as polarization and the deviation from the reversible electrode potential is called the overpotential, η.

$$\eta = E_i - E \tag{2.13}$$

Generally, polarization can be categorized as activation polarization, concentration polarization and may also arise from IR effect. Activation polarization is also called as charge transfer polarization, which is caused by the resistance generated when electrical charges transfer through double layer. Concentration polarization results from the concentration gradient produced between the interface of the electrode and the bulk solution. That is, the rate of electrochemical reaction is much faster than the diffusion of reactants from the bulk solution to the electrode interface, which makes the concentration of reactant at electrode interface less than

that in the bulk solution. The IR drop is caused by the resistance of the electrolyte. Most potentiostats have the function to compensate IR drop.

If only activation and concentration polarization are considered in an electrochemical system, the activation polarization is predominant within small polarization current/potential range. In comparison, concentration polarization is the dominant mechanism when the electrochemical system is polarized far from equilibrium. The relation between these two types of polarization can be illustrated by the polarization curve presented in Figure 2-15. When the polarization current/potential is in the range of activation polarization, two areas, the linear polarization area and the tafel area, are interesting for most researchers. The first one is located approximately ±10 mV from the equilibrium potential and the second one is around ±50 mV. The details about these two areas will be introduced in the following sections.

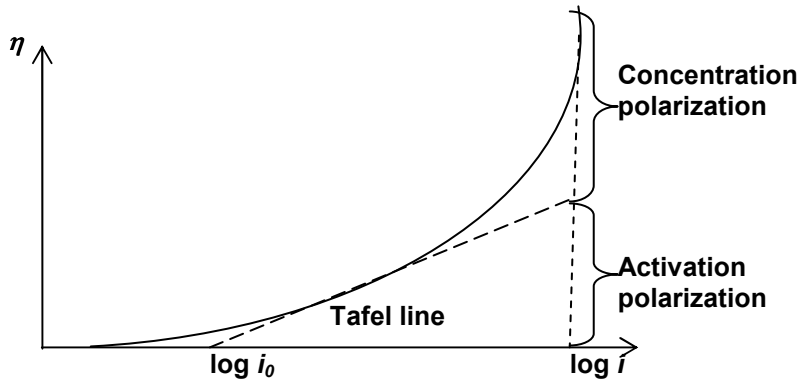

Figure 2 - 15: Polarization (η) as a function of log i (the continuous line indicates the total polarization, i_0 = the exchange current density).

2.7.2.2 Tafel slope

At polarization values approximately larger than 50 mV, there is a linear relationship between the overpotential and the logarithm of the current density as presented by Tafel line in Figure 2-15. This relationship can be represented by the Tafel equation (2.14) (Piron, 1991).

$$\eta = a + b\log i \tag{2.14}$$

where η is the overpotential, and a and b are constants, which can be predicted theoretically for many reaction mechanisms. Experimentally, the Tafel slope, b, can be obtained by measuring the slope of (*dE/dlog i)* plot. Specifically, for cathodic polarization, the Tafel slope is denoted as b_c; for anodic polarization, the slope is designated as b_a.

2.7.2.3 Linear polarization

The linear polarization technique has been discussed thoroughly by many researchers. For example, Barnartt (1986) discussed how the principle of linear polarization was developed. Some researchers (Leroy, 1973; Makrides, 1973; Mansfeld, 1973, 1976a, 1976b, 1986; Nisancioglu, 1986) discussed the problems associated with its applications and made some efforts to improve it. Errors in the technique have been documented thoroughly by Leroy (1973), Makrides (1973) and Mansfeld (1973). Since the technique is well known, the principle is only briefly introduced here.

When a metal is polarized with a low current in an electrolyte (i.e., for potentials that is about ±10 mV from the corrosion potential), a linear relation between the potential and the current applied to the electrode can be expressed as shown in equation 2.15 (Barnartt, 1986).

$$I_{corr} = \frac{b_a b_c}{2.3(b_a + b_c)} \left(\frac{dI}{d\Phi}\right)_{\Phi_{corr}} \tag{2.15}$$

which is valid when the relation between current (I) and potential (Φ) follows the equation:

$$I = I_{corr}\{\exp\frac{2.3(\Phi - \Phi_{corr})}{b_a} - \exp\frac{-2.3((\Phi - \Phi_{corr})}{b_c}\} \tag{2.16}$$

In equation (2.15), $(d\Phi / dI)_{\Phi_{corr}}$ is the slope of the potential-current plot at the corrosion potential and it is called the polarization resistance, R_p; b_a, b_c are the Tafel slopes of the anodic and cathodic polarization curves respectively; I_{corr} is the corrosion current. Using K to substitute for $b_a \cdot b_c /(2.3(b_a + b_c))$, the equation can be rewritten as:

$$R_p = \frac{K}{I_{corr}} \tag{2-17}$$

If the value of K is known and R_p is measured from experiment, the corrosion current can be calculated from this equation. The values of b_a, b_c are different for different materials, and some approximated values are usually used in the calculation. Besides, the slope of potential-current curve is often obtained when Φ is not close to Φ_{corr}. The inaccuracy of Tafel slope value limits the application of polarization resistance technique. Mansfeld (1973) solved this problem by graphical analysis of polarization curves in the range of linear polarization. Furthermore, he developed a method to obtain accurate Tafel slopes and polarization resistance simultaneously from polarization curves in the vicinity of corrosion potential (linear polarization region) and the result was in agreement with the data obtained by computer simulations.

2.7.3 Theory of electrochemical impedance spectroscopy measurement

2.7.3.1 Types of EIS measurement

Electrochemical impedance spectroscopy is one of the electrochemical transient techniques used in corrosion studies. In a general sense, a sinusoidal potential is applied on the measurement system with small amplitude and responded by the sinusoidal current changes with time. This response usually can be obtained by the direct measurement of AC impedance Z. Three methods are generally used to measure AC impedance: the AC bridge technique, a frequency response analyzer (FRA) technique and a Lissajous-figure approach.

1. Alternating Current Bridge

The AC bridge method is based on the balance between the electrochemical cell and the equivalent impedance consisting of a variable resistor and a capacitor. Figure 2-16 shows the structure of this measurement system.

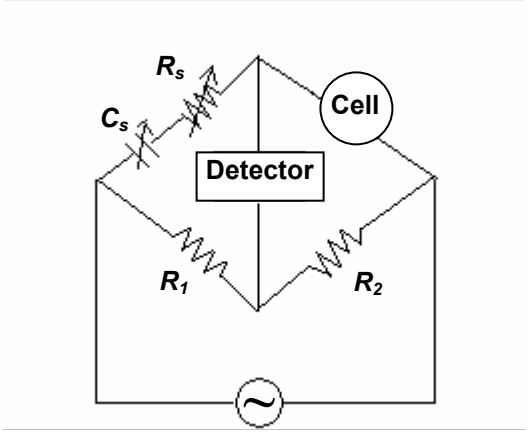

Figure 2 - 16: Sketch of AC bridge for EIS measurement (Brett and Brett, 1993)

When the bridge is balanced, Z_s/R_1 is equal to Z_{cell}/R_2, in which $Z_s = R_s - i/C_s\omega$. Thus equation (2.18) holds true, in which Z_{cell} is the impedance of electrochemical cell under study, R_s is the variable resistance, C_s is the variable capacitance, and R_1 and R_2 are resistances with known values (Brett and Brett, 1993).

$$Z_{cell} = \frac{R_2}{R_1}(R_s - i\frac{1}{\omega C_s}) \tag{2.18}$$

Generally, the impedance of an electrochemical cell can be easily expressed in a complex plot as the one shown in Figure 2-17. The real part refers to the resistance in the electrochemical cell and the imaginary part stands for the capacitance of the cell. Equation (2.19) and (2.20) express these two parts.

$$R_{cell} = \frac{R_2}{R_1}R_s \tag{2.19}$$

$$C_{cell} = \frac{R_2}{R_1}\frac{1}{\omega C_s} \tag{2.20}$$

2. Frequency Response Analyzer (FRA)

The combination of a phase-sensitive detector and a frequency response analyzer is the method usually used in EIS measurements today. The principle of this technique is illustrated in Figure 2-18. In this figure, the electrode system includes a potentiostat and a three-electrode system.

In this system, a sinusoidal potential, mixed with a DC potential in the potentiostat, is applied to the three-electrode system. Then the responding current is

compared with original input signals in the analyzer. Through the response analyzer, the real and imaginary parts of the electrochemical system impedance under study are obtained. This method is appropriate for a frequency range of 10^{-4} to 10^{6} Hz.

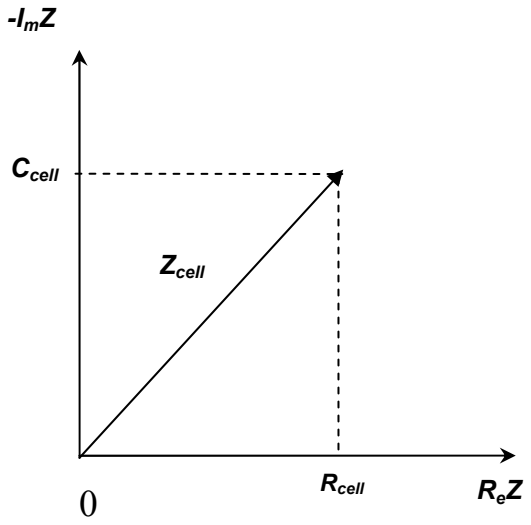

Figure 2 - 17: Complex expression of electrochemical impedance

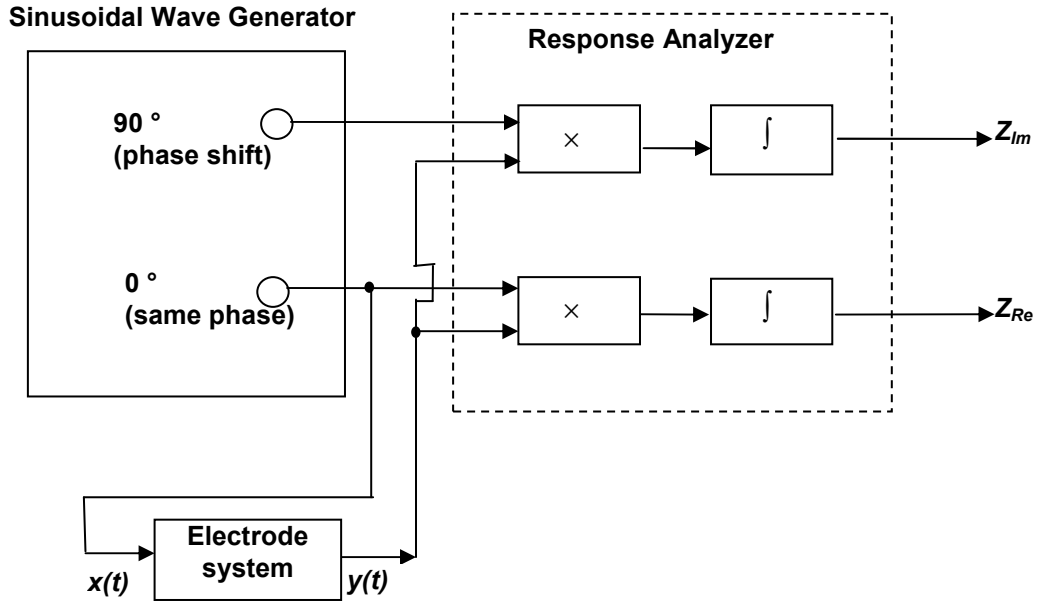

Figure 2 - 18: Scheme of phase-sensitive detectors and frequency response analyzer ×: multiply processor; ∫: integral processor; *x(t)*: sinusoidal perturbation; *y(t)*: response from the electrode system (Bard and Faulkner, 2000).

3. Lissajous-Figure Approach

This method is a direct approach of determining the important variables from a Lissajous figure. This figure can be generated by inputting a perturbation to the system and recording the response as shown in Figure 2-4 (Brett and Brett, 1993).

In this method, the perturbation takes the form of

$$E(t) = \Delta E \sin \omega t \tag{2.21}$$

and the responding current is in terms of

$$I(t) = \frac{\Delta E}{|Z|} \sin(\omega t + \theta) \tag{2.22}$$

where ω is the applied frequency for AC potential and θ is the phase shift between the resulting current and the imposed potential.

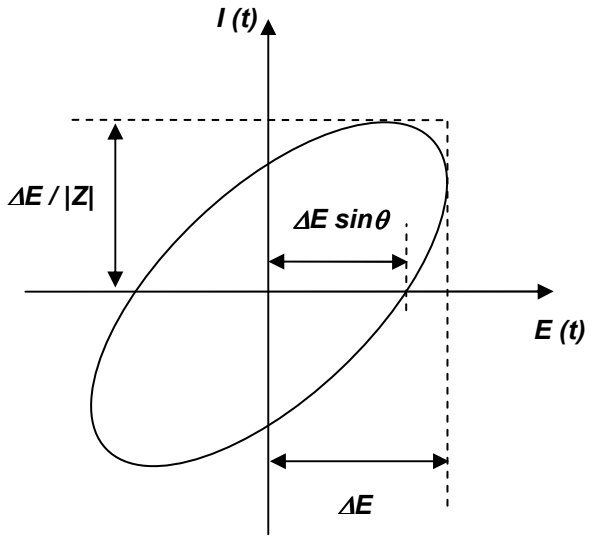

Figure 2 - 19: Lissajous figure for impedance measurement (Brett and Brett, 1993)

2.7.3.2 Analysis of EIS measurement results

After the EIS measurement, it is necessary to analyze the spectrum, obtain the equivalent circuit of the system under study, and calculate the parameters related to the electrochemical kinetic processes.

1. Equivalent Circuit of EIS in Simple Electrochemical Systems

The equivalent circuit in a simple electrochemical system commonly consists of three parts: a resistor representing solution resistance, R_Ω, a capacitor

representing the double layer capacitance, C_d, and a Faradic impedance, Z_F, to describe the electrode reaction processes. The Faradic impedance, Z_F, is often expressed by a series combination of resistance and capacitance, such as a charge transfer resistance, R_{CT}, in series with a Warburg impedance, Z_W. The equivalent circuit is validated by following a rule that the least number of components should have to be used to represent the system. The general form of the equivalent circuit is shown in Figure 2-20.

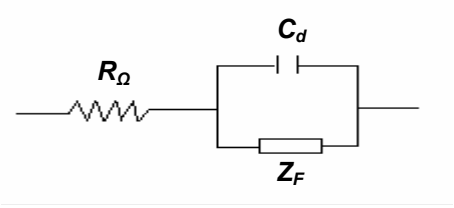

Figure 2 - 20: the equivalent circuit of a simple electrochemical system

2. Plot Patterns of EIS

There are three ways to plot the electrochemical impedance spectrum. The more frequently used plots are the Nyquist and Bode plots. The other plot, the Randles plot, is limited to analyzing in-phase components such as resistors. Only Nyquist plot will be discussed here. More information of other two plot patterns can be found in any EIS reference books (Brett and Brett, 1993).

The Nyquist plot represents both in-phase (resistors) and out-of-phase components (capacitors) in a complex plane, in which the x-axis is the real part, Z', of the impedance and y-axis is the imaginary part, Z'', of the impedance. The following Figure 2-21 is an example of Nyquist plot for a simple electrochemical system.

In this figure, R_Ω and R_{CT} represent the solution resistance and the resistance of charge transfer process respectively. C_d is the double layer capacitance and σ is the diffusion impedance. Figure 2-21 can be explained from two sides. At high frequency (approximately infinity), the kinetics is the controlling step, which means the Warburg impedance is negligible. Therefore, the equivalent circuit is the parallel combination of R_{CT} and C_d in series with R_Ω. Based on the knowledge of electrical circuit, the corresponding impedance of the system can be expressed as

$$\overline{Z} = Z' + jZ'' = R_{\Omega} + \frac{R_{CT}}{1 + j\omega R_{CT} C} = R_{\Omega} + \frac{R_{CT}}{1 + \omega^2 C^2 R_{CT}^{\ 2}} - \frac{j\omega C R_{CT}^{\ 2}}{1 + \omega^2 C^2 R_{CT}^{\ 2}} \qquad (2\text{-}23)$$

which is simplified to be

$$[Z' - (R_{\Omega} + \frac{1}{2} R_{CT})]^2 + (Z'')^2 = (\frac{R_{CT}}{2})^2 \qquad (2\text{-}24)$$

Equation (2.24) is the equation of a circle with a radius of $R_{CT}/2$ and the intercepts of this equation on the x-axis are at (R_{Ω}, 0) and ($R_{\Omega} + R_{CT}$, 0), as shown in Figure 2-21.

At low frequency, the system is controlled by diffusion processes, which means the Warburg impedance is predominant. The corresponding expressions of impedance are shown in equations (2.25) and (2.26).

$$Z' = R_{\Omega} + R_{CT} + \sigma\omega^{-\frac{1}{2}} \qquad (2\text{-}25)$$

$$Z'' = -\sigma\omega^{-\frac{1}{2}} - 2\sigma^2 C_d \qquad (2\text{-}26)$$

It is clear that a plot of Z' vs. Z'' should be a straight line with a unit slope, the intercept of which is ($R_{\Omega} + R_{CT} - 2\sigma^2 C_d$).

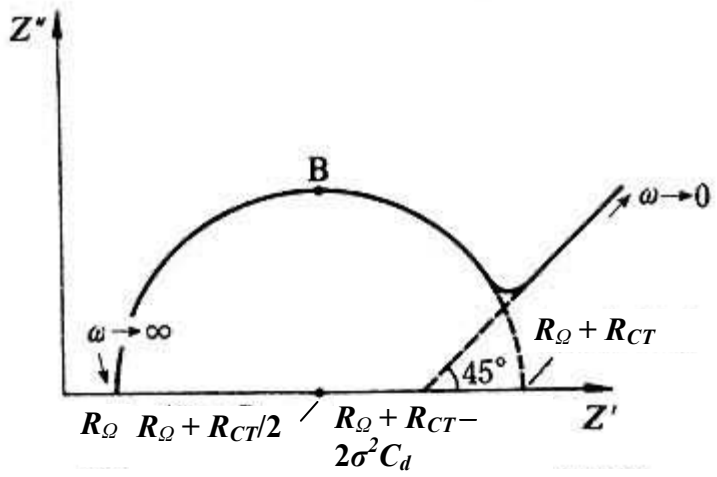

Figure 2 - 21: Nyquist plot of a simple electrochemical system: O + ne^- →R (Bard and Faulkner, 2000).

2.7.3.3 Work done by other researchers

EIS has been applied to corrosion studies for many years. There is a great deal of literature on this subject, but the number that focused on localized corrosion is very limited. This can be attributed to the dynamic nature of localized corrosion processes. The stability is one of the requirements to guarantee the validity of the impedance data. However, the stable condition is hard to achieve when localized corrosion is proceeding, which may interfere with the validity of the data. Mansfeld (1981) and Mansfeld et al. (1982, 1986, 1989), Keddam et al. (1983) and Oltra and Keddam (1988) have investigated localized corrosion processes with EIS and have been able to obtain reasonable data. For example, the large scatter in the EIS data and inductive behavior at the lowest frequencies were observed when Al/SiC metal matrix composites were exposed to 0.6 N NaCl by Trzaskoma et al. (1983). However, Mansfeld et al. (1989) did not observe the same behavior in later studies and attributed the original scatter and induction to experimental artifacts. In addition, Dawson and Ferreira (1986a, 1986b) have reported impedance data for pitting and crevice corrosion of for stainless steel type 316 in 3% NaCl solution. In their experiments, EIS data were found to fit to the model consisting of a Warburg impedance and a parallel combination of negative resistors and capacitors. For copper corrosion, EIS has been used to examine the properties of copper oxide film. Feng et al. (1997) studied the influence of pH, immersion time and rotation speed of the electrode on copper corrosion and film growth using EIS, in which the rate controlling steps were determined with the aid of an XPS. Palit and Pehkonen (2000) further conducted a study on the stability of artificial copper oxide film in various waters for distribution systems. A Cu (II)-inhibitor complex polymeric film was found on copper surface when Cicileo et al. (1999) investigated the effect of inhibitors on copper corrosion in natural aqueous NaCl solution. EIS data was fitted to a model and used to calculate the parameters describing the properties of the film structure.

2.8 Other Experimental Techniques for Crevice Corrosion Study

2.8.1 Electrochemical testing techniques for localized corrosion study

2.8.1.1 Optical interferometry

In recent years, a new instrument called the Optical Transducer was introduced by Habib (1990a, 1990b, 1990c, 1994, 1995, 1999 and 2002), Habib and Al-Mazeedi (2003), and Habib et al. (1993). The corresponding methodology is called optical interferometry. The instrument combined an electrometer and a 3D-interferometric microscope and was developed for testing different corrosion phenomena. It can be used to obtain electrochemical parameters such as cathodic and anodic current densities, and to examine the microstructure of corrosion products produced by stress corrosion cracking, corrosion fatigue, dissolution of anode or/and cathodic deposition. The instrument system structure is shown in Figure 2-22.

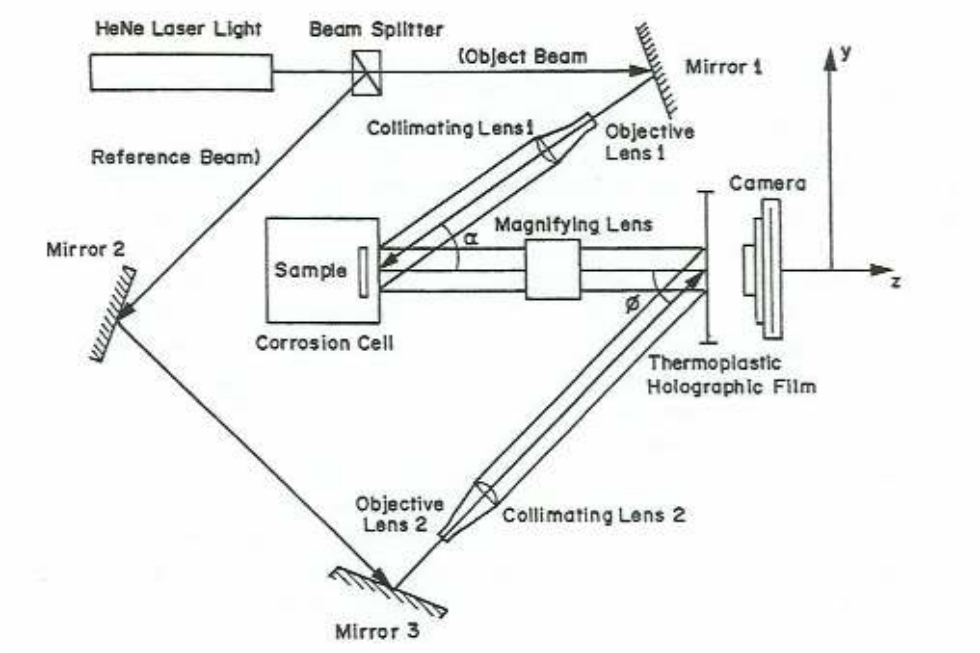

Figure 2 - 22: An off-axis holographic interferometry system for corrosion studies (Habib, 1999).

This instrument was used to monitor the initiation stage of localized corrosion for an aluminum brass and pure copper samples in situ. Interferometric perturbations were observed in the crevice, which were interpreted as the occurrence

of crevice corrosion or pitting corrosion within a depth between 0.3 μm to several micrometers (Habib, 1999). In addition, the Optical Interferometry used the number of fringe evolutions appearing in the samples to evaluate the rate change of anodic dissolution of copper alloys. This method was compared with electrochemical techniques such as EIS and a good agreement was achieved between their results (Habib and Al-Mazeedi, 2003).

2.8.1.2 Electrochemical noise analysis (ENA)

The operating principle of the electrochemical noise can be described as the response of potential difference and current to physical processes. These physical processes might involve: (i) the creation and removal of gas bubbles on a surface, (ii) the variation of the concentration of a solution nearby the surface of a metal, (iii) the turbulent flow of the solution, and (iv) fluctuations caused by producing corrosion products during localized corrosions (Dawson, 1996).

Hladky and Dawson (1981) showed that the noise signature of crevice corrosion has a unique character and can be obtained in seconds after the initiation of crevice corrosion starts. Schneider and Pohl (2002) also reaffirmed the viewpoint that ENA is a very useful technique for detection of the early stage of crevice corrosion processes.

2.8.1.3 Scanning chemical microscope

As one of the influencing factors on crevice corrosion, pH in the crevice is very important because it indicates the occurrence of some chemical/electrochemical process in the crevice. For example, pH of the solution inside the crevice decreases due to the hydrolysis of metallic ions. Recently, a new instrument was developed called a scanning chemical microscope (SCHEM), which can be used to measure pH. The advantage of SCHEM lies in the in situ inspection of pH and the measurement of the pH distribution in a crevice. Sagara et al. (2002) used the SCHEM to monitor the pH variation in austenitic stainless steel crevices. It was found that areas of low pH were the locations where the crevice corrosion occurred.

2.8.1.4 Electrochemical frequency modulation (EFM)

For most electrochemical methods used to determine corrosion rate, Tafel parameters are necessary for interpreting the experimental data. However, those parameters are not always reachable for some electrochemical measurement systems. The development of the EFM technique solves this problem. In this technique, two sine-wave potential perturbations with different frequency are mixed and applied to the system. Consequently, the resultant current response is made up of current components at multiple frequencies, including harmonics and intermodulation frequencies. With the aid of mathematical expansion, the current response can be interpreted in terms of corrosion rate. Moreover, the unique feature of this method, "causality factors", guarantees the validation of inherent data. Recently, EFM was successfully applied in acidic/neutral environment for mild steel with satisfactory results (Bosch et al., 2001).

2.8.2 Materials characterization techniques applied on copper

2.8.2.1 X-ray photoelectron spectroscopy

Metal oxide films are often analyzed by X-ray photoelectron spectroscopy (XPS). For example, the oxide films on Al and an Al-Sn alloy were analyzed by XPS after immersion in a 3.5 wt% aqueous sodium chloride solution (Venugopal et al., 1997). Copper corrosion in alkaline media has also been investigated by surface analysis techniques such as ion-scattering spectroscopy (ISS) and XPS. For example, the anodic films of copper formed in Na_2SO_4 solutions with a pH of 12 was studied by Kautek and Gordon (1990), by which the thickness and composition of the film was found. In Feng et al.'s work (1997), XPS was used to identify corrosion products of copper produced at different pH. Moreover, a protective monoclinic CuO layer was found to cover copper surface at pH of 12 and 13.

2.8.2.2 Ellipsometer

Ellipsometer is an advanced tool for measuring the refractive index and the thickness of semi-transparent thin films. The measurement range of ellipsometer is from 1 nm up to several microns. Based on the refractive index information, the composition of materials can be identified and the characterization of surfaces can

be achieved. Yamashita et al. (1980) used this technique to investigate the passivation behavior of copper electrodes in 0.5 M KOH and verified that the film was composed of two layers, Cu_2O and $Cu(OH)_2$. In the work of Ord et al. (1987), an ellipsometer was used to study the processes involved in the growth, conversion and removal of copper oxides in sodium carbonate solution at pH 12. It was found that ellipsometric study was not appropriate to detect the outer surface of the film because of the film's inhomogeneous structure.

2.8.2.3 Scanning electron microscopy (SEM)

High resolution images of the morphology of a specimen and precise composition analysis are two main functions of the SEM, which makes it one of the most useful techniques in materials research. These two functions are realized by a scanning electron probe and a moving sensor/receiver for secondary x-rays respectively. In addition, SEM can be applied to both metals and non-metals. For non-metal materials, they have to be plated with a layer of silver so that they can get a good conduction for SEM operation.

In the work of Badawy and AI-Kharafi (1999), , a passive Cu (I) film was observed on the alloy surface in aqueous solutions by X-ray photoelectron spectroscopy (XPS) and electron scanning microscopy (SEM). Furthermore, it was found that the stability of the passive film depended on the solution pH and the alloy chemistry.

Feng et al. (1997) conducted a similar research to study the corrosion behavior of copper in aqueous solutions of different pH values. The morphologies of the copper surface formed in solutions of different pH after 24 hours immersion results are shown in Figure 2-23. The corrosion product is a Cu_2O film, but the exact structure in each photograph looks different. The compactness of the film increases with the increasing pH, which indicates that the protection of the film is improved. For pH = 3, there are only few crystals observed, while the crystals almost cover the entire surface at pH of 5 and 7.6. For pH = 10, the surface is very smooth and the passive. In Figure 2-23 (f), a CuO film is observed and the monoclinic crystals with pores cover the whole surface at pH = 13. The film provides protection similar to those at pH of 5 and 7.6

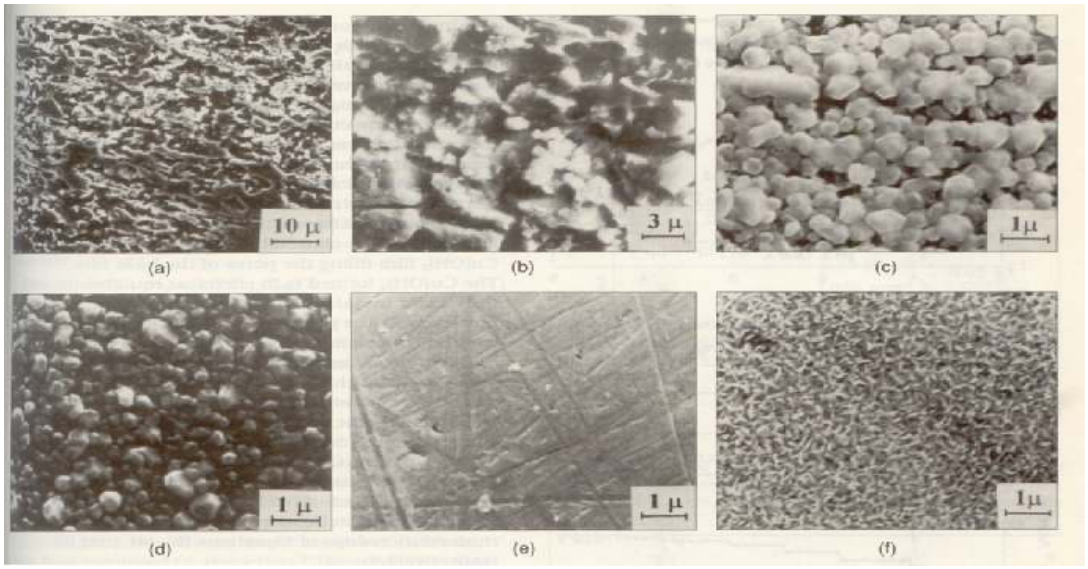

Figure 2 - 23: SEM micrographs for copper surfaces formed in solutions of various pH after 24h of immersion at 30 ºC. (a) and (b) pH 3; (c) pH 5; (d) pH 7.6; (e) pH 10; and (f) pH 13 (Feng et al., 1997).

2.8.2.4 In situ Raman spectroscopy

Raman spectroscopy is often used in analyzing the composition of surface species. In most cases, the anodic film formation on metals and alloys in corrosive environments is studied by electrochemical techniques. But the composition of corrosion products usually can not be determined. In situ spectroscopic studies of the film formation process provide a good supplement to electrochemical studies. It can identify surface species and related species to specific electrode reactions. Therefore Raman spectroscopy has been widely used for corrosion studies. Hamilton et al. (1986) used in situ Raman spectroscopy and cyclic voltammetry simultaneously to study anodic film growth and dissolution on Cu and Ag in strongly alkaline solutions. In this work, Cu_2O and some hydroxides were observed on the metal surface during the formation of anodic film. This was the first time that the Raman spectra of copper hydroxides formed by electrochemical reactions were reported.

2.8.2.5 Atomic force microscopy (AFM)

Atomic Force Microscopy (AFM) was developed in mid-1980s as a daughter technique to scanning tunneling microscopy (STM) in the family of scanning probe

microscopy (SPM). Different from STM's metal probe, the AFM probe is made from amorphous Si_3N_4 or crystalline Si. The surface-probe interactions result from intermolecular van der Waals forces. Similar to SEM, AFM provides a high resolution surface morphology, but it has an advantage over SEM that it can monitor surface reactions in situ.

In recent years, AFM has been more and more applied to in situ electrochemical studies, especially for film analysis. For example, Gong et al. (1995) used AFM to investigate the processes involved in the oxidation of a thin copper film. In this work, the nucleation, aggregation and growth of Cu_2O grains were observed as temperature increased. AFM was also used to observe pit growth in the pitting corrosion of a thin copper film (Li and Lampner, 1999). Besides detecting solid corrosion products, AFM is used to examine liquids like sulfuric acid. Wang (2004) used AFM in the ac non-contact mode to observe micro-liquid of dilute sulfuric acid when it was deposited on SUS304 steel surface. In addition, Skolnik et al. (2000) discussed several methods to analyze results from the AFM in order to quantify surface characteristics such as roughness.

2.9 Summary

In this chapter, the corrosion behavior of copper and its alloys is introduced. In addition, crevice corrosion is explained from the mechanistic and the influencing factors perspectives. Some basic electrochemical knowledge and the methods for measuring corrosion rate are discussed including weight loss, polarization resistance and AC impedance. The literature for designing and fabricating a single crevice assembly are also reviewed based on recent publication on it. Then some advanced techniques and their applications to corrosion studies are presented, including scanning electron microscopy (SEM), atomic force microscopy (AFM), in situ Raman spectroscopy, electrochemical noise analysis (ENA) etc..

CHAPTER 3

EXPERIMENTAL TECHNIQUES

There are several possible approaches to studying crevice corrosion of copper. A multiple-crevice assembly that has previously been used to study crevice corrosion of stainless steels and nickel alloys was used to study copper in this work. Four kinds of electrochemical measurements were conducted: corrosion potential measurement; potentiodynamic measurement; potentiostatic measurement; and electrochemical impedance spectroscopy (EIS). The corrosion potential was monitored by measuring the open circuit potential to see if it changed during the initiation period. Potentiodynamic and potentiostatic measurements were used to monitor film formation behavior. EIS was used to obtain detailed information on film growth and to examine the rate determining steps in the RCC of copper. For surface analysis, atomic force microscopy (AFM) with one nanometer resolution was used to obtain images of the surface and provide a physical picture of the morphology of the corroded surface. The Raman spectroscopy was used to determine the composition of the corrosion products.

3.1 Experimental Apparatus

3.1.1 Specimen preparation

In a previous study of RCC, alloy 400 (70Ni-30Cu) showed crevice-related corrosion after exposure to room-temperature seawater for 45 days (ASM International, 2001). The corrosion extended from the crevice to the bold surface and a mixture of crevice corrosion and RCC was observed. Corrosion was found to occur just outside the crevice mouth and the corrosion was quite shallow even after immersion in seawater for 2 months (ASM International, 2001). In another

investigation, Klein et al. (1991) examined RCC of a 90Cu-10Ni alloy and found that corrosion was severe on the outside surface. Based on these data, it could be concluded that the higher the percentage of copper in the alloy, the greater is the propensity for RCC.

In light of this, annealed copper with 99.9% purity (ASTM-F-68-93) was chosen for the experiments in this study (supplier: Copper and Brass Sales Inc., Canada) and its chemical composition is listed in Table 3-1. A reference metal which undergoes normal crevice corrosion was also studied to compare the differences between these two types of crevice corrosion. Type 304L stainless steel was chosen since it has poor corrosion resistance in seawater and classic crevice corrosion was likely to occur.

Table 3 - 1: Chemical composition of copper (ASTM-F-68-93).

Element	Cu	Pb	Zn	Bi	Cd	O	P	S	Se	Te	Sb	As	Fe	Mn	Ni	Ag	Sn
Unit	%	ppm	ppm	ppm	ppm	ppm	ppm	ppm	ppm	ppm	ppm	ppm	ppm	ppm	ppm	ppm	ppm
Specified value	Min. 99.99	Max. 5	Max. 1	Max. 1	Max. 1	Max. 5	Max. 3	Max. 15	Max. 3	Max. 2	Max. 4	Max. 5	Max. 10	Max. 0.5	Max. 10	Max. 25	Max. 2
Measured value	99.99	1	0.3	0.2	0.2	2	2	8	2	0.5	1	1	4	0.3	t	8	1

The geometry of the sample is an important factor that affects the accuracy of crevice corrosion experiments. In this study, two different types of copper specimens were used for exposure tests and electrochemical measurements.

One type of specimen was a copper coupon made from a copper rod machined to an outer diameter of 20 mm and an inner diameter of 8 mm as shown in Figure 3-1. The used copper coupons were refinished to get rid of any corrosion product after each experiment. These coupons were used in the electrochemical tests.

The other type of coupon was a square copper sheet with a central hole. The length of the square was 20 mm and the diameter of the center hole was 8 mm (Figure 3-2). The copper sheet was quite thin (thickness = 1 mm), which allowed many coupons to be mounted onto an insulated stainless steel bolt, separated by

Teflon washers, for long term exposure tests at elevated temperature, as shown in Figure 3-3.

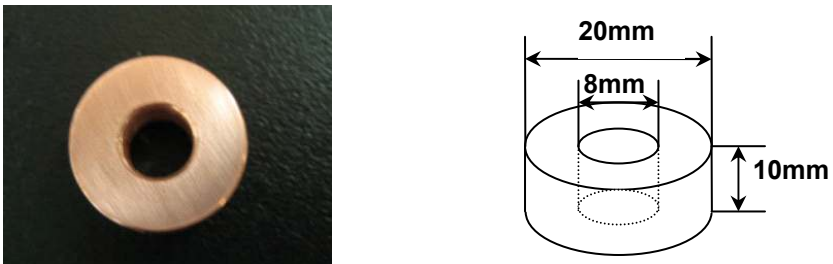

(a) (b)

Figure 3 - 1: (a) Photograph of a copper coupon; (b) Sketch of a copper coupon.

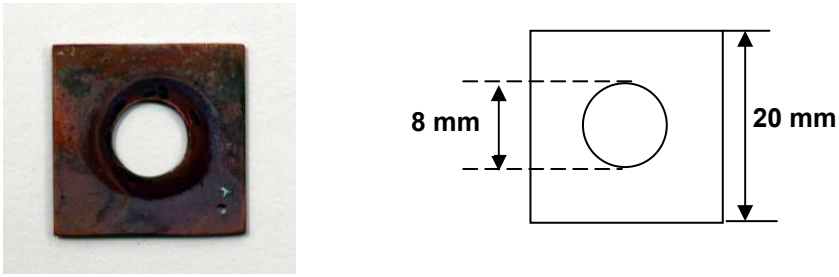

(a) (b)

Figure 3 - 2: (a) Photograph of a square copper coupon; (b) Sketch of square copper coupon.

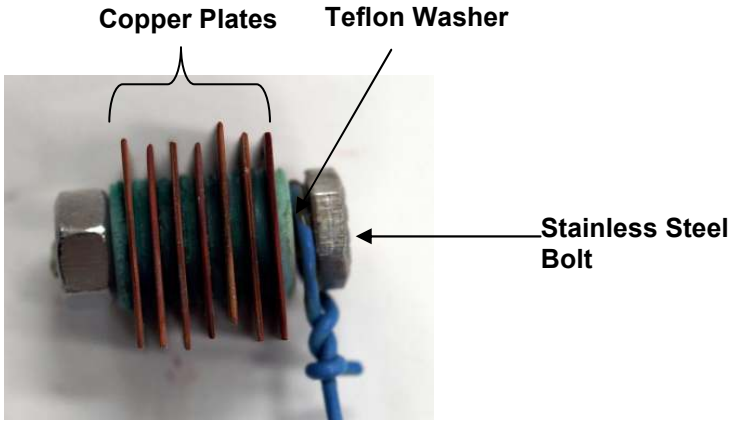

Figure 3 - 3: Photograph of square coupons used in the elevated temperature exposure test.

The stainless steel sample used to perform the comparison experiment was a rectangular piece (L: 50 mm × W: 19 mm × H: 2 mm) with a 10 mm-diameter central hole.

After each specimen was mechanically formed by cutting and milling, it was wet ground on 600 grit silicon carbide paper, rinsed in distilled water and cleaned in ethanol.

A 0.5 M aqueous sodium chloride solution was chosen as the electrolyte because it is close to the concentration of NaCl in sea water. AnalaR® Sodium Chloride (EMD^{TM}, USA) was used to prepare the solution with a purity of 99.5 wt%.

3.1.2 Electrochemical system

3.1.2.1 Electrodes

An electrochemical experimental system is composed of electrodes and electrochemical instruments. Electrodes are classified into three types by their functions: working electrode; reference electrode; and auxiliary or counter electrode. The working electrode is the sample being studied. The reference electrode provides a relatively fixed potential as a reference to measure the potential of the working electrode. Finally, the auxiliary or counter electrode completes the electrochemical circuit. In this study, the working electrode assembly consisted of three parts: the electrode holder, sample, and crevice assembly, as shown in Figure 3-4. A multiple crevice assembly was chosen because it is relatively easy to build up and has some reference standard to follow up. In comparison, an artificial single crevice is very hard to manufacture, which will be detailed in recommendation section of this thesis.

The crevice assembly was fitted with two grooved washers and the copper coupon was placed in between them. The washers were made of PTFE with a radial groove and a diameter of 16mm, which is referenced by ASM standard (G48-03). A plastic keeper nut was used to hold the crevice assembly together. All others parts were made of stainless steel. It should be noted that all stainless steel parts in the solution was covered by Teflon sleeve to avoid contacting the medium. Teflon^{TM} was chosen in many places of working electrode since it provides a very good

corrosion resistance and thermal resistance, which can be used during a large temperature range (T_g: -97 °C – T_m: 327 °C).

When assembling the crevice parts, it was necessary to avoid a situation where galvanic corrosion could occur. Teflon™ tape was wrapped around the cylinder tip to insulate the copper from stainless steel. A copper wire, with a diameter of 1 mm, went through the groove on the washer and attached to the coupon in order to connect it to the electrochemical measurement system. In order to leave enough space for the electrode holder and copper wire, the size of the hole in the copper coupon was slightly larger (D = 8 mm) than the cylinder tip to provide space for the Teflon™ tape as well as to ensure tight contact between the wire and the coupon.

The reference electrode used in this study was a saturated calomel electrode (SCE) with 4 M KCl/AgCl solution and with a potential of 0.242 V v/s SHE (standard hydrogen electrode) at 25 °C. A carbon rod was chosen as the auxiliary electrode. Figure 3-5 shows the photograph of the three-electrode system used in this study.

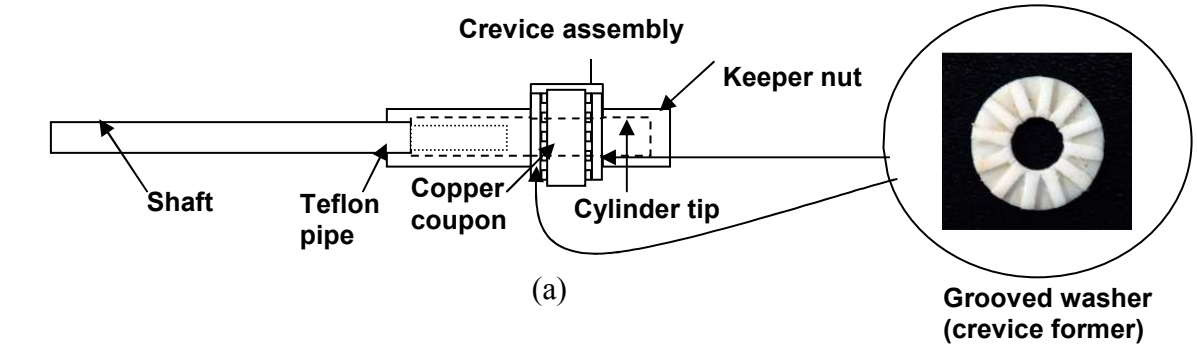

(a)

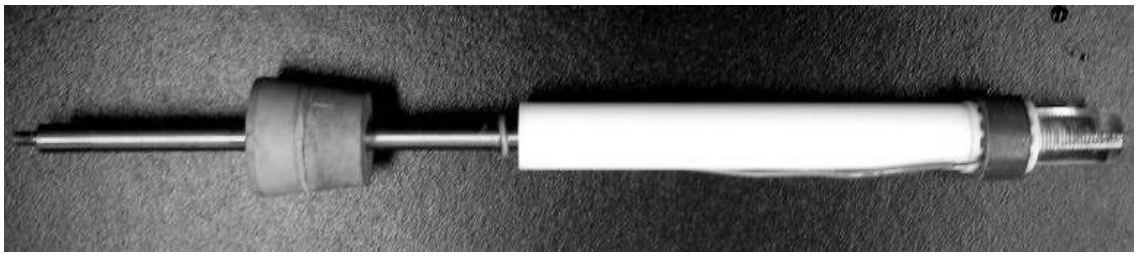

(b)

Figure 3 - 4: (a) Sketch of the working electrode; (b) photograph of working electrode.

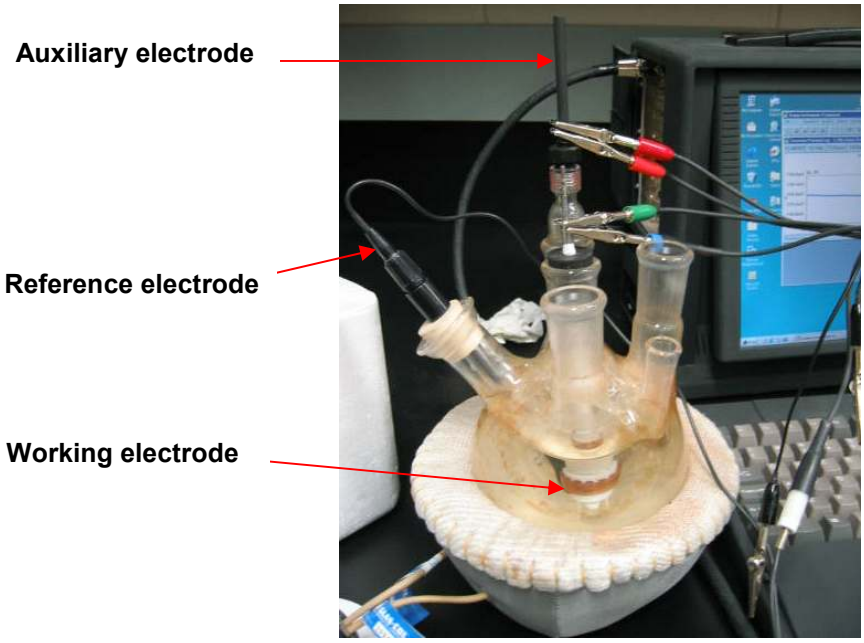

Figure 3 - 5: Photograph of the three-electrode system.

3.1.3.2 Electrochemical instrument

The electrochemical instrument employed in this study was a Gamry PC4™ instrument. It is equipped to accomplish the work of potentiostat, galvanostat, zero resistance ammeter, and an electrochemical noise apparatus. A sinusoid generator that allows AC impedance measurement to be conducted up to a frequency of 100 kHz is also included. An ECM8™ Electrochemical Multiplexer was also used in this study, which connects up to 8 electrochemical cells to one potentiostat. These two instruments are shown in Figure 3-6.

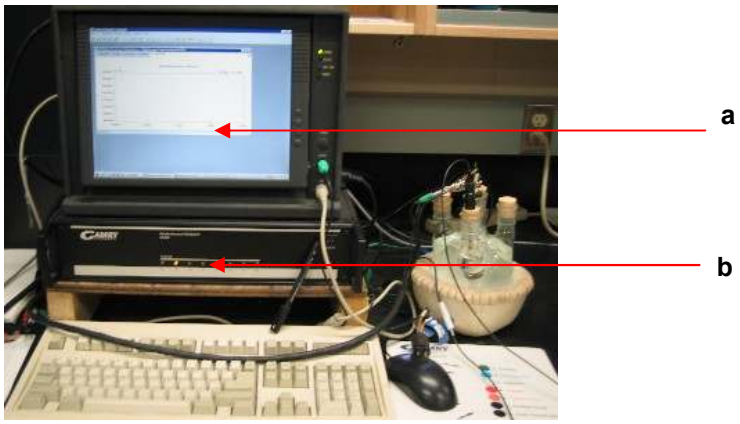

Figure 3 - 6: Photograph of the electrochemical measurement system: (a) Gamry PC4^{TM} instrument; (b) ECM8^{TM} Electrochemical Multiplexer.

3.1.3.3 Glassware

A standard six-necked electrochemical flask, a schematic of which is shown in Figure 3-7, was used in the electrochemical experiments. For short term exposure tests, covered standard laboratory beakers were used.

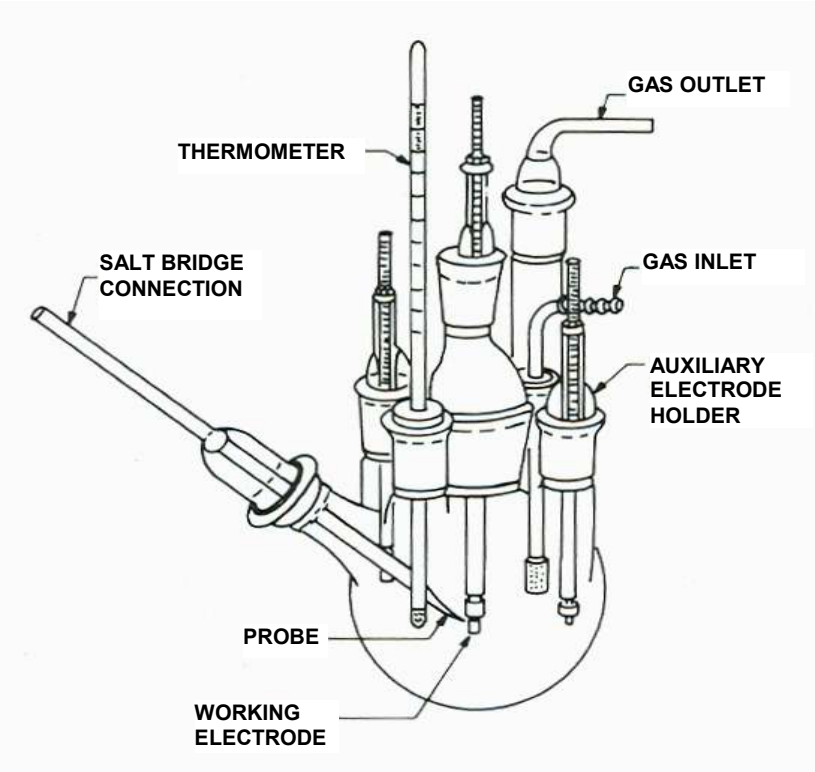

Figure 3 - 7: Schematic of a standard polarization test cell (Dean, 1976).

3.2 Electrochemical Measurements

3.2.1 Corrosion potential measurement

Corrosion potential measurements were conducted at room temperature. The washer-like copper coupon assembly was immersed in 0.5 M NaCl solution for 40 days at 298 K. Corrosion potential was measured once a day. Two replication measurements were performed.

To ensure that the crevices were completely wetted, the working electrode was assembled with the lock nut in a loose position and placed into the aqueous solution for 30 minutes before tightening the lock nut. Corrosion potential was obtained by the open-circuit measurement using the potentiostat.

For the elevated temperature experiments, a water bath was used to maintain constant temperature of solution. The water bath system consisted of a recirculating heater; a plexiglas cover used to reduce the evaporation of the water; and an insulated container. A schematic of the apparatus is shown in Figure 3-8.

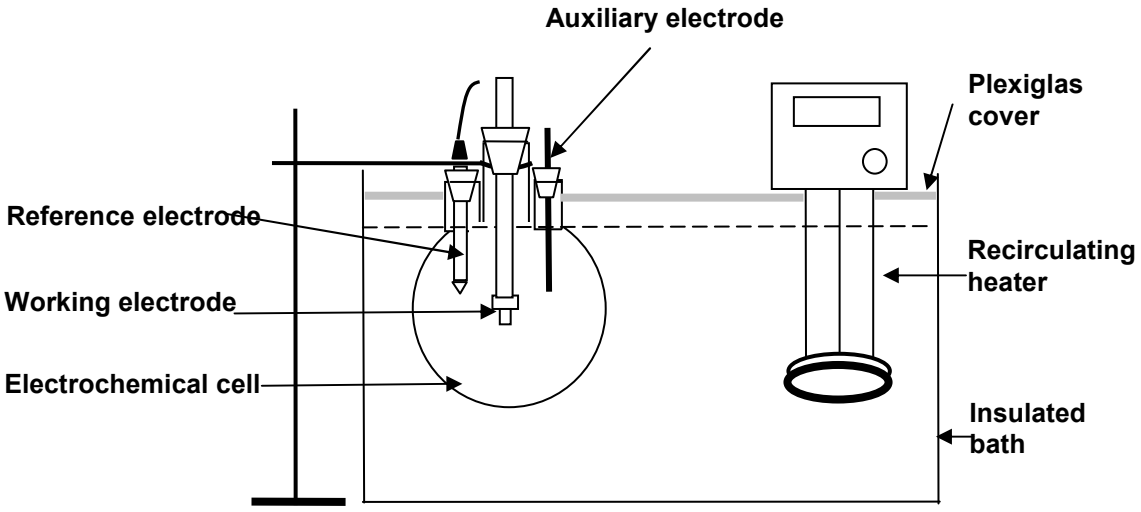

Figure 3 - 8: Schematic of the apparatus used to conduct the elevated temperature measurement.

The washer-like copper coupons were used in corrosion potential measurements and two replication measurements were performed at 50 ºC. The same technique used to measure E_{corr} in the room temperature experiments was used for the elevated temperature. The square copper samples were also used for a 30-day exposure test but no electrochemical measurements were conducted, as this test was only observational.

In order to observe the influence of oxygen on the RCC process, a deoxygenated apparatus was designed and built. The apparatus consisted of a nitrogen cylinder and a PVC glass tube for conveying nitrogen to the electrochemical cell as shown in Figure 3-9.

In this study, nitrogen (99.998 vol% purity) was bubbled into the solution for 4 hours to reduce the partial pressure of oxygen to a very low value. In order to control the flow rate of nitrogen, a regulator was used and the pressure was kept at 50 psi. The electrochemical cell was then sealed with a rubber stopper. A corrosion

potential measurement was performed in the deoxygenated cell every day for 31 days at the room temperature. The same measurement technique was used to detect corrosion potential as was used in the solution open to air at room/elevated temperature.

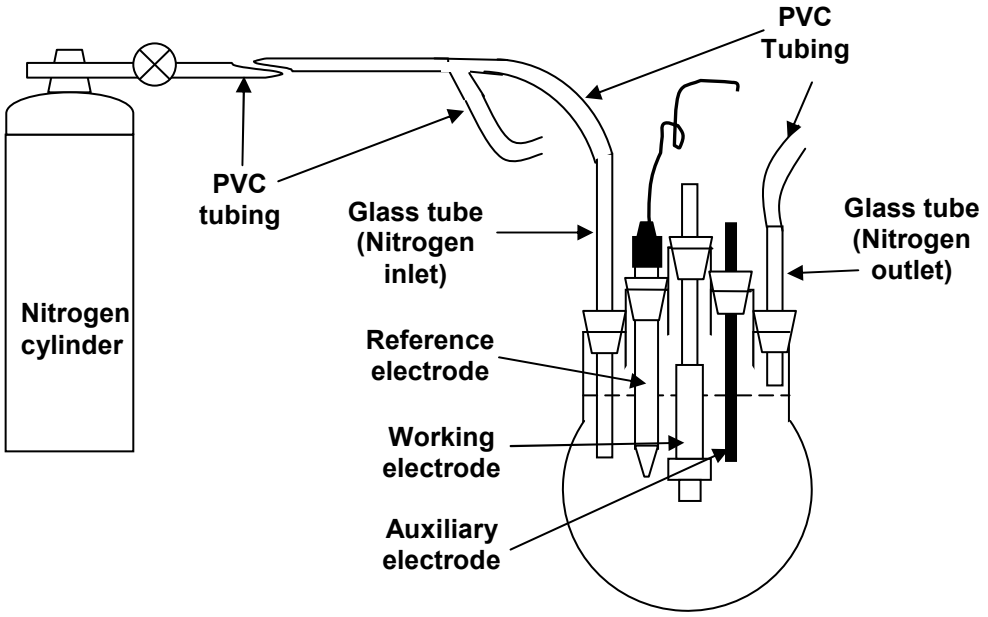

Figure 3 - 9: Sketch of electrochemical apparatus showing the deoxygenating system.

3.2.2 Potentiodynamic measurement

A Potentiodynamic scan is a transient electrochemical method and the scan rate is a key in performing this techniques. If the scan rate is too high, important kinetic data may not be captured, but if the scan rate is too low, the experiment can become very lengthy. A scan rate was chosen such that a small change in scan rate did not significantly affect the shape of the scan for subsequent scans. A scan rate of 2 mV/s was initially tested (this is a value typically used for measurements on stainless steels) and slower rates (1 mV/s, 0.5 mV/s, 0.3 mV/s, 0.1 mV/s) were also tried. The best rate was found out to be 0.3 mV/s. Scans performed at slower rates did not show significant changes in their characteristics. Thus all scans were performed at this rate at room temperature. Furthermore, since the reactions at higher temperature would spend less time than at room temperature, 0.3 mV/s is slow enough for the high-temperature scans. Therefore, it was applied to elevated

temperature scans too. The electrochemical settings for the potentiodynamic measurements are summarized in Table 3-2.

Table 3 - 2: Electrochemical settings of the potentiodynamic scan at room temperature.

Parameters	Initial E (V vs. E_{oc})	Final E (V vs. E_{oc})	Scan rate (mV/s)	Sampling period (s)
Value	-0.1	1.0	0.3 mV/s	5

Copper crevice assemblies were immersed in a 0.5 M NaCl solution and exposed to the atmosphere at room temperature. Potentiodynamic scans were performed after 5, 8, 11, 14, 17 and 21 days. A second set of tests were performed at 50 ºC and the potentiodynamic scans were conducted after 7, 14, 21 and 40 days.

In addition, cyclic potentiodynamic polaraization (CPP) was conducted at room temperature for creviced copper coupon to study the susceptibility of metals to localized corrosion and passive stability. By this way, crevice corrosion parameters, such as critical crevice potential (breaking down potential), E_{crit}, and repassivation potential, E_{rep}, can be determined easily.

3.2.3 Potentiostatic measurement

Compared with potentiodynamic measurements, potentiostatic measurements observe the corrosion phenomena under the conditions of a steady potential applied to the system. Potentiostatic scans are especially suitable for an electrochemical process controlled by activation polarization. In an active-passive system, the resultant current to an applied external potential may pass the same value during the activation process and the passivation process. This means one current might be corresponding to multiple potential values. Therefore, compared with galvanostatic scan, potentiostatic scan ensures that the complete polarization curve for active-passive systems is recorded. In order to reach steady state, each potential applied to the system was kept constant for 10 minutes at room temperature and the corresponding current density was recorded. The range of applied potential was from 20 mV to 180 mV versus E_{corr} with an interval of 10 mV.

3.2.4 Electrochemical impedance spectroscopy (EIS)

Literature on the applications of EIS shows that EIS has great advantages over other techniques in studying film formation. Moreover, the results of EIS can be analyzed to determine rate controlling-steps. EIS is a good means to observe the variation of corrosion current during film formation.

A coupon, prepared as described in section 3.1.1 of this thesis, was immersed in 0.5 M NaCl solution. An EIS measurement was conducted daily by the corrosion measurement system. Automatic frequency scanning was employed in a frequency range between 10^5 to 10^{-5} Hz at a signal amplitude of 10 mV rma. It is noted that although EIS is usually assumed to be non-destructive, the destructiveness in practice is dependent on the magnitude of the AC potential applied to the system. If the potential is within ±50mV vs. E_{corr}, the surface of the metal will not be damaged (Globle Spec, Inc., 2005).

3.3 Surface Analysis

In this study, AFM was used for mapping the surface structure and the Raman spectroscopy was used for composition analysis.

3.3.1 Atomic force microscopy (AFM) measurements

Atomic Force Microscopy (Molecular Imaging Inc., USA) was used in this study. It allows surface examination on the nanometer scale with lateral resolution of 1 nm and vertical resolution of 0.1 nm. It has two operation modes, namely: contact mode and tapping mode. In the contact mode, AFM operates in direct contact with the surface of samples, and the feedback mechanism is the constant deflection method. In the tapping mode, AFM works by the resonance frequency of the cantilever. In this study, all AFM images were obtained in the contact mode because contact mode is better for the detection of solid sample.

Four samples were scanned, each of which was pictured with two dimensions, 30 μm × 30 μm and 10 μm × 10 μm. It was noted that the sample can not be larger than 20 mm × 20 mm due to the size of sample holder. The sample used for exposure test was mounted on the holder using a two-sided tape.

3.3.2 Raman spectroscopy

Raman spectroscopy is an *in situ* spectroscopic technique, the principle of which is the interaction of photons with the vibrations of chemical bonds. This method is widely used for analyzing surface compositions resulting from electrochemical processes and observing *in situ* formation of corrosion products during electrochemical experiments.

In this study, a Renishaw System 2000 Raman spectrometer (Renishaw plc., United Kingdom) operating at a wavelength of 514 nm was used to analyze the composition of the corrosion products. The radiation energy was 5 mW at the contacting sample surface. Unused and corroded copper coupons were observed. The bold surface and crevice wall of coupon from an exposure test were studied using Raman spectroscopy.

3.4 Summary

Two types of experiments were conducted in this study: electrochemical measurements and surface analysis. Table 3-3 summarizes the electrochemical techniques used in this study, including corrosion potential measurement, potentiodynamic scans, potentiostatic measurement and EIS measurements.

Table 3 - 3: Summary of the electrochemical measurements conducted.

Type	Temperature	Exposed to Atmosphere / Deoxygenated	Time	Sampling Period
Open Circuit Potential measurement	Room temperature	Open	40 days	1 day
	50 °C	Open	30 days	1 day
	Room temperature	Deoxygenated	31days	1 day
Potentiodynamic Measurement	Room temperature	Open	Change scan rate	N/A
			21 days	3 days
	50 °C	Open	40 days	1 week

Table 3 - 3 cont.

Type	Temperature	Exposed to Atmosphere / Deoxygenated	Time	Sampling Period
Potentiostatic Measurement	Room temperature	Open	2 hours	10 minutes
EIS	Room temperature	Open	20days	8days

The surface analysis focused on the physical characteristics and the chemical composition of corrosion products observed on the surface of the creviced copper coupon. Raman spectroscopy was used to examine the composition of the corrosion products while AFM served as the imaging tool. All measurements were conducted at room temperature and the details are listed in Table 3-4.

Table 3 - 4: Summary of surface analysis applied to RRC study.

Sample type	1	2	3
Atomic Force Microscopy	High temperature sample	Deoxygenated sample	Untreated sample
Raman Spectroscopy	At the mouth of the crevice (in the crevice)	Red product (outside crevice)	Black product (outside crevice)

CHAPTER 4

RESULTS AND DISCUSSION

This chapter presents the results with a discussion of their significance. The results of the exposure tests are first presented and this is followed by the results of corrosion potential measurement. After that, the physical and chemical characterization results are presented. Based on these results, a hypothesis is postulated. Finally, potentiodynamic scans, potentiostatic measurements and EIS are discussed.

4.1 Room Temperature Experiments

4.1.1 Reproduction of RCC

4.1.1.1 Phenomena of different types crevice corrosion

Assembled with grooved washer (crevice formers), a stainless steel specimen and a copper coupon were immersed in a 0.5 M NaCl solution at room temperature, which was open to the atmosphere, for one month. It was observed that the stainless steel was corroded along the crevice wall, as shown in Figure 4-1.

Figure 4 - 1: Photograph of crevice corrosion on a type 304L stainless steel sample after one month immersion in 0.5M NaCl at room temperature.

In Figure 4-2, the exposure test result of a copper coupon is presented. On the bold surface, a red-brown product accumulated along the periphery of the copper coupon and the inner part of the periphery was covered by yellow green corrosion products. Some black areas were also observed between each crevice wall. In the crevice, the crevice wall can be recognized by its flower shape with a color of shiny metal similar to that of pure copper. In addition, there was some red/orange products observed at the mouth of crevices.

Figure 4 - 2: Photograph of crevice corrosion on a copper coupon after one month immersion in 0.5M NaCl at room temperature.

4.1.1.2 Discussion of phenomena

Based on the phenomena observed on these two materials, a comparison was made on the corrosion properties of these two materials. As far as stainless steel is concerned, the crevice corrosion features were the same as the characters of classic crevice corrosion due to the corroded crevice and relatively corrosion-free bold surface. Conversely, copper behaved uniquely with an attacked bold surface and relatively corrosion-free crevice. This phenomenon was also found by Wyche et al. (1959) and is defined as reverse crevice corrosion in this thesis. Specifically, in RCC, the various colors indicate that different corrosion products, such as copper oxides, were produced at different locations on the bold surface.

It was found that if the lock nut was screwed very tightly, the solution was not able to penetrate into the crevice and this resulted in the absence of corrosion. In addition, uniform corrosion was found on the bold surface of the metal as shown in Figure 4-3.

Figure 4 - 3: Photograph of a copper coupon which shows a lack of crevice corrosion as the solution was unable to penetrate into the crevices.

4.1.2 Processes involved in RCC

4.1.2.1 Variation of open circuit potential during RCC processes

A creviced copper coupon was immersed in 0.5 M NaCl solution at room temperature and the corrosion potential was measured once a day for 40 days. As a comparison, the corrosion potential of an uncreviced copper coupon was also measured once a day for 40 days. Two replication measurements were conducted, but the RCC phenomenon only occurred for the first test. The reason for the poor reproducibility can be attributed to the inability to create repeatable crevice geometries. It is very hard to create two identical crevices without an advanced technique to control the accurate crevice dimension. In these experiments, a micro-adjusting torque wrench was tried to measure the tightness of the lock nut to guarantee the same crevice dimensions for each experiment. However, this did not work for the PTFE washer, which might be due to the softness of the PTFE material.

For the test where RCC occurred, the variation of corrosion potential for RCC can be observed as shown in Figure 4-4. In this figure, the corrosion potential of creviced copper coupon remained constant at approximately -0.2 V_{SCE} during the first five days. On the sixth day, the corrosion potential increases to approximately -0.05 V_{SCE}. The potential remained above -0.2 V_{SCE} until the 20 day of the experiment. Then the potential droped to approximately -0.3 V_{SCE}, and it remained there until the experiment was terminated. In contrast, as seen in Figure 4-4, the corrosion potential of a non-creviced copper coupon was found to be quite stable at a

value of approximately -0.2 V_{SCE}, indicating that uniform corrosion was occurring. On the basis of three distinct variations of potential, three phases, in which different corrosion phenomena occur, can be speculated. The detailed discussion will be presented in section 4.1.2.4.

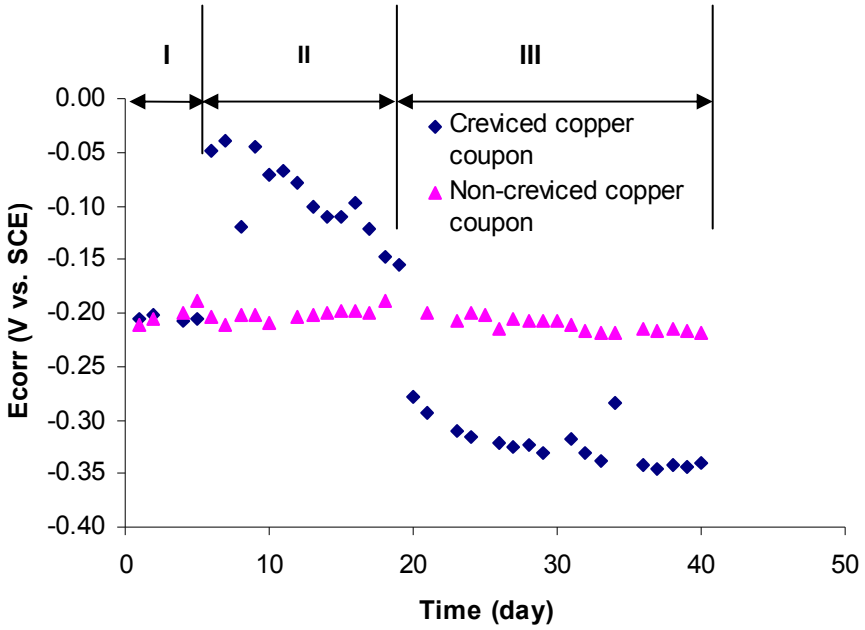

Figure 4 - 4: The classification of different stages of copper reverse crevice corrosion I: Incubation (uniform corrosion); II: Film formation-rupture; III: Reverse crevice corrosion.

4.1.2.2 Composition analysis of corrosion products formed in RCC

The samples used in the exposure test were examined by Raman spectroscopy. A typical sample is shown in Figure 4-5. Location I refers to the crevice surface and locations II and III refer to the bold or external surface.

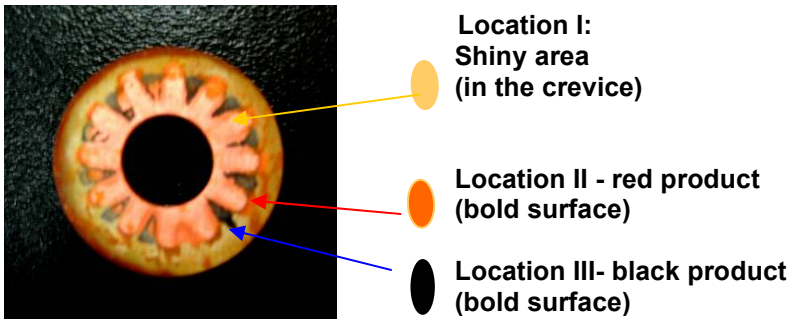

Figure 4 - 5: Photograph of the sample that was analyzed by Raman Spectroscopy.

In order to identify the elements or compounds in the corrosion products, some reference spectra of potential corrosion products were collected from the literature and these are presented in Figure 4-6 (Hamilton, 1986). These reference spectra were achieved from the detection of pressed powder sample of relevant compounds. The excitation wavelength is 488 nm.

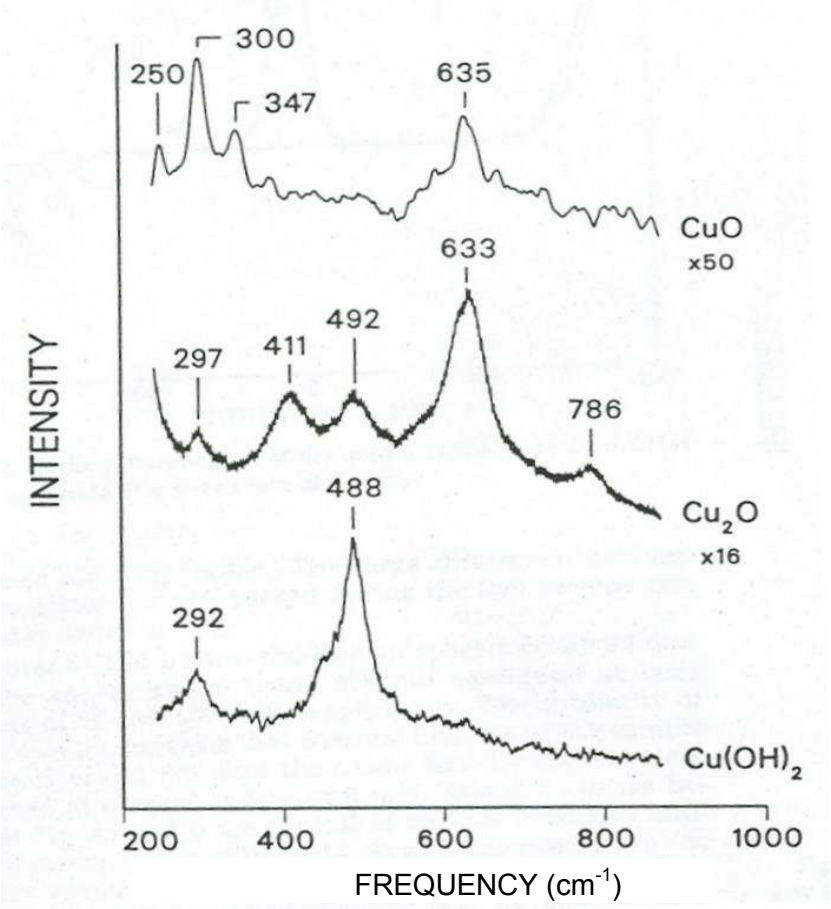

Figure 4 - 6: Reference spectra of Cu_2O, CuO and $Cu(OH)_2$ standards. Spectrum from CuO has been digitally smoothed (Hamilton, 1986).

As a comparison, a Raman spectrum of an unused copper coupon was obtained and is shown in Figure 4-7. Because the unused copper has a purity of 99.99%, there are no peaks in the spectrum as there is no vibration between chemical bonds.

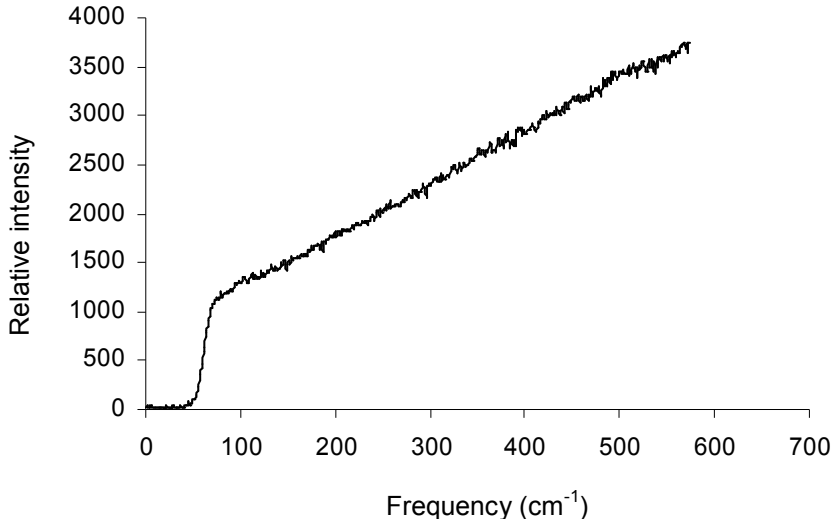

Figure 4 - 7: Raman spectrum for a pure copper coupon.

The Raman spectrum for Location I of Figure 4-5 is shown in Figure 4-8. It is seen that it is similar to the reference spectrum of Cu_2O shown in Figure 4-7.

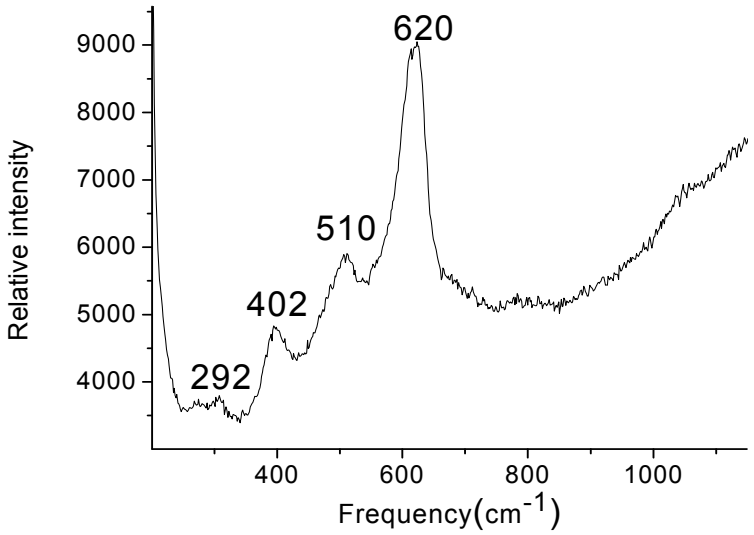

Figure 4 - 8: Raman spectra for Location I in Figure 4-5.

Another spectrum was obtained very close to Location I and this spectrum (Figure 4-9) is identical to the spectrum produced by pure copper (Figure 4-6). It can be summarized that the composition in the crevice is Cu_2O and reduced copper. The evidence of copper reduction is its shinny appearance of the crevice surface. Although the sheen is similar to copper, the color differs from the original copper

coupon. The coexistence of these two compounds in the crevice may result from the oxidation of copper at the initial stage and the reduction of part of it during a later stage. Because the oxidation occurred earlier than the reduction, the red Cu_2O can not be observed in the crevice by naked eyes in Figure 4-5, which means part of Cu_2O was reduced to copper and covered by the newly produced copper.

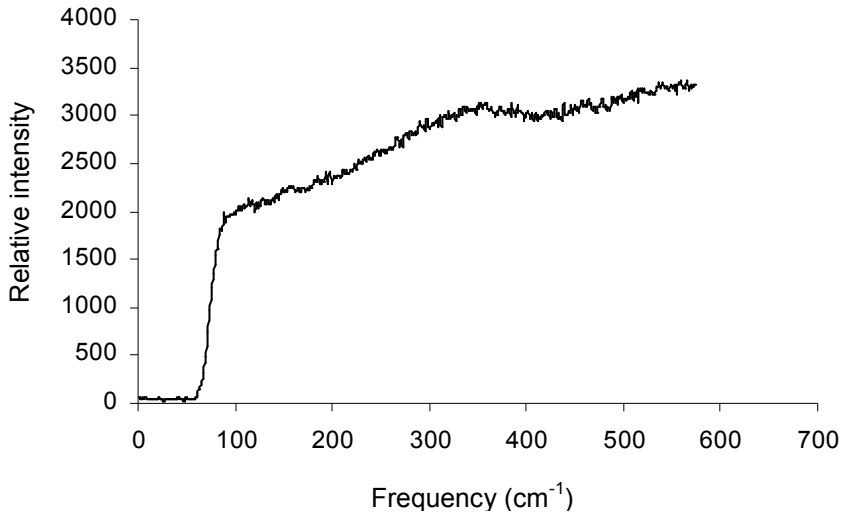

Figure 4 - 9: Raman spectrum for areas near Location I in Figure 4-5.

For the external surface (Location II), five peaks at 300, 411, 523, 634 and 787 cm^{-1} were observed. These are shown in Figure 4-10 and the peaks can be attributed to the formation of Cu_2O. The slight discrepancy between the locations of the peaks might be due to the change of electrical/magnetic field around chemical bonds or measurement temperature. That is, the environment for this study was probably not identical to that of the literature for providing the reference spectra.

Figure 4-11 shows the Raman spectrum obtained from Location III on the bold surface. An interesting new feature is shown in this figure. It can be seen that there are two peaks at 323 and 610 cm^{-1} which may be attributed to the formation of CuO (Hamilton et al., 1986; Frost, 2003; Xu et al., 1999; McCann et al., 1999; Chan et al., 1999; Fontana et al., 1978). However, the Raman peaks at 277 and 400 cm^{-1} could be ascribed to $CuCl_2$ as they are quite close to the literature value of 290 and 409 cm^{-1} (Frost, 2003; Chan et al., 1999). Generally, the color of CuO is black and that of $CuCl_2$ is green. It is noticed that no green corrosion product is present at

location III in Figure 4-5, but the Raman spectrum did detect the presence of $CuCl_2$. It is easy to imagine how hard to distinguish green $CuCl_2$ from black CuO if these two colors are mixed, which could be attributed to the concealment of green $CuCl_2$ in the figure. In addition, from Figure 4-5, it can be observed that green color is around the periphery, which indicate only a small amount of CuO was produced in the later phase and it was not enough to cover the whole bold surface.

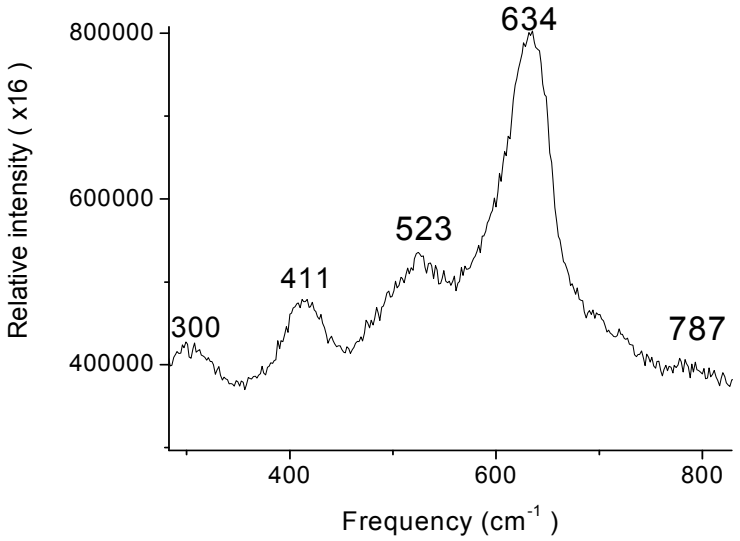

Figure 4 - 10: Raman spectrum for red part at Location II in Figure 4-5.

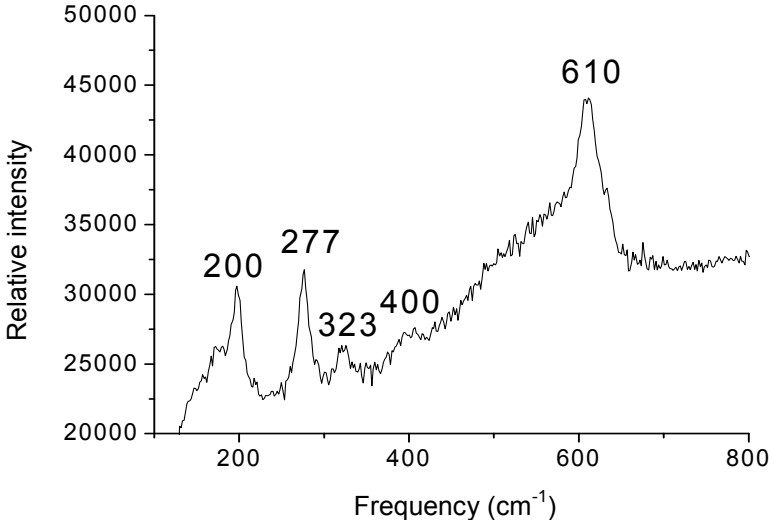

Figure 4 - 11: Raman spectra for black part at location III in Figure 4-28.

4.1.2.3 Surface morphology of RCC

Several micrographs were obtained by AFM that show the surface characteristics of the copper coupon after the immersion test for 40 days in a 0.5 M NaCl solution open to air at room temperature. An unused polished (to 600 grit) copper coupon was first imaged by AFM as a control. The vertical features in the image were due to polishing process as shown in Figure 4-12.

Secondly, a creviced copper coupon was imaged at two areas, the crevice wall and the bold surface. Figure 4-13 shows the morphology of the crevice wall, which shows an unevenly distributed granular structure. Due to the accumulation of corrosion products, it was difficult for the AFM probe tip to get into the deeper areas of the sample. Therefore, it cannot to image the dark area in the this figure. Figure 4-14 is a scan of the metal surface located outside of the crevice. In comparison with Figure 4-13, it is obvious that the corrosion products on the bold surface outside of the crevice are more evenly dispersed.

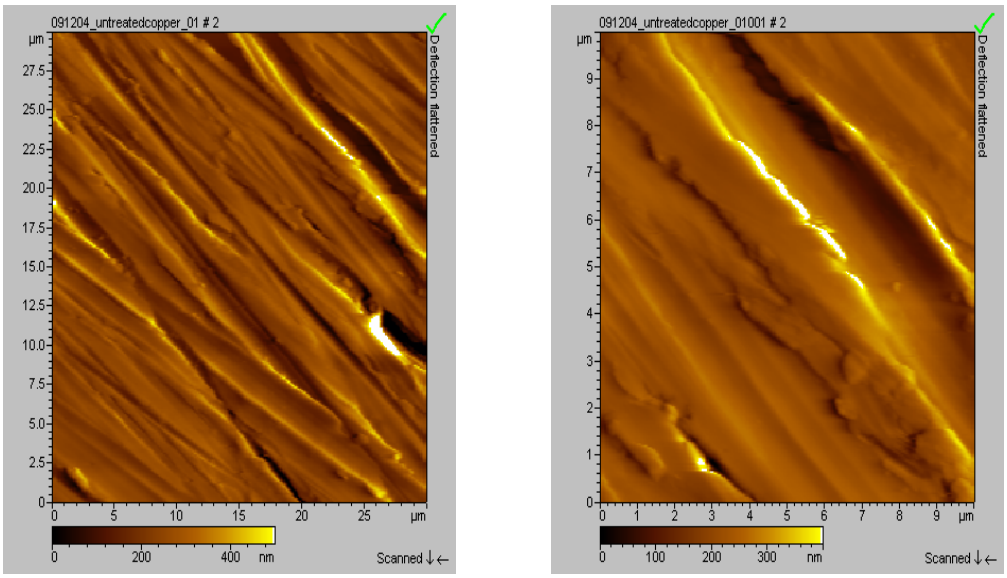

(a) (b)

Figure 4 - 12: AFM Image of unused copper coupon with (a) 30 μm × 30 μm in-plan scan range and a 450 nm z range, and (b) 10 μm × 10 μm in-plan scan range and a 400 nm z-range.

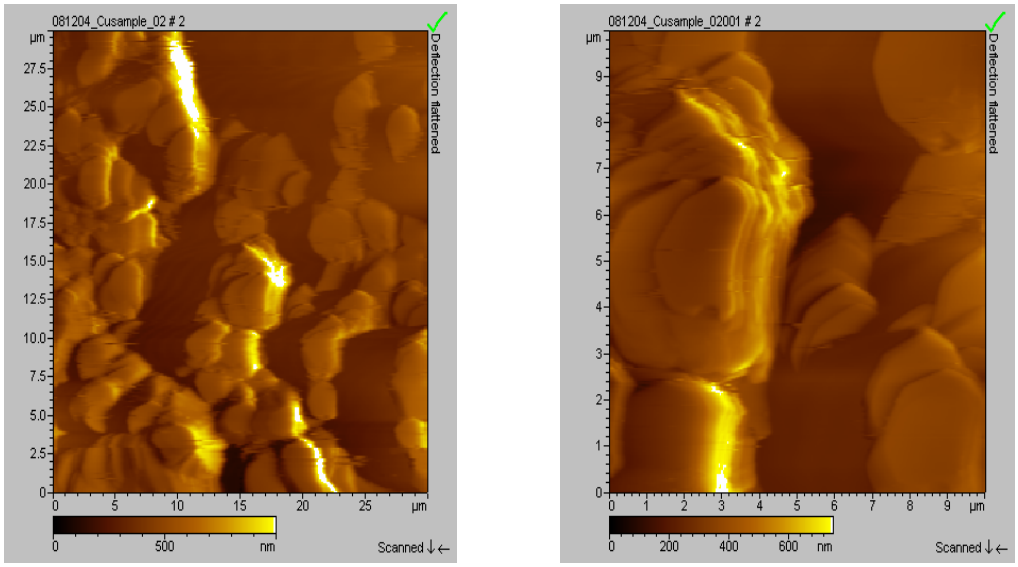

(a) (b)

Figure 4 - 13: AFM Image of the surface in the crevice after the copper coupon was immersed in 0.5 M NaCl solution for 21 days at room temperature with (a) 30 μm × 30 μm in-plan scan range and a 1000 nm z range, and (b) 10 μm × 10 μm in-plan scan range and a 700 nm z-range.

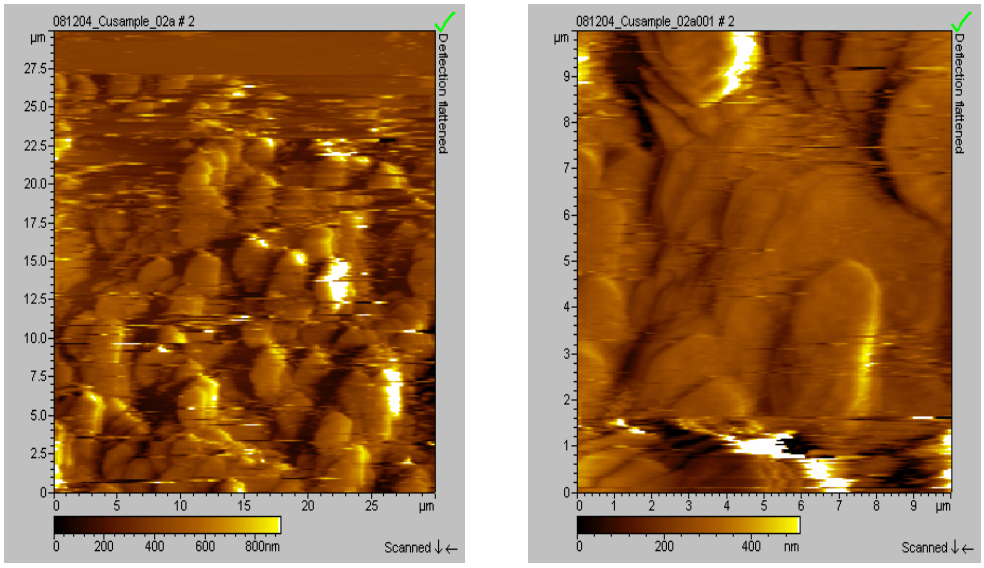

(a) (b)

Figure 4 - 14: AFM Image of the surface out of the crevice after the copper coupon was immersed in 0.5 M NaCl solution for 21 days at room temperature with (a) 30 μm × 30 μm in-plan scan range and a 900 nm z range, and (b) 10 μm × 10 μm in-plan scan range and a 500 nm z-range.

4.1.2.4 Hypothesis of RCC and its evidences

As mentioned in Section 4.1.2.2, there were three distinct variations of corrosion potential during RCC measurement that indicate three different phases in the corrosion processes. It is hypothesized that during the first phase of the RCC process the entire surface of the specimen is corroding uniformly to produce a red Cu (I) product. The supporting evidence for this is the stable corrosion potential, indicating that uniform corrosion occurred during the first 5 days. The possible anodic and cathodic reaction are:

$$\text{Anodic reaction: } Cu \leftrightarrow Cu^{+} + e^{-} \tag{4.1}$$

$$\text{Cathodic reaction: } O_2 + 2H_2O + 4e^{-} \leftrightarrow 4OH^{-} \tag{4.2}$$

This hypothesis can be verified by the result of Feng et al. (1997) in which Cu (I) oxide was found as corrosion product in a solution with a pH varying from 6 to 9.

After the corrosion product accumulates on the surface for five days, both inner and external surfaces are covered with Cu_2O products which are due to Cu (I) hydrolysis. Cu_2O was identified by Raman spectroscopy in the crevice and on the bold surface, which supports the above prediction. Moreover, Cu_2O was the most stable Cu (I) species in neutral solution (Badawy et al., 1997), which makes this prediction more reasonable.

The formation of a relatively complete product layer retards the dissolution of copper and, at that point, the corrosion rate would be reduced. This agrees with Feng et al.'s (1997) findings. Feng et al. mentioned that cubic Cu_2O film is more protective and behaves as a diffusion barrier of copper ions to bulk solution. Therefore, the corrosion potential becomes nobler in phase II, as shown in Figure 4-4. The hydrolysis of copper cations, as expressed by equation 4.3, also initiates acidification of the crevice solution.

$$2Cu + H_2O \leftrightarrow Cu_2O \downarrow + 2H^{+} + 2e^{-} \tag{4.3}$$

In the third phase, it is still unclear how the bold surface becomes anodic. However, it can be imagined that oxygen mass transfer to the bold surface is easier than in the crevice. Meanwhile, the copper oxide product in the crevice cannot migrate out to the bulk solution because Cu_2O is a solid, which also blocks the oxygen transfer into the crevice and offers some protection for the crevice wall.

Although the exact mechanism has not been revealed, based on exposure tests, it can be deduced that the bold surface is more corroded more severely than the crevice. It can be concluded that copper is reduced at some places in the crevice, as shown by Raman spectroscopy. In order to balance the reduction process occurring in the crevices, the oxidation of Cu to Cu (I) occurs on the bold surface, more possibly close to the crevice mouth, the red product of which is identified by Raman spectroscopy as shown in Figure 4-10. Moreover, black corrosion products were observed around the crevice on the bold surface in Figure 4-5, indicating that Cu (I) is oxidized to Cu (II) during this phase, which also balances the reduction process in the crevice. This property of bold surface is distinct from the classic crevice corrosion.

In addition, as reported by Badawy and AI-Kharafi (1999), in acidic solutions, the Cu (I) film was not stable and a disproportion reaction would occur to produce Cu (II) with the deposition of Cu. The deposited copper was observed on the copper alloy surface (Badawy et al., 1997; Johnson et al. 1971). Therefore, the production of copper in the crevice can also be explained by this mechanism.

To summarize, during the third phase, the following reactions may take place in the crevice and the cathodic reaction may predominate:

Anode reaction: $\mathrm{Cu} \rightarrow \mathrm{Cu}^{+} + e^{-}$ (4.5)

Cathodic reaction: $\mathrm{Cu}^{+} + e^{-} \rightarrow \mathrm{Cu}$ (4.6)

On the bold surface, the following reactions may occur during the third phase.

Anodic reactions: $\mathrm{Cu}^{+} \rightarrow \mathrm{Cu}^{2+} + e^{-}$ (4.7)

$$\mathrm{Cu} \rightarrow \mathrm{Cu}^{+} + e^{-} \quad (4.8)$$

Cathodic reaction: $\mathrm{O_2} + 2\mathrm{H_2O} + 4e^{-} \leftrightarrow 4\mathrm{OH}^{-}$ (4.9)

In summary, there are three phases in the reverse crevice corrosion process of copper that correspond to the three potential changes. These phases are a uniform corrosion period, in which corrosion potential was kept constantly at -0.2 V_{SCE}; the film formation phase, at the beginning of which corrosion potential increased to -0.05 V_{SCE}; and a final period of RCC occurrence, in which a constant corrosion potential, lower than first phase, was observed.

4.1.3 Copper crevice corrosion under deoxygenated environment

4.1.3.1 Variation of open circuit potential

Figure 4-15 shows the variation of open circuit potential of a creviced copper coupon which was immersed in a deoxygenated 0.5M NaCl solution for 31 days. During the first week, the corrosion potential ranged from -0.2 V_{SCE} to -0.3 V_{SCE}. Then the potential became stable at approximately -0.4 V_{SCE}. That is, the corrosion potential tends to stabilize after the fluctuations during the first couple of days. The fluctuation is caused by the oxygen residing in the crevice assembly because the working electrode was assembled in air. An improved procedure for assembling the crevice is suggested in the recommendation section of this thesis.

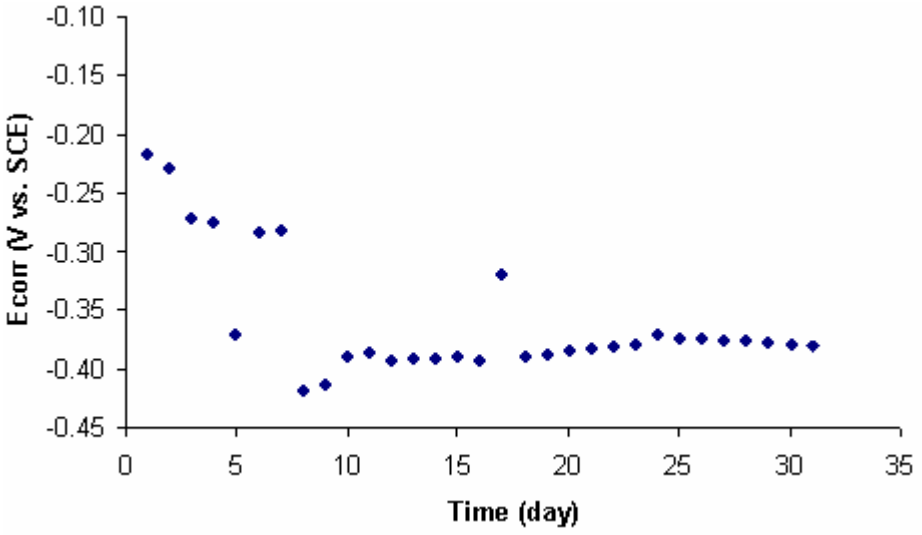

Figure 4 - 15: The open circuit potential of creviced copper coupon immersed in deoxygenated 0.5 M NaCl solution at room temperature over 31 days.

4.1.3.2 AFM Results of Deoxygenated Copper Coupon

The influence of oxygen on the existence of RCC was investigated by AFM. The copper coupon was immersed in a deoxygenated 0.5 M NaCl solution for 30 days. Figure 4-16 shows the images obtained for this coupon. It was found that the bold surface is superficially corroded and the size of corrosion products is different from that obtained for the coupon immersed in the solution exposed to air. In Figure 4-16 (a), the vertical features resulting from polishing can be recognized, which is similar to the morphology of unused copper. That is to say, very little corrosion

occurred on the surface. In Figure 4-16(b), the size of the crystals on the metal surface can be seen.

4.1.3.3 Discussion of deoxygenated experiments

From a thermodynamic perspective, copper does not corrode in a deoxygenated system. However, it was observed that a superficial corrosion took place under deoxygenated NaCl solution. This problem may due to the small trace of oxygen in the system, which may have caused the initial fluctuation of the corrosion potential. Also, because the amount of oxygen in the system would be very small, it is consumed up quickly during the first week. This assumption can be verified from the AFM results, in which very small amount of corrosion products are observed.

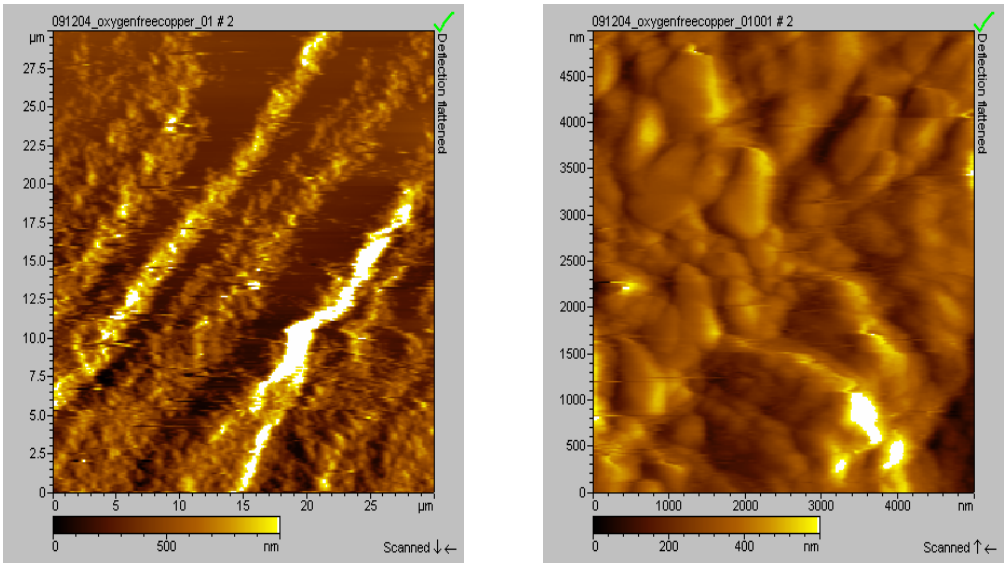

(a) (b)

Figure 4 - 16: AFM image of the bold surface after the creviced copper coupon was immersed in a deoxygenated 0.5 M NaCl solution for 30 days at room temperature with (a) 30 μm × 30 μm in-plan scan range and a 1000 nm z range, and (b) 10 μm × 10 μm in-plan scan range and a 600 nm z-range.

4.1.4 Kinetics of RCC

4.1.4.1 Potentiodynamic Scan

To guarantee the validity of potentiodynamic measurements, the optimum scan rate must be determined. Potentiodynamic scan can be classified into two types, slow-scan and rapid-scan. Rapid-scan refers to the scan rate about 16.7 mV/s which

is used when intense anodic activity is likely. Slow-scan means sweeping at a relatively slow rate of potential change about 0.28 mV/s, and this is used when relative inactivity is likely. In the other words, a rapid potentiostat sweep of potential minimizes film formation so that the currents observed relate to relatively film free or thin film conditions. In comparison, the slow sweep rate experiment allows more time for film formation.

In this study, the rate was initially set at 2 mV/s and then it was decreased in subsequent experiments until there was little change between the experimentally generated curves. Figure 4-17 shows the curves produced by potentiodynamic measurement with the different scan rates.

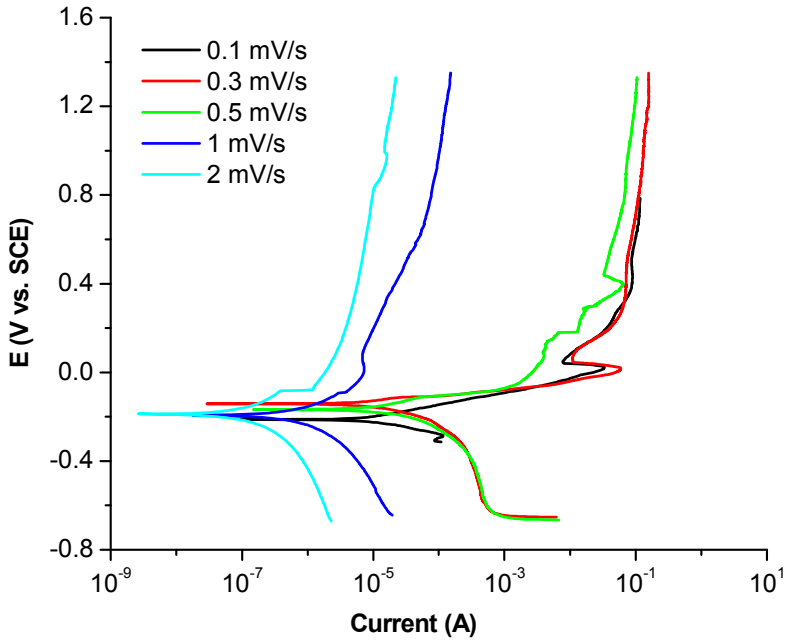

Figure 4 - 17: Influence of different scan rates on potentiodynamic curves on copper crevice corrosion by using copper crevice assembly immersed in 0.5 M NaCl solution for 30 minutes (room temperature).

Compared with the curves obtained by 2 mV/s, the result from 0.3 mV/s reveals more details of the corrosion process in that there is a passivation area which does not appear in higher scan rate measurement. Theoretically, the slower the rate, the more complete the curve, but in practice there is compromise as slow scan rate

experiments are very lengthy and may not see the results of rapid anodic activity. Therefore, an appropriate scan rate has significant influence on the efficiency and validity of experiments. In this study, it was found that reducing the scan rate to less than 0.3 mV/s did not significantly change the shape of the potentiodynamic curve. Therefore, a scan rate of 0.3 mV/s was used for all potentiodynamic measurements at room temperature. It was also used at elevated temperature scans because the reactions should proceed faster at higher temperature and therefore do not need a scan rate slower than 0.3 mV/s.

The polarization behavior of a non-creviced copper coupon and a creviced copper coupon were compared after they had been immersed in 0.5 M NaCl solution open to the atmosphere at room temperature for 30 minutes. In Figure 4-18, two curves looks very similar with each other and no significant distinction presents. That is to say, potentiodynamic scan is not sensitive to RCC and may not provide effective information distinguished RCC from other types of corrosion.

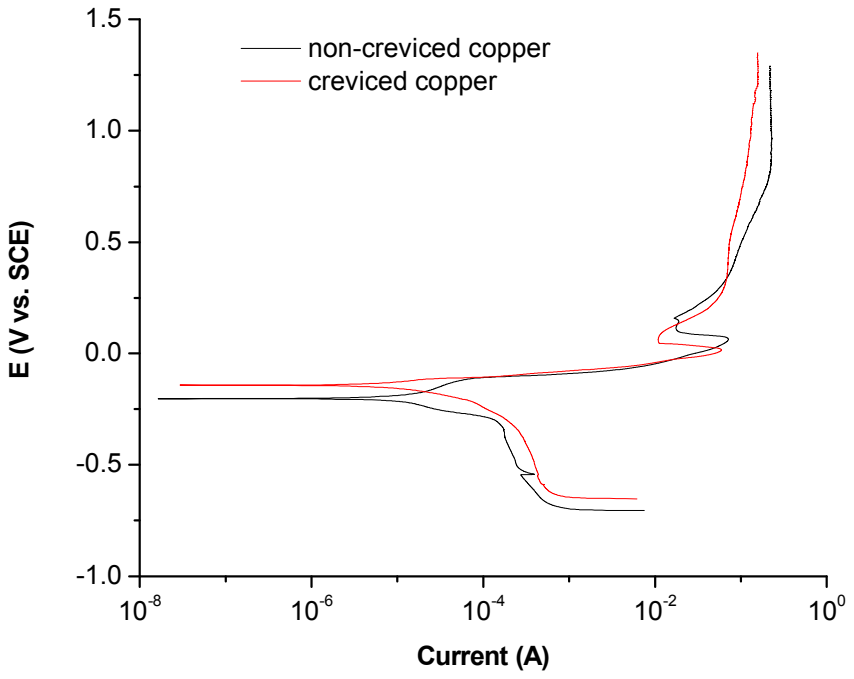

Figure 4 - 18: Potentiodynamic curves for a copper and creviced copper coupon immersed in 0.5 M NaCl solution for 30 minutes (room temperature).

To further study the application of potentiodyamic scans, copper coupons with crevice assembly were immersed in 0.5 M NaCl solution at room temperature and exposed to the atmosphere for 5, 8, 11,14, 17 and 21 days. Several potentiodynamic scans were performed for these. Similarly, the potentiodynamic scans were conducted at 50 ºC after the creviced copper coupons were immersed for 7, 14, 21 and 40 days. Results of the scans conducted at room temperature are given in Figure 4-19.

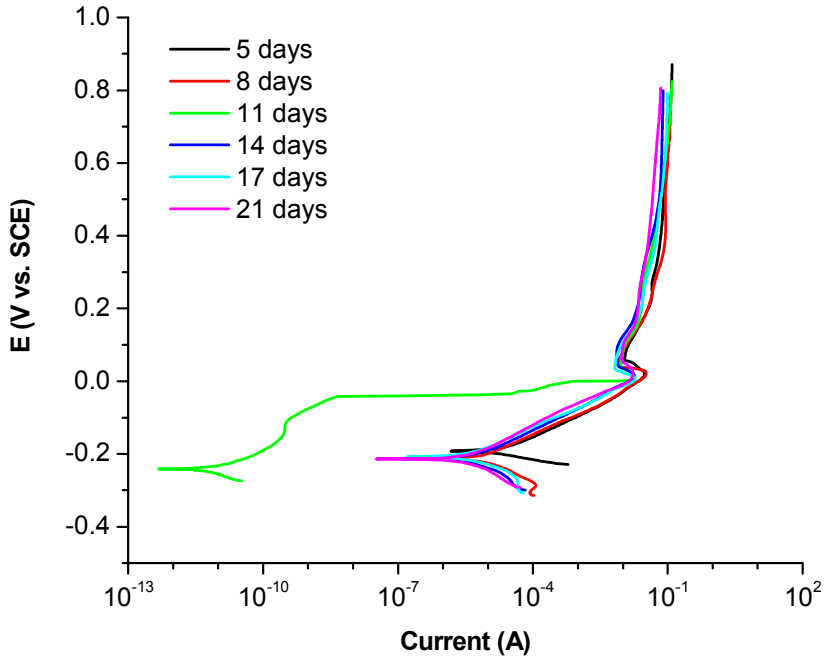

Figure 4 - 19: Potentiodynamic curves for a copper crevice assembly immersed in 0.5M NaCl solution during different time periods (room temperature).

It is found that except for the day eleven scan, the curves are similar for scans taken at different times. Thus, only one typical scan is discussed in detail. Taking the curve obtained at the fifth day as an example, it shows that there might be film formation at approximately 0 V_{SCE}. A linear *E*/log *i* relation with an anodic Tafel slope of 60.3 mV/decade is obtained. The overall corrosion rate and corrosion potential are given in Table 4-1. Benedetti et al. (1995) performed a similar study on non-creviced specimens in 0.5 M NaCl with a pH of 3 and obtained the same anodic

Tafel slope. The similarity of the curves indicates that potentiodynamic scanning is not a good indication of the RCC processes.

Table 4 - 1: Corrosion parameters obtained from potentiodynamic scanning of creviced copper coupon immersed in 0.5 M *NaCl* solution for 5 days at room temperature.

Anodic Tafel Slope (mV/decade)	Cathodic Tafel Slope (mV/decade)	I_{corr} (μA)	E_{corr} (mV)	Corrosion rate (mm/year)
60	35	23	-192	0.063

4.1.4.2 Critical potential and repassivation potential of RCC

In the literature, breakdown potential (critical potential) has been defined as the potential that the sample needs to reach a current density of 20 μA/cm^2. The repassivation potential is the potential for the sample to reach 1 μA/cm^2 in the reverse scan (Evans, 2005). Figure 4-20 shows that the critical potential of RCC is -10 mV_{SCE} and the repassivation potential is -48 mV_{SCE}.

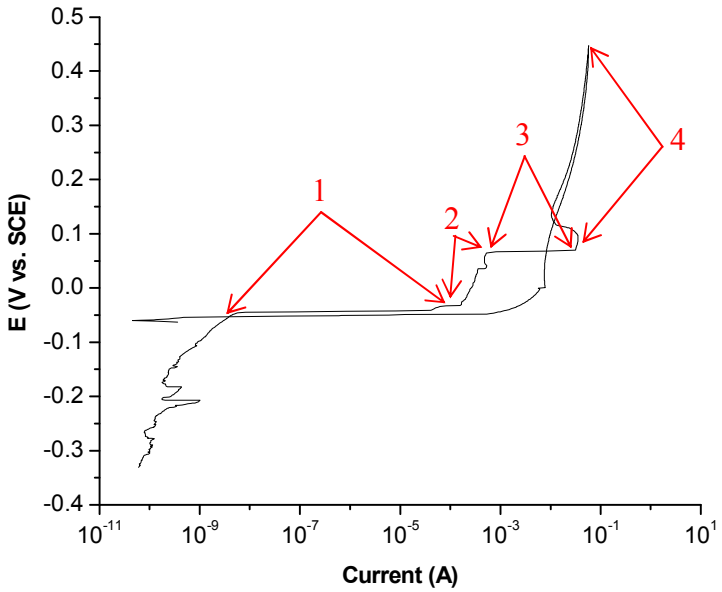

Figure 4 - 20: Cyclic potentiodynamic polarization curve of a creviced copper coupon immersed in 0.5 M NaCl solution open to atmosphere.

Figure 4-20 also indicates some changes of surface status during experiment period, marked as 1, 2, 3 and 4 areas in the figure. Firstly, the current increased fast with the applied potential, which indicates a rapid corrosion process (area 1). After some time, a film formed on the surface while decreased the rate of corrosion, indicated by area 2. Following by this, a sharp increase in corrosion current located in area 3. Finally, a limiting current situation occurred and the current did not increase with potential (area 4).

Potentiostatic measurements were performed in a 0.5 M NaCl solution exposed to the atmosphere at room temperature. The external potential was held between 10 mV vs. E_{corr} to 200 mV vs. E_{corr} with intervals of 10 mV. The potential was held for 30 minutes at each level.

Figure 4-21 shows the results of potentiostatic measurement. It is useful in determining the critical potential for crevice corrosion. It can be seen that the critical potential for copper reverse crevice corrosion is 30 mV (vs. E_{corr}) in 0.5 M NaCl solution under room temperature and it might be changed under other conditions.

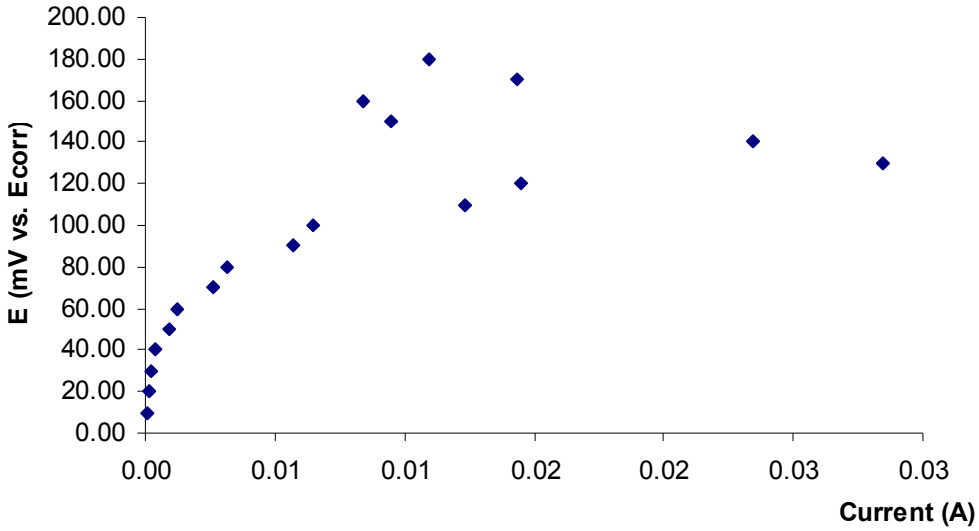

Figure 4 - 21: Potentiostatic curve of a copper crevice assembly immersed in 0.5 M NaCl solution for 2 hours at room temperature.

4.1.4.3 Electrochemical impedance spectroscopy analysis

Electrochemical Impedance Spectroscopy (EIS) was used as another analysis tool and spectra were obtained after samples were immersed in aqueous, air-exposed 0.5 M NaCl for two, 10 and 18 days. Corresponding to the three phases obtained in the open circuit measurements, it was found that there is a different type electrochemical impedance spectrum in each phase.

Figure 4-22 (a) shows the EIS results for a copper crevice assembly that has been immersed for two days. Two time constants are observed in this figure. The first time constant is represented as a semicircle with a diameter of 120 Ω that may be attributed to a charge transfer process. A linear region indicates a second time constant which that may be due to a diffusion process. Thus, during the incubation period of RCC the process is under both charge transfer and mass transfer control. The charge transfer process might be copper dissolution over the entire surface and the diffusion time constant is attributable to the diffusion of oxygen to the surface of the metal.

After 10 days of exposure only one time constant was observed. This capacitive arc, which is shown in Figure 4-22 (b), indicates that charger transfer is now the rate controlling process. In other words, the accumulation of hydrolysis products of copper species on the surface slows down the copper dissolution rate (i.e., a relatively protective film has been formed). The formation of a product film slows down the diffusion of oxygen from solution to bold surface. At the same time, the film might be a poor electronic conductor, which will have some influence on the electron transfer to the cathode. Therefore, the rate of reaction decreases.

Finally, during the RCC stage (18 days of exposure), the Nyquist plot again shows two time constants in which a linear region occurs in the high-frequency region (100 kHz ~ 15.79 Hz), indicating diffusion control, and a charge transfer process is indicated in the low frequency region. The plot is given as Figure 4-22 (c). In the third phase, the diffusion process may be attributed to the oxygen mass transfer to the bold surface and the charge transfer process indicates the reduction of *Cu* (I) to *Cu*.

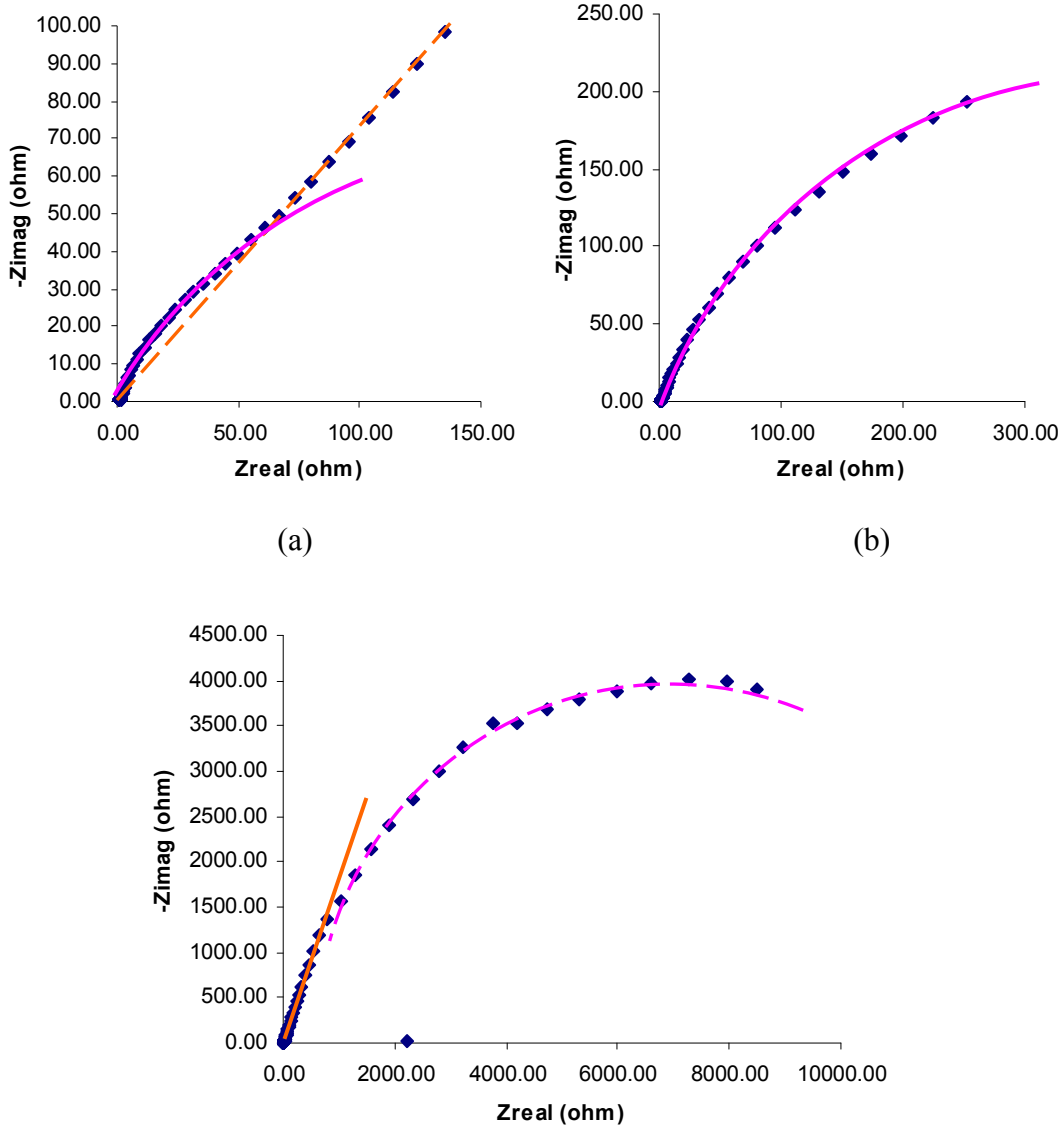

(a) (b)

(c)

Figure 4 - 22: Nyquist plot for a copper crevice assembly in solution of 0.5 M NaCl at room temperature (a) after 2 days; (b) after 10 days; (c) after 18days.

With the aid of Gamry Echem Analyst^{TM}, the impedance data was fit to the selected equivalent circuit models by using Levenberg-Marquardt Method, which is useful to non-linear fitting. Table 4-2 shows best fit models for different time periods and Figure 4-23, 4-24 and 4-25 present the curve fit models.

In Table 4-2, two types of model are fitted, OTCWAR and CPE, corresponding to the two phases/three steps of RCC. OTCWAR is a diffusion model.

Its equivalent circuit can be presented by Warburg impedance (Figure 4-26). The value of Warburg impedance is proportional to $\omega^{-1/2}$. Therefore, Warburg impedance is small at high frequencies. Comparably, Warburg impedance is larger at low frequencies (Gamry Instruments, 2005).

Table 4 - 2: Model Fit Results for Experimental System.

Parameters	2days	10days	18days
R_u (ohm): Uncompensated Solution Resistance	855.2×10^{-3}	1.093	13.52×10^{3}
Y_0 (s): CPE Y_0 Value	1.472×10^{-3}	1.61×10^{-3}	5.749
Alpha : CPE Exponent	685.9×10^{-3}	700×10^{-3}	38.30×10^{-6}
W_d (s) : Warburg Impedance	6.377×10^{-3}	2.081×10^{3}	N/A
R_p (ohm) : Polarization Resistance	87	630	690.2×10^{-3}
Model	OTCWAR	OTCWAR	CPE

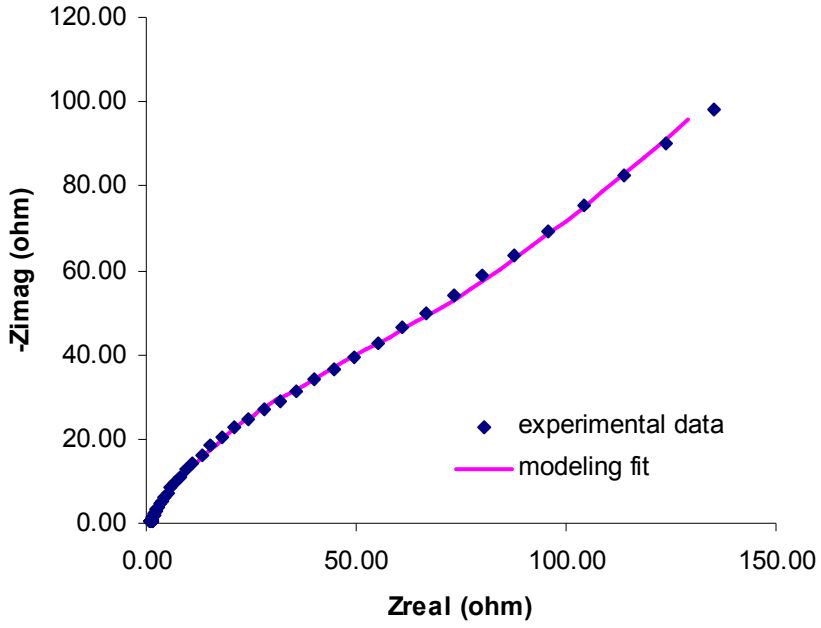

Figure 4 - 23: Diffusion model fit to the EIS data of a creviced copper coupon after the immersion in 0.5 M NaCl solution for 2 days open to air.

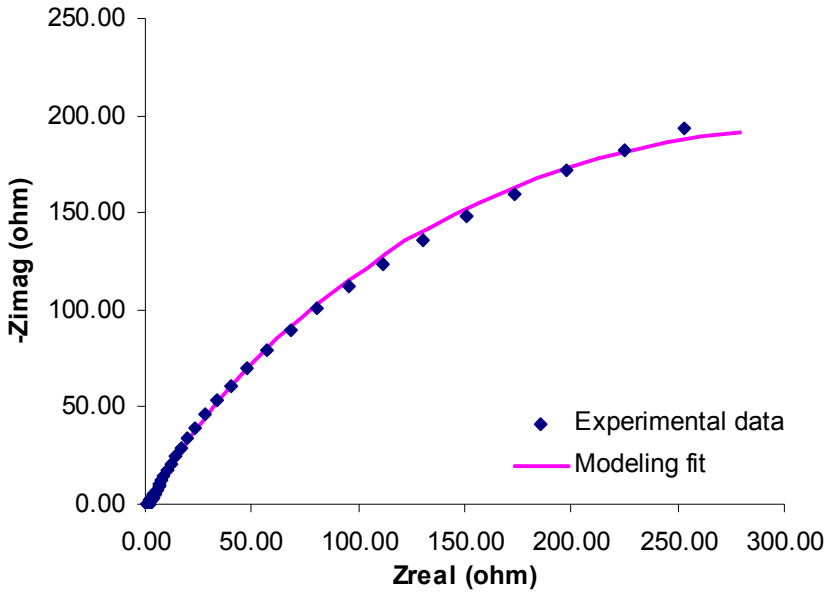

Figure 4 - 24: Diffusion model fit to the EIS data of a creviced copper coupon after the immersion in 0.5 M NaCl solution for 10 days open to air.

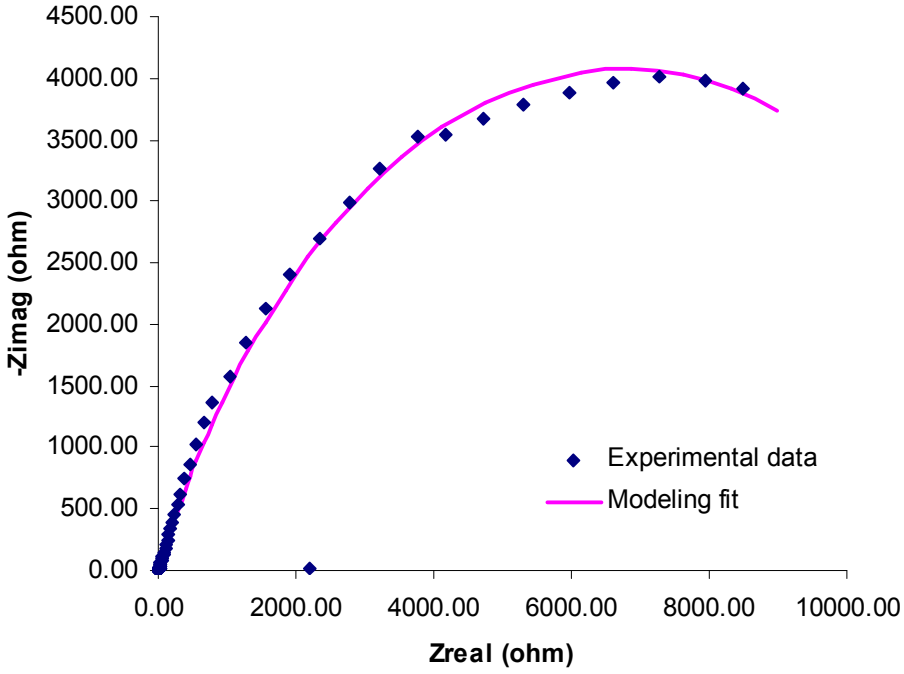

Figure 4 - 25: Depressed Nyquist model fit to the EIS data of a creviced copper coupon after the immersion in 0.5 M NaCl solution for 18 days open to air.

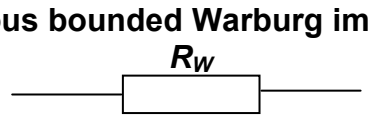

Figure 4 - 26: Equivalent circuit of the diffusion model

CPE stands for Constant Phase Element and that is a Depressed Nyquist Model. CPE is often used to explain deviations brought about by surface roughness, which is the reason why capacitors do not work ideally in practical cases. This model is similar to the Randles cell, the equivalent circuit of which is shown in Figure 4-27. In CPE model, Warburg impedance replaces the double layer capacitor in Randles cell. The CPE model describes the situation in which the center of the charge transfer semicircle is below the Real axis of Nyquist plot, as shown in Figure 4-28 (Gamry Instruments, 2005).

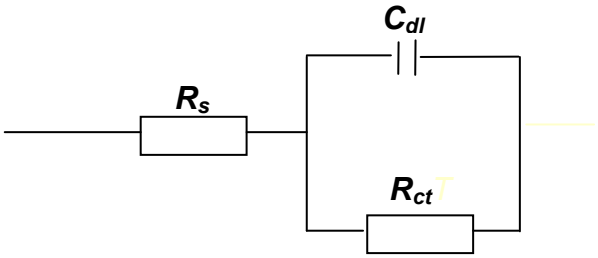

Figure 4 - 27: Equivalent circuit of a Randles cell. R_s: Resistance of solution; R_{ct}: Resistance of capacitor; C_{dl}: Double layer capacitor.

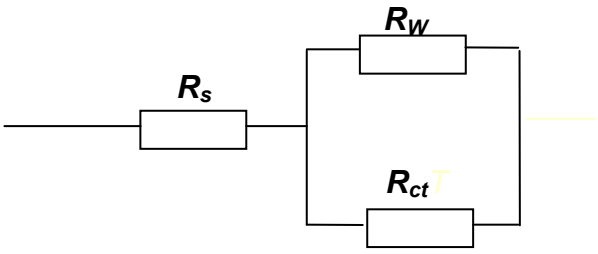

Figure 4 - 28: Equivalent circuit of a depressed Nyquist model. R_s: Resistance of solution; R_{ct}: Resistance of capacitor; R_W: Warburg Resistance.

Based on the modeling results, it is speculated that the diffusion step is the controlling step at the beginning of the RCC procedure, which might be related to the oxygen migration from the solution to the copper surface during the first step or

the mass transfer of copper ions through the corrosion product film during the second step of RCC. During the third step, the controlling step is a result of the combination of charge and mass transfer resistance.

4.2 Elevated Temperature Experiments

4.2.1 Variation of open circuit potential of copper crevice corrosion

Open circuit potential measurements were conducted at 50 ºC for two replication times. However, the results shown in Figure 4-29 and 4-30 are not consistent with one another. In addition, comparing these with the experimental data obtained at room temperature, the results for elevated temperature do not show indications of RCC. The reason will be discussed in section 4.2.5.

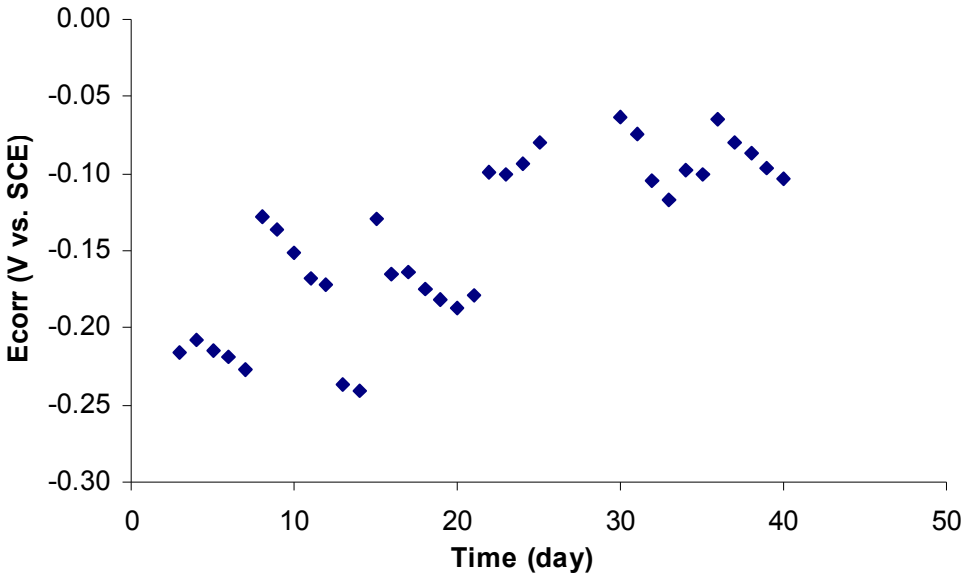

Figure 4 - 29: Variation in E_{corr} for a copper crevice assembly immersed in 0.5 M NaCl at 50 ºC (first round).

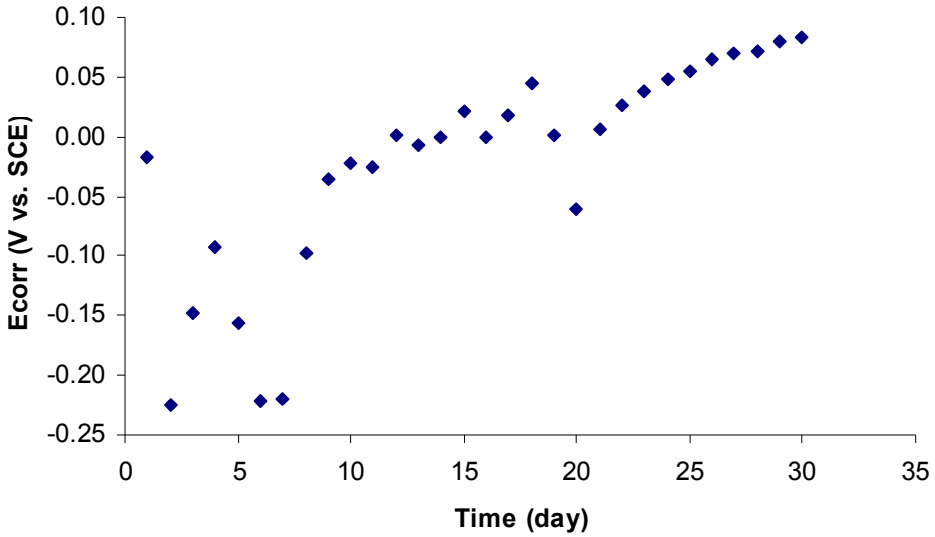

Figure 4 - 30: Variation in E_{corr} for copper crevice assembly immersed in 0.5 M NaCl at 50 ºC (second round).

4.2.2 Exposure tests at elevated temperature

Since RCC was not observed at 50 ºC in the corrosion potential measurements. A nature investigation was performed in which several samples were exposed to 0.5 M NaCl solution at 50 ºC for one month with the solution open to the atmosphere.

It was observed that the corrosion occurred everywhere on the surface of each copper plate and there was no reverse crevice corrosion. The exact appearance of a sample plate after one month of immersion is shown in Figure 4-31.

Figure 4 - 31: Photograph of a copper plate coupon after immersion in 0.5 M NaCl solution for one month at 50 ºC. The solution was exposed to the atmosphere.

4.2.3 Potentiodynamic scan results at elevated temperature

Four creviced copper coupons were immersed in a 0.5 M NaCl solution at 50 ºC for different time periods and measured by potentiodyamic scans. The obtained curves and kinetic parameters were shown in Figure 4-32 and Table 4-3. It can be seen that four curves presented by various colour exhibit dissimilar behavior, unlike the superposition observed in the potentiodynamic curves at room temperature. In addition, the curves do not have the passivation section like that appeared in the curves obtained at room temperature. According to the parameters in Table 4-3, it can be found that the increase of corrosion rate is proportional to the immersion time for first three time periods, 7 days, 14 days and 21 days. However, the corrosion rate of the creviced copper coupon decreases significantly after 40 days immersion.

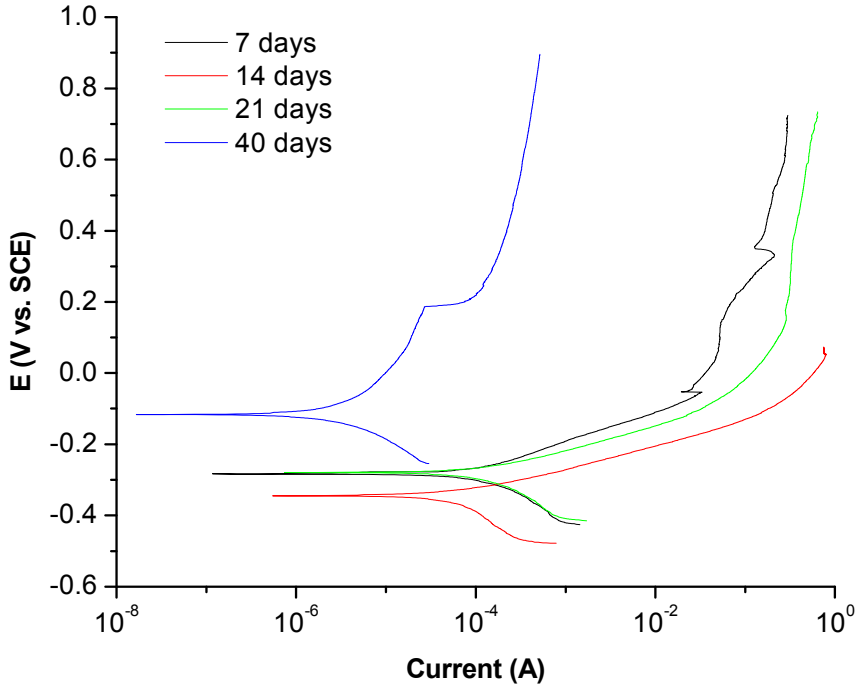

Figure 4 - 32: The variation of potentiodynamic curves for copper crevice assemblies immersed in 0.5 M NaCl solution during different periods (50 ºC).

Table 4 - 3: Corrosion parameters obtained from potentiodynamic scanning of creviced copper coupon immersed in 0.5 M NaCl solution during different time periods at 50 ºC.

Time / Parameters	7 days	14 days	21 days	40days
b_a (mV/decade)	68.30	64.70	71.90	522.8
b_c (mV/decade)	68.10	237.7	171.1	222.4
I_{corr} (μA)	35.40	75.00	151.0	7.510
E_{corr} (mV)	-283.0	-344.0	-279.0	-116.0
Corrosion rate (mm/year)	0.0990	0.210	0.424	0.0210

4.2.4 Surface morphology analysis

Although the elevated temperature creviced copper coupon did not exhibit the distinct features of RCC, it also was investigated by AFM, and the results are shown in Figure 4-34. Since there is was little difference between bold surface and the wall of crevice after using the AFM probe to scan the whole surface of the copper coupon, the image was only taken for the bold surface, in which the corrosion products were accumulated in a form like overlapped shale. In Figure 4-33, it is observed that the distribution of crystals on the whole surface at high temperature is similar to that of bold surface at room temperature.

4.2.5 Discussion

In comparison with the room temperature experiment, the reverse crevice corrosion was not observed at elevated temperatures, as shown by exposure tests and the AFM results. But the copper coupon was attacked more severely by corrosion at 50 ºC because it has higher corrosion rate than that of room temperature, which is based on kinetic parameters obtained from the potentiodynamic scan. However, the exception was found after the coupon was immersed for 40 days. Although mechanism for the corrosion process at elevated temperature was not discovered, some facts should be noticed. Firstly, the crevice formers were assembled at room

temperature and then put in the solution with 50 ºC. This procedure may make the former expand and further affect the width of crevice. The width of crevice is very important for the occurrence of crevice corrosion because classic crevice corrosion only occurs under a specific crevice width and RCC mostly possible follow the same rule. In addition, the Saturated Dissolved Oxygen Concentration (SDOC) is 5.576 mg/L at 50 ºC while it is 8.32 mg/L at 298 K (General Chemistry Online, 2005). Dissolved oxygen is the key for reduction of oxygen and further affects the coupling of cathodic reactions and anodic reactions. Considering the influence of SDOC on the electrochemical reactions and combining with the results from the exposure tests at elevated temperature, it is doubtful that RCC exists at elevated temperature.

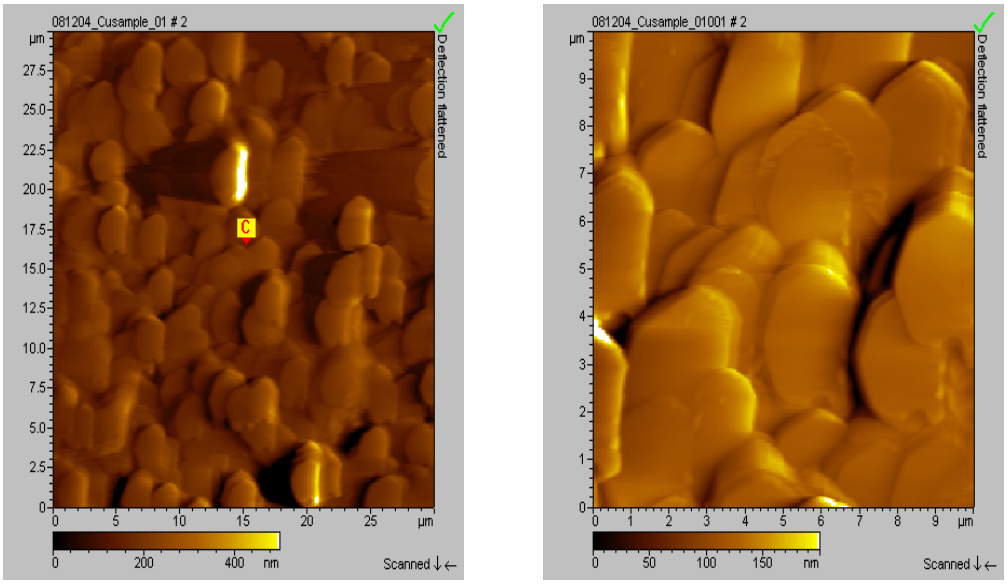

(a) (b)

Figure 4 - 33: AFM Image of the surface out of the crevice after the creviced copper coupon was immersed in 0.5 M NaCl solution for 30 days at 50 ºC with (a) 30 µm × 30 µm in-plan scan range and a 500 nm z range, and (b) 10 µm × 10 µm in-plan scan range and a 200 nm z-range.

4.3 Summary

In Chapter 4, the experimental results were presented and discussed. Based on open circuit potential measurements, it was hypothesized that RCC has three

steps: uniform corrosion, corrosion rate slow-down, and reverse crevice corrosion. This hypothesis was verified, to some degree, by the results from Raman spectroscopy. The relationship between the hypothesis and proofs can be illustrated by Figure 4-34. In this figure, each circle refers to a phase and the cross area of two circles is the transition process.

The AFM results also provide a good visual indication of the morphology of the corroded surface of copper coupon. It was observed that RCC did not occur at the higher temperature and this evidence was reinforced by the AFM photographs since the morphology of the entire surface of the creviced copper coupon exposed at high temperature looked the same. The photograph taken of the coupon in the deoxygenated environment showed that corrosion did not occur when oxygen is absent in electrolyte, which agrees with the results indicated by the open circuit potential measurements.

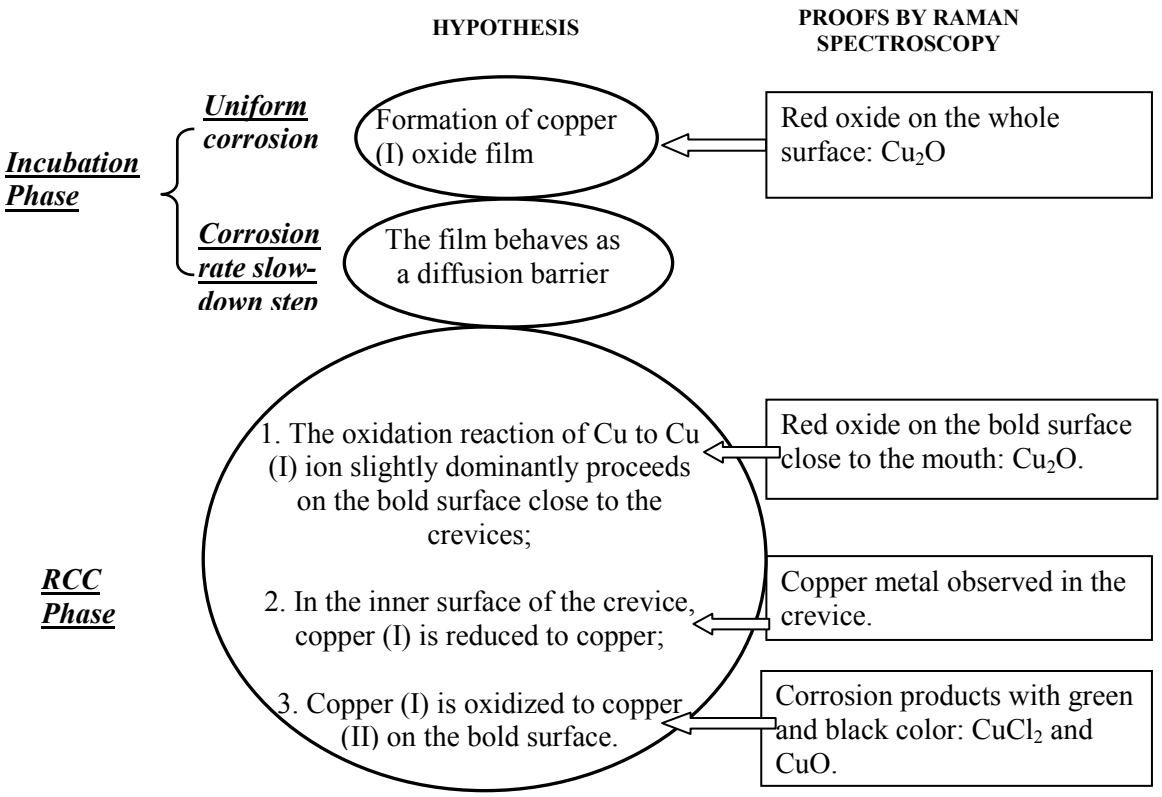

Figure 4 - 34: Diagram of the relationship between RCC phases and Raman spectroscopic results.

Several other electrochemical techniques were employed to investigate kinetic behavior of RCC. Potentiodynamic curves illustrated the polarization performance of RCC, by which corrosion rate can be measured. It was found that the corrosion rate is higher in elevated temperature compared with room temperature, there was an exception though. EIS revealed the rate controlling steps that occur during different phases of RCC. Based on the result of EIS, the rate controlling steps of RCC, in sequence, were diffusion processes from bulk solution to copper surface and the combination controlling of oxygen migration to crevice and the reduction from Cu (I) to Cu.

CHAPTER 5

CONCLUSIONS AND RECOMMENDATIONS

5.1 Conclusions

This research investigated the phenomenon of reverse crevice corrosion in commercially pure copper metal. Both electrochemical and surface analysis measurements were employed for evaluation. The following conclusions are drawn from this research.

1. During the RCC process, two phases with three distinct steps can be observed. They are:

- Step 1: Uniform corrosion. the whole copper surface undergoes uniform corrosion.
- Step 2: Corrosion rate slow-down. A film of Cu (I) oxide retards the diffusion between the solution and copper surface.
  Step 1 and 2 can be integrated into an incubation phase.
- Step 3: Reverse crevice corrosion. Copper ions are reduced in the crevice. Correspondingly, Cu is oxidized to Cu (I) and Cu (I) is oxidized to Cu (II) on the bold surface. This step is also the phase II.

The three steps are marked by significant changes in the open circuit potential.

2. The corrosion behavior of a creviced copper coupon at elevated temperature is different from that exhibited at room temperature. Uniform corrosion was observed on the whole surface of the copper specimen after it was immersed in 0.5 M NaCl aqueous solution for one month at 50 ºC. In addition, the results of the corrosion potential measurement and potentiodynamic measurement were significantly different than that obtained at room temperature. RCC did not occur with a creviced copper coupon at 50 ºC and this was verified by the result of atomic force microscopy.

3. A relatively stable corrosion potential was observed for a creviced copper coupon in a deoxygenated environment at room temperature. With the aid of the atomic force microscopy, it was observed that the little corrosion occurred on the whole surface. Therefore, as expected a deoxygenated environment dramatically reduces the corrosion damage.

4. It was found, via EIS measurements, that

- The rate controlling step in incubation phase is a diffusion process between the solution and the copper surface;
- During the final phase, the corrosion rate is controlled by both the reduction of copper in the crevice (charge transfer), and the change in oxygen transfer rate (mass transfer).

5. Raman spectra showed corrosion products that verified the hypothesis that was formulated from the open circuit potential measurements.

- In the crevice, copper and Cu_2O produced during the first stage were found.
- On the bold surface, CuO, Cu_2O and $CuCl_2$ were the mixed corrosion products.

6. The surface morphologies of creviced copper coupons were dissimilar under different environments, as determined by the AFM.

- At room temperature and open to the air, the surface in the crevice looked like an unevenly distributed granular solid, while the bold surface outside the crevice was covered evenly with corrosion products.
- At 50 ºC and with the solution open to the air, a similar morphology was observed on the whole surface. The granular solid was distributed evenly on the surface, which indicates the occurrence of uniform corrosion.
- In the deoxygenated environment at room temperature, no obvious granular solid was observed and the surface looked relatively smooth. The image was very similar to that of unused copper. Therefore, very little corrosion occurred under this condition.

As can be seen from the above conclusions, this study has discovered a three-stage RCC process for pure copper metal. The RCC characteristics under

different temperatures and different environments were also investigated and some relationships among these factors are also determined.

5.2 Recommendations

The following recommendations are made for future study.

1. Tests with Single Crevice Assembly

In this study, a multiple crevice assembly was used in all experiments. However, it can only provide qualitative information on RCC. In addition, the crevice size was difficult to control, which caused the poor reproducibility of the experiment. Although the multiple crevice assembly is suitable to apply for a primary study of RCC, it is not appropriate for more advanced study.

A single crevice assembly will permit the measurement of solution composition and potential in the crevice which will aid in understanding this phenomenon to a deeper extent.

2. Other Electrochemical Methods

The electrochemical measurements used in this research were open-circuit potential measurement, potentiodynamic measurement, potentiostatic measurement and electrochemical impedance spectroscopy. For future study, these techniques could be supplemented with others such as electrochemical noise and electrochemical frequency modulation. For the surface analysis studies, SEM with the aid of an X-ray photoelectron probe could be used because it can perform imaging and composition analysis at the same time.

3. Use Other Copper Alloy and Environmental Conditions

In all experiments of this study, commercially pure copper was immersed in a 0.5 M NaCl solution. It would be interesting to examine RCC for other copper alloys such as 70Cu-30Ni and 90Cu-10Ni. Furthermore, the composition of the solution could be varied.

4. Modeling of RCC

It would be interesting and useful to develop a numerical model for RCC of copper. Many models have been developed for regular crevice corrosion but none has been developed for RCC of copper.

However, some difficulties may be encountered developing such models. Firstly, some processes involved in RCC are not exactly known and the mechanism of RCC is not well understood. However, computer models are always based on profound background of mechanism. Secondly, in modeling studies, crevices are assumed to have ideal dimensions, which means perfectly smooth side walls and uniform crevice gaps. But in practice, it is hard to fabricate crevices with ideal dimensions.

5. Improvements of Experimental Procedures

In order to improve the reproducibility of RCC, some experimental procedures should be improved. Firstly, it would be preferable to measure the width of the crevice produced at each experiment. Secondly, to minimize residual oxygen in the crevice, for deoxygenated experiments, crevice assembly should be performed with the sample in a oxygen-free environment.

In addition, for Raman spectroscopy measurement, multiple samples can be used and observation can be made at different time periods. This would provide more detailed information that produced corrosion products for each phase. X-ray photoelectron spectroscopy (XPS) can also be used because it can present the thickness profile of the composition of corrosion products.

LIST OF REFERENCES

Abdulsalam, M. I. and Pickering, H. W. (1999) Effect of the Applied Potential on the Potential and Current Distributions within Crevices in Pure Nickel. Corrosion Science, **41**, No. 2, pp. 351 – 372.

Abdulsalam, M. I. (2002) Significance of Temperature Change on the Behavior of Crevice Corrosion. Corrosion **58**, No. 4, pp. 364 – 369.

Alavi, A. and Cottis, R. A. (1987) The Determination of pH, Potential and Chloride Concentration in Corroding Crevices on 304 Stainless Steel and 7475 Aluminum Alloy. Corrosion Science **27**, No. 5, pp. 443 – 451.

Alkire, R. C., and Siitari, D. (1982) Initiation of Crevice Corrosion: II – Mathematical Model for Aluminum in Sodium Chloride Solutions. Journal of the Electrochemical Society **129**, No. 3, pp. 488 – 496.

ASM International (2001) "Engineering Properties and Service Characteristics" in *ASM Specialty Handbook - Copper and Copper Alloys*, Ed. Davis, J. R., ASM International, OH, pp. 385 – 392.

Badawy, W. A., El-Egamy, S. S. and El-Azab, A. S. (1995) The Electrochemical Behaviour of Leaded Brass in Neutral Cl^- and SO_4^- Media. Corrosion Science **37**, pp. 1969 – 1979.

Badawy, W. A., El-Egamy, S. S. and El-Azab, A. S. (1997) Investigation of Corrosion and Stability of Lead-Brass Alloy in Acid and Neutral Solutions Using Electrochemical Impedance Spectroscopy. Corrosion **53**, No. 11, pp. 842 – 851.

Badawy, W. A., AI-Kharafi, F. M. (1999) Corrosion Behavior of Brass Alloys in Aqueous Solutions of Different pH. Corrosion **55**, No. 3, pp. 268 – 277.

Bard, A. J. and Faulkner, L. R. (2000) "Techniques Based on Concepts of Impedance" in *Electrochemical Methods-Fundamentals and Applications*, 2nd. John Wiley & Sons, New York, pp. 368 – 416.

Barnartt, S., (1986) "Electrochemical Nature of Corrosion" in *Electrochemical Techniques for Corrosion Engineering*, Ed. Baboian, R., NACE International, Houston, TX, pp. 1 – 11.

Beccaria, A. M., Mor, E. D. and Poggi, G. (1987) A Study of the Corrosion Products of Aluminum Brass Formed in Sodium Sulfate Solution in the Presence of Chlorides. Corrosion Science **27**, No. 4, pp. 363 – 372.

Benedetti, A. V., Sumodio, P. T. A., Nobe, K., Cabot, P. L. and. Proud, W. G (1995) Electrochemical Studies of Copper, Copper – Aluminum and Copper – Aluminum – Silver Alloys: Impendence results in 0.5M NaCl. Electrochimica Acta **40**, No. 16, pp. 2657 – 2668.

Bernhardsson, S., Eriksson, L., Oppelstrup, J., Puigdomenech, I., and Wallin, T. (1983) A Model for the Initiation of Crevice Corrosion of Stainless Steels in a Chloride Environment. Proc. 9th Scandinavian Corrosion Congress, Copenhagen, Denmark, September 1983, pp. 1 – 6.

Bianchi, G., and Longhi, P. (1973) Copper in Sea-Water, Potential-pH Diagrams. Corrosion Science **13**, No. 11, pp. 853 – 864.

Bosch, R. W., Hubrecht, J., Bogaerts, W. F. and Syrett, B. C. (2001) Electrochemical Frequency Modulation: A New Electrochemical Technique for Online Corrosion Monitoring. Corrosion **57**, No. 1, pp. 60 – 70.

Braun, M. and Nobe, K. (1973) Electrodissolution Kinetics of Copper in Acidic Chloride Solution. Journal of the Electrochemical Society **120**, No. 10, pp. 1666 – 1670.

Brett, C. M. A. and Brett, A. M. O. (1993) "Impedance Method" in *Electrochemistry Principles, Methods, and Applications*, Oxford University Press, New York, pp. 221 – 254.

Chan, H. Y. H., Takoudis, C. G., and Weaver, M. J. (1999) Oxide Film Formation and Oxygen Adsorption on Copper in Aqueous Media As Probed by Surface-Enhanced Raman Spectroscopy. Journal of Physical Chemistry **103**, pp. 357 – 365.

Chin, D. T., and Sabde, G. M. (1999) Current Distribution and Electrochemical Environment in a Cathodically Protected Crevice. Corrosion **55**, No.3, pp. 229 – 237.

Cicileo, G. P., Rosales, B. M., Varela, F. E. and Vilche, and J. R. (1999) Comparative Study of Organic Inhibitors of Copper Corrosion. Corrosion Science, **41**, No. 7, pp. 1231 – 1463.

Cieslewicz, J. M. and Schweitzer, P. A., P. E. (1989) "Copper and Copper Alloys" in *Corrosion and Corrosion Protection Handbook*, Ed. Schweitzer, P. A., Marcel Dekker, Inc., New York, pp. 125 – 152.

Dawson, J. L. and Ferreira, M. G. S. (1986) Electrochemical Studies of the Pitting of Austenitic Stainless Steel. Corrosion Science **26**, No. 12, pp. 1009 – 1026.

Dawson, J. L. and Ferreira, M. G. S. (1986) Crevice Corrosion on 316 Stainless Steel in 3% Sodium Chloride Solution. Corrosion Science **26**, No. 12, pp. 1027 – 1040.

Dawson, J. L. (1996) "Electrochemical Noise Measurement for Corrosion Applications" in *Electrochemical Noise Measurements for Corrosion Applications*, ASTM, West Conshohocken, PA, pp. 3 – 35.

Dean, S. W. (1976) "Electrochemical Methods of Corrosion Testing" in *Electrochemical Techniques for Corrosion*, Ed. Baboian, R., NACE, TX, pp.52 – 60.

DeJong, L. A. (1999), *Investigations of Crevice Corrosion Scaling Laws Using Microfabrication Techniques and Modeling*, a PhD thesis of University of Virginia, pp. 58 – 62.

Evans, K. J., Yilmaz, A., Day, S. D., Wong, L. L., Estill, J. C. and Rebak, R. B. (2005) Using Electrochemical Methods to Determine Alloy 22's Crevice Corrosion Repassivation Potential. JOM, 2005 January, pp. 56 – 61.

Evitts, R., Gad, M. M. A., Watson, M. K. and Postlethwaite, J. (1993) "Crevice Corrosion of Nickel Alloys at Elevated Temperatures: Experimental and Modelling Studies" in *Corrosion/93*, NACE International, Houston, TX, pp. 601:1 – 601:10.

Evitts, R. W., Postlethwaite, J. and Watson, M. K. (1995) Numerical Simulation of the Initiation of Crevice Corrosion of Passive Alloys at Elevated Temperatures. Proc. NACE International Canadian Region Western Conference, NACE International, Houston, TX, pp. 367 – 377.

Evitts, R. W., Watson, M. K. and Postlethwaite, J. (1996) "Numerical Simulation of Crevice Corrosion of Titanium: Effect of the Bold Surface" in *Corrosion/96*, NACE International, Houston, TX, pp. 121:1 – 121:10.

Evitts, R. W. and Postlethwaite, J. (2000) Numerical Investigation of Crevice Corrosion of Titanium at Elevated Temperatures. Proceeding of NACE International Canadian Region Western Conference, NACE International, Houston, TX, pp. 215 – 230.

Feng, Y., Siow, K.-S., Teo, W.-K., Tan, K.-L., and Hsieh, A.-K. (1997) Corrosion Mechanisms and Products of Copper in Aqueous Solutions at Various pH Values. Corrosion **53**, No.5, pp. 389 – 398.

Fontana, Mars G. and Greene, Norbert D. (1967) "Corrosion Forms" in *Corrosion Engineering*, McGraw-Hill, New York, pp. 41 – 44.

Fontana, M. P., Maisano, G., Migliardo, P., and Wanderlingh, F. (1978) Raman Spectroscopy and Local Order in Aqueous Solutions of Strong II-I Electrolytes. Journal of Chemical Physics **69**, No. 2, pp. 676 – 683.

Frost, R. L. (2003) The Raman Spectroscopy of Selected Copper Minerals of Significance in Corrosion. Spectrochimica Acta, Part A **59**, pp.1195 – 1204.

Fu, J. W. and S. Chan (1984) A Finite Element Method for Modeling Localized Corrosion Cells. Corrosion **40**, No. 10, pp. 540 – 544.

Gamry Instruments (2005) Electrochemical Impedance Spectroscopy Primer. An Application Note from Gamry Instruments, pp. 11 – 16.

General Chemistry Online, Date Revised: 09/20/1005; Date Accessed: 10/06/2005. http://antoine.frostburg.edu/chem/senese/101/solutions/faq/predicting-DO.shtml, Aug 24th, 2005.

Giuliani, L., Tamba, A. and Modena, C., (1971) Electrochemical Characterization of Some Cu Alloys in NaCl Solutions. Corrosion Science **11**, No. 8, pp. 485 – 498.

Globle Spec, Inc., Date Revised: N/A; Date Accessed: 10/06/2005. http://www.globalspec.com/specifications/spechelpall?name=ndt_Corrosion_Electrochemical_Instruments&comp=1983, Aug. 25, 2005.

Gong, Y. S., Lee, C. and Yang, C. K. (1995) Atomic Force Microscopy and Raman Spectroscopy Studies on the Oxidation of Cu Thin Film. Journal of Applied Physics **77**, No. 10, pp. 5422 – 5425.

Habib, K. (1990a) Holographic Interferometry of a Polarizaed and Loaded Metallic Electrodes in Aqueous Solution. Applied Optics **29**, No.13, pp. 867 – 869.

Habib, K. (1990b) Holographic Interferometry in Predicting Cathodic Deposition of Metals in Aqueous Solution. Proceeding of SPIE **1230**, pp. 293 – 296.

Habib, K. (1990c) Initial Behaviour of Corrosion Fatigue/Hydrogen Embrittlement of Metallic Electrodes in Aqueous Solutions. Exper. Tech. Physics **38**, No.5/6, pp. 535 – 538.

Habib, K., Carmichael, G., Lakes, R. and Stwalley, W. (1993) Novel Technique for Measuring Stress Corrosion Cracking of Metallic Electrodes in Aqueous Solutions: Theory and Application. Corrosion **49**, No.5, pp. 354 – 362.

Habib, K. (1994) Initiation of Stress Corrosion Cracking of Ti 90-A16-V4 Wire in Aqueous Solution: Non-Destructive Monitoring by Holographic Interferometry. Optics Lasers Engineering **20**, pp. 81 – 85.

Habib, K. (1995) Non-Destructive Evaluation of Metallic Electrodes under Corrosion Fatigue Conditions by Holographic Interferometry. Optics Lasers Engineering **23**, pp. 65 – 70.

Habib, K. (1999) Localized Corrosion of Copper Alloys by Optical Interferometry and Other Techniques. Desalination **124**, pp. 93 – 98.

Habib, K. (2002) Modified Electrochemical Emission Spectroscopy (MEES) of Detection of Crevice Corrosion of Metallic Alloys. Nondestructive Testing and Evaluation **18**, No. 3-4, pp. 109 – 117.

Habib, K. and Hanna Al-Mazeedi (2003) Optical Interferometry as Electrochemical Emission Spectroscopy of Copper Alloys in Seawter. Desalination **158**, pp. 3 – 8.

Hamilton, J. C., Farmer, J. C. and Anderson, R. J. (1986) In Situ Raman Spectroscopy of Anodic Films Formed on Copper and Silver in Sodium Hydroxide Solution. Journal of Electrochemical Society **133**, No. 4, pp. 739 – 745.

Hausler, R. H. (1977) Practical Experiences with Linear Polarization Measurements. Corrosion **33**, No. 4, pp. 117 – 128.

Hebert, K. and Alkire, R. (1983) Dissolved Metal Species Mechanism for Initiation of Crevice Corrosion of Aluminum. Journal of the Electrochemical Society **130**, No. 5, pp. 1007 – 1014.

Heppner, K. L., Evitts, R. W. and Postlethwaite, J. (2002) Prediction of the Crevice Corrosion Incubation Period of Passive Metals at Elevated Temperatures: Part I-Mathematical Model. The Canadian Journal of Chemical Engineering **80**, No. 10, pp. 8497 – 856.

Heppner, K. L., Evitts, R. W. and Postlethwaite, J. (2002) Prediction of the Crevice Corrosion Incubation Period of Passive Metals at Elevated Temperatures: Part II-Model Verification and Simulation. The Canadian Journal of Chemical Engineering **80**, No. 10, pp. 857 – 864.

Heppner, K. L., Evitts, R. W. and Postlethwaite, J. (2004) The Effect of the Crevice Gap on the Initiation of Crevice Corrosion in Passive Metals. Corrosion **80**, pp. 718 – 728.

Heppner, K. L., and Evitts, R.W. (2004) Computation of Mass Transport in Electrolytic Systems. Discrete and Continuous Dynamical Systems, Series B **11**. pp. 29 – 46.

Heppner, K. L., Evitts, R. W., and Postlethwaite, J. (2005) Effect of Ionic Interactions on the Initiation of Crevice Corrosion in Passive Metals, Journal of the Electrochemical Society **152**, pp. B89 – B98.

Hladky, K., and Dawson, J. L. (1981) The Measurement of Localized Corrosion Using Electrochemical Noise. Corrosion Science **21**, No. 4, pp. 317 – 322.

Johnson, J. W., Sun, Y. C. and James, W. J. (1971) Anodic Dissolution of Zn in Aqueous Solutiosns. Corrosion Science **11**, pp. 153 – 159.

Kautek, W. and Gordon II, J. G. (1990) XPS Studies of Anodic Surface Films on Copper Electrodes. Journal of Electrochemical Society **137**, No.9, pp. 2672 – 2677.

Keddam, M., Oltra, R., J., Colson, C. and Desestret, A. (1983) Depassivation of Iron by Straining and by Abrasion: an A.C. Impedance Study. Corrosion Science **23**, No. 4, pp. 441 – 451.

Klassen, R. D., Robergea, P. R. and Hyattb, C. V. (2001) A Novel Approach to Characterizing Localized Corrosion within a Crevice. Electrochimica Acta **46**, No. 24-25, pp. 3705 – 3713.

Klein, P. A., Hays, R. A. and Ferrara, R. J. (1991) The Effect of Electrolytic Chlorination on the Crevice Corrosion Behavior of 70/30 Copper-Nickel and

Nickel-Copper Alloy 400. Proc. Corrosion/91, the NACE Annual Conference and Corrosion Show, Cincinnati, Ohio, pp. 509:1 – 509:15.

Landolt, M., Muller, R. H. and Tobias, C.W. (1971) Crystallographic Factors in High-Rate Anodic Dissolution of Copper. Journal of Electrochemical Society **118**, No. 1, pp. 36 – 51.

Leckie, H. P. (1970) The Anodic Polarization Behavior of Copper. Journal of Electrochemical Society **117**, No. 12, pp1479 – 1483.

Leidheiser, H. (1979) "Aqueous Corrosion" in *The Corrosion of Copper, Tin and Their Alloys*, Robert E. Krieger Publishing Company, Huntington, NY, pp. 71 – 126.

Leroy, R. L. (1973) Range of Validity of the Linear Polarization Method for Measurement of Corrosion Rates. Corrosion **29**, No.7, pp. 272 – 175.

Li, J. and Lampner, D. (1999) In-situ AFM Study of Pitting Corrosion of Cu Thin Films. Colloids and Surface A: Physicochemical and Engineering Aspects **154**, pp. 227 – 237.

Makrides, A. C. (1973) Corrosion in Dilute Acids: Part 1 — A Modified Linear Polarization Technique. Corrosion **29**, No.4, pp.148 – 153.

Mansfeld, F. (1973) Tafel Slopes and Corrosion Rates from Polarization Resistance Measurements. Corrosion **29**, No.10, pp. 397 – 402.

Mansfeld, F. (1976a) "Polarization Resistance Measurements – Experimental Procedure and Evaluation of Test Data" in *Electrochemical Techniques for Corrosion*, Ed. Baboian, R., pp. 18 – 26.

Mansfeld, F. (1976b) "Corrosion Rate Determination", in *Electrochemical Techniques for Corrosion*, Ed. Baboian, R., pp. 113 – 153.

Mansfeld, F. (1981) Recording and Analysis of Alternating Current Impedance Data for Corrosion Studies; Part 1 — Background and Methods of Analysis. Corrosion **36**, No. 5, pp. 301 – 308.

Mansfeld, F., Kendig, M. W. and Tsai, S. (1982) Corrosion Kinetics in Low Conductivity Media – I. Iron in Natural Waters. Corrosion Science **22**, No. 5, pp. 455 – 471.

Mansfeld, F. (1986) “Polarization Resistance Measurements – Today’s Status” in *Electrochemical Techniques for Corrosion Engineering*, Ed. Baboian, R., pp. 67 – 71.

Mansfeld, F., Jeanjaquet, S. L. and Kendig, M. W. (1986) An Electrochemical Impedance Spectroscopy Study of Reactions at the Metal/coating Interface. Corrosion Science **26**, No. 9, pp. 735 – 742.

Mansfeld, F., Lin, S., Kim, S. and Shih, H. (1989) Surface Modification of Al Alloys and Al-Based Metal Matrix Composites by Chemical Passivation. Electrochimica Acta **34**, No. 8, pp. 1123 – 1132.

McCann, L. I., Trentelman, K., and Golding, B. (1999) Corrosion of Ancient Chinese Bronze Money Trees Studies by Raman Microscopy. Journal of Raman Spectroscopy **30**, pp. 121 – 132.

McKay, R. J. (1922) Corrosion by Electrolyte Concentration Cells. Transactions of the Electrochemical Society **41**, pp. 201 – 203.

McKay, R. J. (1925) The Common Occurrence of Corrosion by Electrolyte Concentration. Industrial and Engineering **17**, pp. 23 – 24.

Melchers, R. E. (2001) Temperature Effect on Seawater Immersion Corrosion of 90:10 Copper-Nickel Alloy. Corrosion **57**, No. 5, pp. 440 – 451.

NACE International, Date Revised: 09/10/2003; Date Accessed: 10/06/2005. http://nace.org/nace/content/publicaffairs/cocorrindex.asp

Nisancioglu, K. (1986) “The Error in Polarization Resistance and Capacitance Measurements Resulting from Nonuniform Ohmic Potential Drop to Flush-Mounted Probes” in *Electrochemical Techniques for Corrosion Engineering*, Ed. Baboian, R., pp. 45 – 55.

Oldfield, J. W., and Sutton, W. H. (1978) Crevice Corrosion of Stainless Steels I – A Mathematical Model. British Corrosion Journal **13**, pp. 13 – 22.

Oldfield, J. W., Masters, G. L., and Stokes, K. R. (1996) “Prediction of Initiation and Propagation of Crevice Corrosion on Aluminum Alloys in Sea Water by Mathematical Modelling” in *Proceeding of Corrosion 96*, pp. 512:1 – 512: 16, 1996.

Oltra, R and Keddam, M (1988) Application of Impedance Technique to Localized Corrosion. Corrosion Science **28**, No. 1, pp. 1 – 18.

Ord, J. L., DeSmet, D. J. and Huang, Z. Q. (1987) An Ellipsometric Study of the Anodic Oxidation of Copper in pH 12 Sodium Carbonate. Journal of Electrochemical Society **134**, No. 4, pp. 826 – 832.

Palit, A. and Pehkonen, S. O. (2000) Copper Corrosion in Distribution Systems: Evaluation of a Homogeneous Cu_2O Film and a Natural Corrosion Scale as Corrosion Inhibitors. Corrosion Science **42**, No. 10, pp. 1669 – 1851.

Pardo, A., Otero, E., Merino, M.C., Lopez, M.D., Utrilla, M.V., Moreno, F. (2000) Influence of pH and Chloride Concentration on the Pitting and Crevice Corrosion Behavior of High-Alloy Stainless Steels. Corrosion **56**, No. 4, pp. 411 – 418.

Piron, D. L. (1991) "Electrode Rate Process and Overpotential" in *The Electrochemistry of Corrosion*, NACE, Huston, TX, pp. 75 – 101.

Polan, N. W. (1987) "Copper and Copper Alloy" in *ASM handbook - Corrosion*, Ed. Davis, J. R. and Destefani, J. D., ASM International, OH, pp. 610 – 616.

Postlethwaite, J. (1983) Electrochemical Tests for Pitting and Crevice Corrosion Susceptibility. Canadian Metallurgical Quarterly **22**, No. 1, pp. 133 – 141.

Postlethwaite, J., Evitts, R. W. and Watson, M. K. (1994) "Modelling the Initiation of Crevice Corrosion of Passive Alloys at Elevated Temperatures" in *Proceeding of EMCR '94, 5th International Symposium on Electrochemical Methods in Corrosion Research*, Materials Science Forum, Trans Tech Publications, Switzerland, pp. 121 – 132.

Pourbaix, Marcel (1974) "Establishment and Interpretation of Potential – pH Equilibrium Diagrams" in *Atlas of Electrochemical Equilibria in Aqueous Solutions*, National Association of Corrosion Engineers, Houston, Tex, pp. 384 – 392.

Royuela, J. J. and Otero, E. (1993) The Assessment of Short Term Data of Pipe Corrosion in Drink Water- II. Copper. Corrosion Science **34**, No. 10, pp. 1595 – 1606.

Sagara, M., Noda, K., Katada, Y. and Kodama, T. (2002) Application of Scanning Chemical Microscope to Crevice Corrosion Process of Stainless Steel. Electrochemical Society Proceedings **2002-24**, pp. 411 – 420.

Schafer, G. J., and Foster, P. K. (1959) The Role of the Metal-Ion Concentration Cell in Crevice Corrosion. Journal of the Electrochemical Society **106**, p. 468.

Schneider, M. and Pohl, H. (2002) Crevice Corrosion Investigation on AA 6013: Application of Electrochemical Noise Analysis. British Corrosion Journal **37**, No. 4, pp. 298 – 304.

Sharland, S. M. (1988) A Mathematical Model of Crevice and Pitting Corrosion – II The Mathematical Solution. Corrosion Science **28**, No. 6, pp. 621 – 630.

Skolnik, A. M., Hughes, W. C. and Augustine, B. H. (2000) A Metallic Surface Corrosion Study in Aqueous NaCl Solution Using Atomic Force Microscopy (AFM). Chemistry Educator **5**, No. 1, pp. 8 – 13.

Smialowska, Z. S. and Mankowski, J. (1978) Crevice Corrosion of Stainless Steels in Sodium Chloride Solution. Corrosion Science **18**, No. 11, pp. 953 – 960.

Steinsmo, U., Rogne, T., Drugli, J. M. and Gartland, P. O. (1997) Critical Crevice Temperature for High-Alloyed Stainless Steels in Chlorinated Seawater Applications. Corrosion **53**, No. 1, pp. 26 – 32.

Trzaskoma, P. P., McCafferty, E. and Crowe, C. R. (1983) Corrosion Behaviour of SiC/Al Metal Matrix Composites. Journal of Electrochemical Society **130**, No. 9, pp. 1804 – 1809.

Turner, M. and Brook, P. A. (1973) The Anodic Behavior of Copper in Static and Flowing Hydrochloric Acid Solution. Corrosion Science **13**, No. 12, pp. 973 – 983.

Vankeerberghen, M. (2004) Critical Characteristic Dimension or Geometry for Determining the Susceptibility of a Crevice to Crevice Corrosion. Corrosion **60**, No. 8, pp. 707 – 717.

Venugopal, A., Veluchamy, P., Selvam, P., Minoura, H. and Raja, V.S. (1997) X-Ray Photoelectron Spectroscopic Study of the Oxide Film on an Aluminum-Tin Alloy in 3.5% Sodium Chloride Solution. Corrosion **53**, No. 10, pp. 808 – 812.

Walton, J. C., Cragnolino, G., and Kalandros, S. K. (1996) A Numerical Model of Crevice Corrosion for Passive and Active Metals. Corrosion Science **38**, No. 1, pp. 1 – 18.

Wang, R. (2004) An AFM and XPS Study of Corrosion Caused by Micro-liquid of Dilute Sulfuric Acid on Stainless Steel. Applied Surface Science **227**, pp. 399 – 409.

Wood, R. J. K. and Fry, S. A. (1989) The Synergistic Effect of Cavitation Erosion and Corrosion for Copper and Cupro-Nickel in Seawater. Journal of Fluids Engineering **111**, No. 9, pp. 271 – 279.

Wyche, L. R., Voigt, L.R., and Laque, F.L. (1959) Corrosion in Crevice. Journal of the Electrochemical Society **106**, pp. 468 – 470.

Xu, J. F., Ji, W., Shen, Z. X., Li, W. S., Tang, S. H., Ye, X. R., Jia, D. Z. and Xin, X. Q. (1999) Raman Spectra of CuO Nanocrystals. Journal of Raman Spectroscopy **30**, pp. 413 – 415.

Yamashita, M., Omura, K. and Hirayama, D. (1980) Passivating Behavior of Copper Anodes and its Illumination Effects in Alkaline Solutions. Surface Science **96**, pp. 443 – 460.